NUMERICAL STUDIES ON CORNEAL BIOMECHANICS AND DEVELOPMENT OF SILICA-COLLAGEN CORNEAL HYBRIDS

Submitted By:

DIBYENDU MANDAL
Doctor of Philosophy (Engineering)

Department of Mechanical Engineering
Faculty Council of Engineering & Technology
Jadavpur University
Kolkata, INDIA

2019

JADAVPUR UNIVERSITY
KOLKATA-700032

INDEX NO.: 42/14/E

1.	**Title of the thesis:**	**Numerical Studies on Corneal Biomechanics and Development of Silica-Collagen Corneal Hybrids**.
2.	**Name, Designation & Institution of the Supervisor/s:**	**Dr. Amit Karmakar** *Associate Professor* Department of Mechanical Engineering Jadavpur University **Dr. Himadri Chattopadhyay** *Professor* Department of Mechanical Engineering Jadavpur University
3.	**List of publication:**	**1. Dibyendu Mandal**, Himadri Chattopadhyay, Amit Karmakar, Kumaresh Halder, Finite Element approach towards Impact Analysis on Biomechanical Nature of Cornea, *2018, 29(12), 2465-2470, Biomedical Research.* **2. Dibyendu Mandal**, Himadri Chattopadhyay, Amit Karmakar, A Fractional Calculus Approach in Mathematical Modeling of the Viscoelastic Response of Human Cornea, *Mathematical Biosciences - Under Review*
4.	**List of Patents:**	Nil
5.	**List of Presentations in National / International :**	1. Presented a paper "*A 3-Dimensional FEM approach towards Impact Analysis on Corneal Biomechanics for prevention of Ocular Injury*" National Conference on Computing, Electronic Devices, Materials, Manufacturing and Thermal Engineering, MCKV Institute of Engineering, 2016. 2. Presented a paper "*Simulation of Eye Injury Due to Blunt Body Impact*" in India Altair Technology Conference, Pune, 2013.

सूयाद्भवान्त भूताान
सूर्येण पालितानि तु ।
सूर्ये लयं प्राप्नुवन्ति यः सूर्यः सोऽहमेव च । चक्षुर्नो
देवः सविता चक्षुर्न उत पर्वतः ।
चक्षुर्धाता दधातु नः । आदित्याय विद्महे सहस्रकिरणाय
धीमहि । तन्नः सूर्यः प्रचोदयात् ।

(Suryopanishad)

EVERYTHING OWES THEIR ORIGIN TO THE SUN, IS NURTURED BY THE SUN AND ALSO TERMINATES IN HIM. OUR EYES ARE BUT THE REFLECTION OF HIM ONE WHO RULES OVER THE TIME. LET OUR EYES BE PROTECTED BY THE ALL-SEER. WE SEEK THE BLESSINGS OF THE LORD OF MYRIAD RAYS.

CERTIFICATE FROM SUPERVISORS

This is to certify that the thesis entitled --

"Numerical Studies on Corneal Biomechanics and Development of Silica-Collagen Corneal Hybrids" submitted by **Shri Dibyendu Mandal** who got his name registered on 30th October 2014 for the award of Ph.D. (Engg.) degree of Jadavpur University is absolutely based upon his own work under the supervision of *Dr. Amit Karmakar,* Associate Professor, Department of Mechanical Engineering, Jadavpur University and *Dr. Himadri Chattopadhyay*, Professor, Department of Mechanical Engineering, Jadavpur University and that neither his thesis nor any part of the thesis has been submitted for any degree/ diploma or any other academic award anywhere before.

Signature of the Examiner with date

_____ _____

Signature of Supervisor with date **Signature of Supervisor with date**

_____ _____

Seal of the Supervisor **Seal of the Supervisor**

DEDICATIONS

With immense gratitude I dedicate this thesis to my ***Family*** & my ***closest Friend*** who is now a family to me.

From the core I dedicate this piece of work to my ***Grandparents*** who used to dream with me to witness this day.

I feel always overwhelmed to dedicate any of my work to my Guru, The bard ***Rabindranath Tagore*** as he played a key role in my life through his creativity which never let me get frustrated or down.

বিপদে মোরে রক্ষা করো এ নহে মোর প্রার্থনা —
বিপদে আমি না যেন করি ভয়।
দুঃখতাপে ব্যথিত চিতে নাই বা দিলে সান্ত্বনা,
দুঃখে যেন করিতে পারি জয় ॥

1906 A.D.

ACKNOWLEDGEMENT

After a long struggle here comes another opportunity to show gratitude to them who have always been with me in this struggle.

The first person who is struggling, scolding, pacifying and mentoring me since my Masters days and whom I want to thank for accepting me as his student and taught all simple small basics of research and thesis writing is *Dr. Himadri Chattopadhyay*. I like to thanks *Dr. Amit Karmakar* for this thesis to happen.

I thanks my parents and my brothers and sisters and the full family whom I upon whenever I am down.

I thank to my school and college teachers and my tutors for believing in me.

Thank you *Majumder Miss* and *Mita Miss.*

There is nothing to give to the Almighty as Tagore told "Whatever I give to thee are all that You have given me". So, a heartfelt gratitude to the Almighty.

I like to thanks all my lab-mates and my dear friends.

Moreover a thanks to all who have supported me and kept faith in me till now.

Dibyendu Mandal, 2019

ABSTRACT

Human cornea exhibits viscoelastic behavior as in other living tissues. The cornea is mainly dominated by the stroma which constitutes 90% of the corneal thickness. A number of experiments on tensile strip of human bovine corneas show that the tissue exhibits anisotropic, non-linear, rate dependent, viscoelastic mechanical stress-strain response and also a highly nonlinear creep response that depends on the applied stress.
The work comprises two different areas; the first one is related to mathematical modeling of viscoelsticity of cornea. The second part is related to development of corneal substitute.

The first phase of the work is a computational analysis of a blunt body impact on corneal viscoelastic behavior; simultaneously comparison is drawn between the tissue behaviors with corresponding cases considering the tissue to be elastic in other simulated model.
A simulation model of eye is set up based on the information of cadaver eyes done in the earlier works in this domain. Three dimensional models of corneal tissue were subjected to blunt body impact at different velocities in ALTAIR platform to study the nature of injury on the tissue material. The variation in the strain due to impact on the cornea for the material behaviors, range in the order 10^{-2}±0.002 and that for the stress, the magnitude gets almost double for elastic nature of cornea. The results shows that the viscoelastic biomechanics of the tissue predict higher resistance to any foreign body impacting on the surface of cornea preventing it from further indentation into the tissue. The viscoelastic model provided in this work can be incorporated for the synthesis of artificial corneas and soft contact lenses.

A mathematical approach has been taken further in this work to trace out the rate dependent, anisotropic and viscoelastic response. Two basic classical models have been taken into account to compare and predict the rate dependent response. On one hand as the K-V Model shows similar nature, Maxwell Model violates the same with a large discrepancy and thus giving rise to the Fractional operator FMM. Fractional calculus approach has hence been taken into account in modeling human corneal viscoelastic

behavior. The degree of both elasticity and viscosity is much convenient to consider when described in terms of the fractional order parameters. FMM plays an essential role to study viscoelastic properties. This paper presents modeling of the human cornea when subjected to simple stress in the order of few MN/m^2 by FMM. The governing fractional equation involving two fractional parameters α and β have been considered to model the stress-strain relationship of human cornea. The analytical solution of the fractional equation has been obtained for values of α and β using Laplace transform methods. The effect of the fractional parameter values on the stress-deformation nature has been observed and studied. A comparison between experimental values and computational values for the various fractional order of the Maxwell model equation clearly describes the mathematical model of choroidal and scleral strips and also shows range of values of the parameters for which the mathematical model depicts the real time stress-strain relationship of human cornea. It can also be seen that this model concludes to the Classical Maxwell model as a special case for α = β = 1 and that human eye does not clearly obey the Maxwell model viscoelastic property.

The experimental part of the study is mainly focused on the synthesis and development of Silica-Collagen Hybrids that can substitute normal healthy cornea of human. The main issue that concerns the patients and doctors after a donor corneal transplant is Auto-Immune Rejection by host body which may be due to biocompatibility, haemocompatibility or cytotoxicity. The research thrives for synthesis of a composite comprised of Collagen, the basic protein that can be abundantly found in human body and silica which is biosafe and biocompatible to physiological system and can act as a scaffold for tissue engineering and drug delivery. The starting materials of the synthesis are diluted Silica precursor and two types of collagen-I and III which is predominantly found on the epithelium and basement membrane of the cornea. Sol Gel technique has been applied for the synthesis of the composite and finally lyophilized after the pH has been stabilized around 7.2-7.4 to obtain dehydrated silica collagen composite. Optical property of the developed composite closely mimics the collagen hybrids from earlier work in this field. The composite exhibits crystallinity as it evidenced from its XRD plot.

Other material characterizations, viz. FTIR and SEM have been performed on the sample to identify the nature of the composite.
Despite significant advance in the research front, one of the major concern is the price of commercial collagen and unavailability of indigenous components. This is the reason which has given path to extraction of nascent collagen from fish skin in this research.

Sperata Aor, commonly known as Indian Catfish has a thick layer of epidermal tissue which is a reserve of basic protein, collagen and fats. The objective of the work is to extract the collagen present in the skin. The skin has been carefully removed and treated with stock solution to loosen the non-protein bonds and further treated with butyl alcohol to remove fats. To loosen the thick fibres of the skin it is finally suspended in acetic acid and finally filtered and washed with deionized water followed by centrifugation and salting. Salting helps to remove any traces of acetic acid and finally pH has been maintained and lyophilized for 48hours in -60^{o}C which lead to a porous spongy mesh of collagen. The presence of Amide A and Amide I&II confirms the material thus extracted is predominantly collagen type I. SEM images has shown fibrillar structures with some knotted structure which also confirms it to be Collagen. This collagen can be used for preparation of tissue engineering scaffolds and for development of Biomimetic structure exhibiting both physiological and electrical properties.

In conclusion the studies in the thesis has been organized under three major sections which have given better understanding on the physiology and biomechanical behavior of the delicate tissue whose damage may cause severe injury and even death sometimes. Through the experimental investigation an insight has been developed about Sol-Gel technique and the property and structure of the collagen protein for possible application in drug delivery and tissue engineering.

CONTENT

LIST OF FIGURES

LIST OF TABLES

CHAPTER 1
INTRODUCTION

1.1 INTRODUCTION

Biology is the branch of science that deals with the study of living things and mechanics is the study of motions and applied loads that causes them while biomechanics is the study of the structural and functional behavior of biological systems such as humans, animals, plants, organs, and cells by means of mechanical science. Biomechanics is a branch of engineering, as it applies engineering sciences to analyze biological systems. Some simple applications of Newtonian mechanics or materials sciences can supply correct approximations to the mechanics of many biological systems. Applied mechanics, most notably mechanical engineering disciplines such as continuum mechanics, mechanism analysis, structural analysis, kinematics and dynamics play prominent roles in the study of biomechanics.

Herein, biomechanics is the development, extension and application of mechanics for the purposes of better understanding of the influence and application of mechanical loads on the biological structures, properties and function which makes the domain of biomechanics wide. It comprises of the effects of loads of wind and gravity on the plant growth, flights of birds and human gait and athlete performances to summarize in short among many other analysis and studies. Additionally, biomechanics also deals many health issues, disease, injury, and their path of treatment in biotic society.

1.2 BRIEF ANATOMY OF HUMAN EYE

Humans are profoundly visual animal groups as a significant piece of data about the world comes to Central Nervous System (Brain and Spinal Cord) through eyes and the vast majority of the social and scholarly data is put away and transmitted as words, pictures, and contemplations to which vision gives access and importance. Along these lines, the better learning of human eye gives an exact flawlessness to the world and circle of understanding. Ocular mechanical examination and study give a reasonable idea and pathway to tread away different wounds and sicknesses which could prompt lethal issue or could assert life. A layoff of human eye has been shown in Figure 1.1.

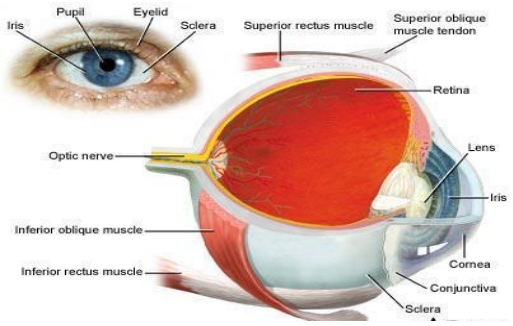

Fig.1.1: *The Human Eye*

1.2.1. Geometry of Human Eye

The eyeball is comprised of two circles joined at the limbus (intersection of the cornea and sclera). The cornea is the littler front circle of sweep 7.8 mm, and the sclera is the bigger back circle of range 17 mm.

The general geometry of the grown-up human eye is relatively round, more accurately ovoid fit as a fiddle. It can be considered as two circles with their focuses 5 mm apart (*Grand and Hage, 1980*). Geometrically, a circle with a range of 12 mm can speak to the back bit of the eye while the foremost part can be portrayed by a small circle having a sweep of 8 mm. Actually, the back of the eye is marginally straightened and its range of ebb and flow changes around the eye. For example, the level tropical range is typically bigger in the nasal side contrasted and the transient side. In an investigation on the state of human eye utilizing an MRI of 22 tests, demonstrates that all things considered that the eyes were 23.0 mm long, 22.7 mm wide, and 22.4 mm high(*Atchison et al., 2004*). A ton of variety had additionally been seen between subjects as the pivotal length of the eye extended from 21.4 to 24.3 mm, the width from 20.6 to 24.6 mm and the stature ran from 20.4 to 24.0 mm.

By and large, there is variety in eye measure between people, yet the normal pivotal length of the globe is 24 mm (extend 21-26 mm). The level length is around 23.5 mm. Figure 1.2 demonstrates a romanticized geometry of Eye proposed by *Reno, 2010*.

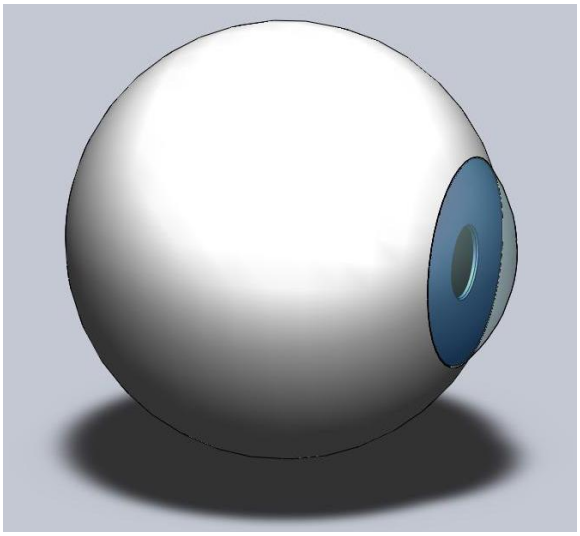

Fig.1.2: *Idealized Geometry of Human Eye (Reno. 2010)*

1.2.2 Components of Human Eye

The basic structure of human eye includes:

1. The Protective Structures

- The Orbit
- The Lids
- The Sclera

2. The Anterior Segment

- The Cornea
- The Aqueous Humour
- The Iris
- The Pupil
- The Crystalline Lens and Ciliary Muscle

3. The Posterior Segment

- The Retina
- The Vitreous Humour

1.2.2.1 Corneo-scleral shell

The external layer of the eye frequently referred to as the corneo-scleral shell, is an intense sinewy tissue that encases and secures the intraocular structures (*McBrien and Gentle, 2003; Ethier et al., 2004*). The corneo-scleral shell is made out of the cornea anteriorly and the sclera posteriorly (Fig.1.4). The cornea and the sclera meet at the limbus. The external layer of the eye contains up to 90% collagen (*McBrien and Gentle, 2003*), giving it its quality. An imperative capacity of the corneo-scleral shell is to keep up a settled hub length with the end goal that the light is centered around the retina at untouched. Along these lines, the external layer of the eye needs to oppose the variety in intraocular weight, which is the liquid weight inside the eye, and the powers produced by the additional visual muscles amid eye developments. It likewise needs to give an inflexible structure to the ciliary muscle to guarantee exact settlement.

The cornea is straightforward because of its avascularity and to the profoundly consistent course of action of its collagen strands. The stroma, which is the primary piece of the cornea, comprises layers of lamellae stacked together. Each layer has its own favored course and inside every lamella, the collagen fibrils are close equidistant and impeccably parallel to each other (*Pinsky et al., 2005).* The thickness of the cornea is around 500 μm in the middle and increments to around 650 μm at the outskirts. The sclera is the white

piece of the eye which is obscure because of the sporadic course of action of its collagen filaments. A favored collagen fiber introduction in the sclera can be found close to the additional visual muscle connection destinations (*Thale et al., 1996*) and around the optic nerve (*Thale and Tillmann,1993*). The thickness of the sclera is most minimal anteriorly and builds consistently to achieve a maximum of around 1.25 mm at the back of the eye (*Le Grand and El Hage, 1980a*). The sclera is the primary load-bearing part of the eye (*Girard et al., 2008*). Figure 1.3 demonstrates the external and internal shell of the human eye containing watery cleverness and vitreous diversion individually.

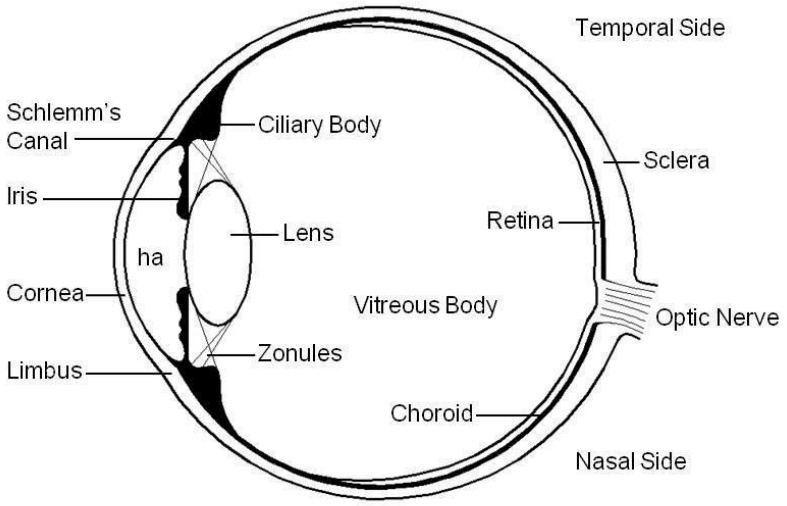

Fig.1.3: *Horizontal Section of Human Eye; ha is the Aqueous Humor (Reno, 2010)*

1.2.2.2 Middle tunic

The middle tunic is made up of the iris, the ciliary body, and the choroid. These structures are highly vascularised and pigmented. The iris is a circular structure that lies between the lens and the cornea and the eye color is determined by the color of iris. Iris musculature relaxes and contracts to control the diameter of the pupil and therefore the amount of light entering the eye based on the ambient illumination. In bright light the pupil diameter can contract upto 2 mm whereas complete darkness produces a pupil diameter of about 8 mm (*Le Grand and El Hage, 1980a*).

The ciliary body is composed of the ciliary muscle and the ciliary processes. The ciliary muscle can be classified into three types based on the orientation of the muscle fibres: longitudinal, radial, and circular. The main function of the ciliary muscle is accommodation which is required to bring near objects into focus. During accommodation, the ciliary muscle contracts pulling the ciliary body forward and inward

(*Tamm et al., 1991*). The inward movement causes a release of tension of the zonules leading to a change in shape of the lens. The main function of the ciliary process is the production of aqueous humor which is a liquid that nourishes avascular tissues such as the lens and the cornea. Aqueous humor fills the space of the anterior chamber which lies between the posterior surface of the cornea and the anterior surface of the iris and the lens. Aqueous humor flows from the ciliary processes around the iris and drains mainly into Schlemm's canal located at the angle of the iris and the limbus. Proper balance between aqueous humor production and outflow is critical for the maintenance of normal intraocular pressure (IOP).

The choroid is a layer of highly vascularised tissues situated between the retina and the sclera. The main function of the choroid is to supply oxygen and nutrients to the outer retina where the energy-demanding photoreceptors (rods and cones) are located. The blood vessels in the choroid swell and contract with the cardiac cycle which causes variation in choroidal thickness producing a change in IOP known as the ocular pulse (*Ethier et al., 2004*).

1.2.2.3 The lens

The lens is a transparent optical component capable of adjusting its refractive power to focus light coming from different distances. The lens is suspended by the zonules which are attached to the ciliary body. When focusing on a near object, the tension on the zonules is released causing the lens to fatten and change its curvature which results in an increase in dioptric power. The result is a close object focused on the retina and a clear image. With accommodation at rest, the lens accounts for roughly 1/3 of the total refractive power of the eye and its dioptric power range available for accommodation is around 10 dioptres (D) in young adults (*Allen and O'Leary, 2006*). The dioptre is commonly used in optometry as a measure of the optical power of a lens and is equal to the reciprocal of the focal length in metres. For instance, a 4 D lens brings parallel rays of light into focus at a distance of 1/4 metres behind the lens. The dioptre is also used to specify the optical power of the eye.

1.2.2.4 Vitreous body

The vitreous body is a transparent gel that fills the space of the vitreous chamber which lies between the posterior surface of the lens and the anterior surface of the retina. Its main functions are to support and inflate the eye; to provide nutrients and eliminate cellular waste; and to maintain the vitreous pressure. Studies in monkeys showed that during accommodation, the vitreous pressure increases while the anterior chamber

pressure (IOP) decreases such that a pressure gradient across the lens is present (*Young,1981*).

1.2.2.5 Retina

The retina is the innermost layer of the eye consisting of light sensitive tissue. Light striking the retina is converted into nerve impulses sent to the brain via the optic nerve (*Reno, 2010*).

1.3 OCULAR BIOMECHANICS

Regardless of advanced experimental and clinical methods some visual mechanisms still remain generally unknown. Ocular biomechanics represents a subset of the field of biomechanics related to human eye. By definition, biomechanics combines the laws of physics, applied mathematics and engineering concepts to study a biological phenomenon, describe parts in motion, couples associated and the forces acting upon them during activity. This systematic biomechanical approach has numerous advantages; particularly, this treatment has been very successful in the understanding of physiological processes.

As any other biological entity the eye also needs to perform a series of complex and interrelated activities in order to work adequately and sufficiently. If any of these activities is somehow altered, the entire system may suffer. (Moreover, some of the treatments used to correct a given anomalous condition interfere with present eye activities, partially modify them and, thus, may cause unwanted secondary effects.). Studying the various ocular phenomenon is of great medical relevance for the understanding of these processes and their treatments, their causes and also the consequences. A detailed investigation on the functioning of primary eye systems is not only important for the clinical ophthalmologic practice, but also crucial for general concepts of human eye. Such ocular biomechanical studies provide a platform for the correct explanations for normal as well as diseased pathological performances and thus show directions for diagnostics and treatment of some ocular abnormalities thus reducing the scope for a riskful surgery.

The combination of various experimental studies, both in vivo and in vitro, and mathematical descriptions of phenomena is of invaluable help to analyze and explain the visual mechanisms and gain a better insight into ophthalmologic conditions. Important data, provided by experiments, are interpreted within the context of an analytical framework, while theoretical simulations are used to test the consistency of sets of previous experimental measurements, suggesting where further laboratory studies are

needed. Numerical analysis has been helpful in the understanding of biomedical processes by means of computer simulations. Other major contributions brought to the medical community by computational facilities include the ability to analyze, manage and visualize vast amounts of data. The integration of these techniques has become widely accepted as investigative tools for systematic analyses.

A detailed review of literature has been provided in the next chapter.

1.4 ORGANIZATION OF THESIS

The thesis has been organized into chapters. This present chapter introduces the introductory area of the complete research work.

- In this chapter a concise introduction has been provided on the anatomy and physiology of human eye and various aspects of biomechanics and its mathematical formulation.
- *Chapter 2* contains a comprehensive Literature Survey of the full thesis which has supported the research methodically, technically and mathematically.
- Mathematical formula and constitutive equations has been discussed here in this chapter briefly which has been further broadly described in *Chapter 3* along with various conditions that has been applied to those equations to obtain results with its proper discussions according to the nature of human soft collagenous tissue.
- *Chapter 4* gives a brief summary of the Impact nature of Cornea due to impacting foreign projectile at various deformation speed leading to variation in resulting strain on the tissue.
- The next section of the thesis has been discussed in *Chapter 5*that deals with the mathematical biomechanics for fractional order derivatives of the conventional viscoelastic models and the nature of the corneal tissue in accordance with the aforementioned models.
- *Chapter 6* discusses the experimental rig for the development and synthesis of Human Collagenous tissue and mechanical and morphological characterization and discussion of the so formed collagen composite. This chapter also discuss about the extraction of natural collagen from biological tissue.

The complete research has been summarized under this heading which gives a brief but complete understanding and content of the present thesis.

References:

Allen P.M., O'Leary D.J., 2006. Accommodation functions: Co-dependency andrelationship to refractive error. Vision Res. 46, 491-505.

Atchison D.A., Jones C.E., Schmid K.L., Pritchard N., Pope J.M., Strugnell W.E., Riley R.A., 2004. Eye shape in emmetropia and myopia. Invest. Ophthalmol.Vis. Sci. 45, 3380-3386.

Ethier C.R., Johnson M., Ruberti J., 2004.Ocular biomechanics and biotransport.Annu.Rev.Biomed. Eng. 6, 249-273.

Genest R., 2010. Effect of Intraocular Pressure on Chick Eye Geometry, FiniteElement Modeling, and Myopia

Girard M.J.A., Downs J.C., Burgoyne C.F., Suh J.K.F., 2008. Experimental surfacestrain mapping of porcine peripapillary sclera due to elevations of intraocular pressure. J. Biomech. Eng. 130, 041017-1-041017-6.

Le Grand Y., ElHage S.G., 1980. Description of the Human Eye, in: Physiologicaloptics, first ed. Springer, Berlin, 25-42.

Makris N., Constantinou M.C., 1991. Fractional-Derivative Maxwell Model ForViscous Dampers. Journal of Structural Engineering 117(9), 2708-2724

McBrien N.A., Gentle A., 2003. Role of the sclera in the development and pathologicalcomplications of myopia.Prog.Retin. Eye Res. 22, 307-338.

Ostrander L.E., Lee B.Y., Testing Viscoelastic Properties of Biological SoftTissue, 0-7803-0785-2

Peña E. ,Peña J.A., Doblare´M., 2008. On modeling nonlinear viscoelastic effects inligaments, J. of Biomech. 41, 2659– 2666

Pinsky P.M., van der Heide D., Chernyak D., 2005.Computational modeling ofmechanical anisotropy in the cornea and sclera. J. Cataract Refract. Surg. 31, 136-145.

Tamm E., Lütjen-Drecoll E., Jungkunz W., Rohen J.W., 1991.Posterior attachment ofciliary muscle in young, accommodating old, presbyopic monkeys. Invest. Ophthalmol. Vis. Sci. 32, 1678-1692.

Thale A., Tillmann B., 1993. The collagen architecture of the sclera- SEM andimmunohistochemical studies. Ann. Anat. 175, 215-220.

Thale A., Tillmann B., Rochels R., 1996. Scanning electron-microscopic studies of thecollagen architecture of the human sclera - normal and pathological findings.Ophthalmologica. 210, 137-141.

Young F.A., 1981. Primate myopia. Am. J. Optom. Physiol. Opt. 58, 560-566.

CHAPTER 2
LITERATURE REVIEW

2.1 LITERATURE SURVEY

Eye is one of the most important sensing organs in human body and very much prone to various external injuries. Therefore, the study of the human eye and its various aspects have always been a vital topic of importance in biology related science and engineering. One of the major engineering challenges with the eye is its proper modeling both mathematical and mechanical and its further use in various constructive ways be it artificial lens designing or even study the impact of changes due to its mechanical properties. A slight change in the properties of eye predicts ocular trauma or several other ophthalmologic disabilities or abnormalities. Prediction of any disease specific changes can also be made on how the properties vary. Many a number of works including mathematical modeling, simulation based analysis or a direct in-vitro experimental pathogenesis has been done in this respect to trace out the mechanical properties and hence a variation in them in the past few years. In this work, we have mainly stressed on the similarity and differences of a human corneal structure with a conventional viscoelastic or partly elastic mechanical model and a newly generated fractional calculus model. In that regard a lot of studies have been observed showing and thus proving the Viscoelasticity of a number of soft tissues including human eye and also on how and why the fractional calculus have been preferred in this case. The theoretical computed values and nature can be drawn comparison with few experimental works performed lately or recently.

The whole state of art is broadly classified into several areas of interest: as few authors have experimented and worked on human cornea experimentally or mathematically, whereas other works on viscoelastic soft tissues proves the behavior of human cornea, also a section of Fractional Maxwell Model also can be shown which describes how it can be used in modeling viscoelastic properties.

2.1.1 Studies on Cornea & Its Properties

Cornea of several other animals except humans has been an area of interest too in many literatures. *Boyce et al., 2006* did a study on the viscoelastic response of bovine corneas characterized using in vitro load-controlled uniaxial tension. The cornea's structural performance is dominated by the stroma which constitutes 90% of the cornea thickness. Another literature comparison was made with regard to mechanical anisotropy. *Kampmeier et al., 2000* found that porcine corneas were stiffer along the Inferior-Superior (IS) axis than the Nasal-Temporal (NT) axis, which is consistent with the present observations on bovine corneas where the effect was much less pronounced. As expected, the cornea exhibited significant Viscoelasticity as evidenced by: (a) asymmetry in the ramp loading–unloading response (b) corresponding hysteresis in the stress–strain

response (c) exponential recovery at low stresses after ramp cycles, and (d) time-dependent creep behavior at a variety of hold stresses.

Another work on the Viscoelastic material properties of the peripapillary sclera in normal and early glaucoma monkey eyes by *Downs et al., 2004* had the purpose to test the hypothesis that changes in the viscoelastic material properties of peripapillary sclera are present within monkey eyes at the onset of early experimental glaucoma. It showed that peripapillary sclera from the early-glaucoma eyes exhibited an equilibrium modulus (7.46 $\pm$ 1.58 MPa) that was significantly greater than that measured in normal eyes (4.94 $\pm$ 1.22 MPa; mean $\pm$ 95% confidence interval, $P<0.01$, ANOVA). As a conclusion the long-term viscoelastic material properties of monkey peripapillary sclera are altered by exposure to moderate, short-term, chronic IOP elevations. In an investigation of the role of scleral creep in the axial elongation of chick and tree shrew eyes with induced myopia also demonstrated that In both chick and tree shrew, posterior and equatorial scleral samples from myopic eyes had significantly (P, 0.05) greater creep extensions than equivalent samples from control and normal eyes (n 5 10, each group) (*Phillips et al., 2000*).

Hence resultantly, it can be well defined and concluded that animal cornea or scleral strips do exhibit time dependent anisotropic viscoelastic behavior under various abnormal or appropriate conditions.

Next discussed section is dealing with the biomechanical properties of human and bovine corneas that present the similarity and dissimilarities among them both mechanically and property wise. *Ahmed et al., 2008* and *Yanjun et al., 2000* both throws light on the comparison between the corneas of both. Ahmed extracted Thirty seven human donor corneas and thirty four ex-vivo porcine corneas and tested them under inflation conditions to determine their short-term stress-strain behavior and long-term creep behavior up to 2.8 h (10,000 s). Human and porcine corneas were observed to have almost the same form of behavior under short and long-term loading. They both exhibited non-linear stress-strain behavior and reacted to sustained loading in a similar fashion. However, human corneas were significantly stiffer than porcine corneas. They also crept less under long-term loading and could sustain their stress state for longer compared to porcine corneas.

*Yanjum*on the other hand directly accepted that as it is difficult to obtain human corneas,pig corneas are often substituted as models for cornea research. Instron apparatus was accounted in this case to determine the tensile strength, stress–strain relationship, and stress-relaxation properties of both human and bovine corneas. The work stated that the tensile strength and stress–strain relation were very similar but significant differences

between the two tissues were observed in the stress-relaxation relationship. *Yanjum* also stressed on the point that the porcine cornea relaxed much more than human cornea.

In the terminology of material science, the cornea is a complex anisotropic composite with non-linear elastic and viscoelastic properties. It is a composite because its properties are determined by the interaction of disparate materials like collagen and a polyanionic ground substance and anisotropic because its properties are not directionally uniform. The cornea is also highly heterogeneous in the central to peripheral, anterior to posterior and rotational dimensions (*William & Steven, 2006*).

Viscoelastic property in cornea arises from the time-dependent nature of biomechanical responses in biological soft tissues. And henceforth, these properties are represented by the phenomena of hysteresis, stress relaxation and creep. Results on the distribution of strain in the human cornea indicate that the strain distribution is unexpectedly non uniform with statistically significant variations between regions and with a minima occurring approximately half-way between the apex and the limbus (*Thomas et al.,1997*). Thus the anisotropic time dependent nonlinear nature of human cornea has beenstudied and analysed greatly which predicts the viscoelastic stress-strain response of the same (*Nguyen et al., 2008; Khaow et al., 2014; Long & Brian, 2007,2006*; *Alberto,2013).*

Christian et al., 2009 presented three consecutive papers in the two following year on the Viscoelastic response of passive eye muscles in primates. The 1st paper conducted an in-vivo study of the mechanics of passive eye muscles in deeply anesthetized and paralyzed monkeys and static forces and consequently step responses were applied to derive the mechanical properties which seemed similar to various biological tissues. In the second and the third paper the same specimen were studied under natural elongation forces and concluded of the earlier discussed behavior. Works on the determination of the elastic moduli of human cornea clearly served our purpose in this case as it illustrated the stress-strain time dependent nature of cornea and hence demonstrated the viscoelastic nature of the tissue which is the most important surveying topic in this work (*Friberg and Lace,1988;Ahmed and David, 2007;Hsichun et al., 1996).*

Two more important factors to be kept in mind while modeling human cornea are the elasticity and viscosity of the muscles which combines to produce the time dependent viscoelastic nature actually (*Nguyen et al., 2008)*. Change in either of them deflects the normal behavior thus giving rise to the unwanted error of hysteresis; accordingly change in the mechanical properties of elasticity and viscosity produces change in hysteresis. Low hysteresis can be associated with either high elasticity or low elasticity, depending on the viscosity (*Dianne at al., 2007*).

2.1.2 Studies on Viscoelasticity

That viscoelastic property prevails in biological soft tissues have been proved and explained by many a works. *Lee & Bok* in their book mentioned of an experimental work to assess instrumentation and methods for measuring the pressure and deformation of soft body tissues, mainly points to the rate dependent viscoelastic anisotropic properties of biological soft tissues and hence design and testing of a viscoelastic testing instrument consisting of a centre indenter. This determination and study of the Viscoelasticity of the soft tissues helped in evaluation of skin and other soft tissue damage from mechanical causes including edema, ulceration & necrosis.

Zhang, 2005 also proposed such a piece of work where he postulated a new method for evaluating the viscoelastic properties of biological tissues such as tendons and ligaments. This method obtains the complex modulus of these tissues to characterize their viscoelastic properties. With this method, the stresses and strains measured in time are first transformed (using FFT), and the complex modulus is then obtained. The complex modulus contains sufficient information about the viscoelastic characteristics of the biological tissues. With this method, the mechanical properties of biological tissues can be measured without making prior assumptions regarding their structures, and the measurements can be made in real time. In another study based on measurement of the elastic properties of blood vessels the proposed method was based on the deformation of the Polyvinyl alcohol (PVA) samples representing artificial networks of arteries as well as on the applied stress inducing the deformation and it was concluded that the modulus of elasticity of blood vessels being three times larger than the modulus of elasticity of PVA, it is thus possible to derive mechanical properties of blood vessels (*Ilic et al.,2005*).

As a result Viscoelasticity was noticed even as a non-uniform change in elasticity in collapsible blood vessels and that did have some effect or the other on the pathology (*Tracy & Gary, 2000*). A change in blood Viscoelasticity can also be observed during a cardiac surgery (*Thurston et al., 1989*). Other examples of viscoelastic soft tissues can be those of muscles (*Levin & Wyman, 1927*), lung tissues (*Béla et al., 1994*), brainstem (*Ning et al., 2006*), aortic valves (*Grashow et al., 2006*), pericardium (*Sacks, 2000*) and articular cartilage (*Hayes and Mockros, 1971*).

2.1.3 Studies on Fractional Model

The growing utility and field of fractional mathematical modeling specifically Fractional Maxwell Modeling (FMM) for viscoelastic behavior exhibiting tissues and objects have significantly increased in the past few years. Fractional derivative model has been proposed for modeling viscous dampers by a number of literatures.

Among them as for example, *Markis et al., in 1991* presented a paper where A fractional-derivative Maxwell model is proposed for viscous dampers, which are used for vibration isolation of piping systems, forging hammers, and other industrial equipment, as well as for vibration and seismic isolation of building structures. The proposed model is validated by dynamic testing and very good agreement between predicted and experimental results is obtained and results obtained are useful to the design of vibration-isolation systems (*Lewandowski & Chorazyczewski, 2010*).

Similar works by *Lyan et al., 2012* also proves how the model can be validated to model non-linear viscoelastic dampers used in seismic isolation. Cumulatively the fractional calculus modeling does not only help in precisely describing time dependent nature of any objects but also provides a few advantages over generalized models including incorporating lesser number of parameters, easy access and solution by various mathematical formulations such as Laplace Transform, Fourier Transform etc. (*Vasily,2008; Lili et al., 2013; Magdy et al., 2013; Jiaguo & Mingyu)*

Studies on the stress relaxation Modulus and mechanical properties of PMMA and PTFE (Plymethylmethacrylate and Polytetrafluorethylene) has been carried out, pointing out that there exists not only one time of relaxation as the classic Maxwell model predicts but two distributions of relaxation time which can be approached by using a fractional Maxwell's model in which the stress appears as two non-integer order derivatives of the strain.

The two polymers studied in the article by *Hernández-Jiménez et al., 2001*, present a clearly viscoelastic behavior where the deformation of the sample is not instantaneous when applying a load and as a consequence, after the initial deformation process, if we keep the total strain constant, the plastic deformation of the sample increases and the value of their elastic deformation decreases and therefore the stress also decreases — the phenomenon of stress relaxation.

Kai & Ke in 2011 made a further study on the works of *Jiménez* and hence postulated more appropriate fractional parameters that fit experimental data appropriately.

Articles based on viscoelastic fluid modeling showed the use of fractional model mostly, be it a periodic unidirectional flow (*Hayat et al., 2004*) or a non-periodic viscoelastic fluid flow. The fractional derivative Maxwell model is an advanced model for analyzing the oscillating flow. It is obtained by replacing the time derivative of the integer order of the Maxwell model with the Riemanne Liouville fractional calculus operators. This generalization allows one to define precisely non-integer order derivatives for different

materials. Moreover, experimental research has illustrated that a better agreement of the experimental data could be achieved with the fractional Maxwell model than the ordinary Maxwell model (*Makris, 1991*; *Dao and Ti, 1998*).

With the fractional Maxwell method, *Tan et al., 2003* studied four unsteady flows of a viscoelastic fluid between two infinite parallel plates. *Hayat et al., 2004* also took the fractional Maxwell model into account and discussed three types of unidirectional flows which were induced by general periodic oscillations of a plate.

Yin and Zhu, 2006 solved the oscillating flow of a viscoelastic fluid in a pipe with the fractional derivative Maxwell model. *Qi and Xu, 2007* calculated the unsteady flow of the viscoelastic fluid in a channel. *Jia and Hua, 2008* investigated the oscillating flow in a pipe with a simpler and clearer technique solving the fractional derivative Maxwell method, instead of the Laplace transform and inverse Laplace transform used by *Yin and Zhu*.

Fractional derivative Maxwell Model also helped in the study oscillating flow in rolling motion (*Yan et al., 2011*) and also in a pipe (*Youbing & Zhu, 2006*).

The continuous wavelike muscle contraction and relaxation of the physiological vessels such as oesophagus, stomach, intestines, sometimes in the ureters, and blood vessels (arteries, veins, capillaries etc.) and other hollow tubes i.e., the peristaltic flow of viscoelastic fluid has been considered with the Fractional model as well. *Tripathi et al.,2010* discussed the effect of relaxation time, fractional parameters and amplitude on the pressure difference and friction force across one wavelength for such a peristaltic viscoelastic fluid flow. Another paper presented by *Tripathi in 2011* presented the effect of endoscope on peristaltic transport of fractional Maxwell fluids through the gap between two concentric uniform tubes under the assumptions of large wavelength and low Reynolds number.

Unsteady flows due to a constantly accelerating plate (*Corina et al., 2009*), in any channel (*Haitao&Mingyu, 2007*), in a pipe (*Yang & Zhu, 20190)*, between two side walls perpendicular to a plate (*Vieru et al., 2008*), between two parallel plates (*Tan et al.,2003*), between two cylinders (*Muhammad et al., 2012*) have also been proposed and modeled by Fractional approach and hence the Fractional Maxwell Model has been incorporated.

2.1.4 Studies on development of Corneal composite

Recently there is an emergence in the field of synthesizing corneal substitute by various researchers. Cadaver eyes have a major problem of physiological auto rejection which

may lead to various medical problems which may lead to serious fatality to the patients. So, the idea of corneal scaffold has come to light to provide better biocompatibility and minimal rejection issues.

In 2004, *Liu* with the research team developed a simple crosslinked collagen composite. In this research, 10%Porcine type I collagen with pH around 5, was mixed with 1-ethyl-3-(3-dimethylaminopropyl) carbodiimide (EDC) and *N*-hydroxysuccinimide (NHS). The homogenous solution was cured to corneal dimensions and implanted into rabbits and minipigs by lamellar keratoplasty. A follow up of the implant has been done up to 6 months after surgery. The cross linked collagen showed better clarity than the original tissue and post-surgical physiological issues were minimal. Whereas the cross linked collagen enhanced growth of cells on the scaffolds and there was no loss in the thickness of the implanted scaffold and had better host and graft interaction. *Liu W.* in 2008 developed a transparent hydrogels as corneal substitutes from concentrated recombinant human type I and type III collagen solutions crosslinked with 1-ethyl-3-(3-dimethyl aminopropyl) carbodiimide (EDC) and N-hydroxysuccinimide (NHS). It has been observed that in this case also the product so formed has superior clarity when compared with original tissue. Both type I and type III hydrogels showed cell growth and proliferation which is a desirable characteristic of a scaffold which also showed commendable strength and elasticity for surgical issues. These synthetic cornea had been implanted in minipigs which were kept under follow up for 12 months and it had been noticed that the optical clarity remain unchanged with regeneration of new cells, nerves and tear films.

Hybrids were synthesized from collagen and silica derivatives and cured to corneal dimensions by *DiVito* in 2012. The structural characteristics had been studied by SEM and mechanical strength was measured using suture pullout tests. The refractive index and transmittance were measured by using an Abbe refractometer and a spectrophotometer. The material formed was further implanted in rabbits to analyze the cell growth rate and epithelialization in culture medium. In the full study it had been observed that this artificial cornea can mimic the original corneal tissue in a superior way. Further in 2015, *Hayes et al.* crosslinked recombinant human collagen type III (RHCIII) with and without 2-methacryloyloxyethyl phosphorylcholine (MPC) and characterized for their nanostructural behavior in TEM, XRD, Spectroscopy and refractometry. TEM showed that loose bundles of fine collagen filaments were present within both RHCIII and RHCIII-MPC implants, which X-ray scattering showed to lack D-banding. Due to high water content (90%), very fine collagen filaments (2–9 nm) and lack of cells, the collagen hydrogels transmitted almost all light incident on it in the visible range. They also transmitted a large proportion of UV light compared to the corneal tissue.

References:

Boyce B.L., Jones R.E., Nguyen T.D., Grazier J.M., 2007. Stress-controlled viscoelastictensile response of bovine cornea. J. of Biomech 40,2367–2376.

Cao L., Li Y., Tian G., Liu B., Chen Y.Q., 2013. Time domainanalysis of the fractional order weighted distributed parameter Maxwell model. Computers and Mathematics with Applications 66, 813–823.

Dao Y.S., Ti Q.J., 1998. Study on the constitutive equation with fractional derivative forthe viscoelastic fluids-modified Jeffreys model and its application. Rheol.Acta 37, 512-517.

DiVito M.D., Rudisill S.G., Stein A., Patel S.V., McLaren J.W., Hubel A., 2012. Silica Hybrid for Corneal Replacement: Optical, Biomechanical, and Ex Vivo Biocompatibility Studies. Investigative Ophthalmology and Visual Science 53(13), 8192-8199.

Downs J.C., Francis Suh J.K., Thomas K.A., Bellezza A.J, Hart R.T., Burgoyne C.F., 2005.Viscoelastic Material Properties of the Peripapillary Sclera in Normal and Early-Glaucoma Monkey Eyes. Invest Ophthalmol Vis Sci.46, 540–546

Dupps W.L. Jr., Wilson S.E., 2006. Biomechanics and wound healing in thecornea.Exp. Eye Res. 83,709-720.

Elsheikh A., Wang D., Pye D., 2007.Determination of the Modulus ofElasticity of the Human Cornea. J Refract Surg.;23,808-818.

Elsheikh A., Alhasso D., Rama P., 2008. Biomechanical properties of humanand porcine corneas. Experimental Eye Research 86 783e790

Ezzat M.A., El-Karamany A.S., El-Bary A.A., Fayik M.A., 2013.Fractional calculus in one-dimensional isotropic thermo-viscoelasticity. C. R. Mecanique 341, 553–566.

Fetecau C., Athar M., Fetecau C., 2009. Unsteady flow of a generalized Maxwell fluid with fractional derivative due to a constantly accelerating plate. Computers and Mathematics with Applications 57, 596-603.

Friberg T.R., Lace J.W., 1988. A comparison of the elastic properties of human choroid andsclera. Exp. Eye Res. 47, 429-436.

Glass D.H., Roberts C.J., Litsky A.S., Weber P.A., 2008. A Viscoelastic Biomechanical Model of the Cornea Describing the Effect of Viscosity and Elasticity on Hysteresis. Invest Ophthalmol Vis Sci. 4, 3919–3926.

Grashow J.S., Yoganathan A.P., Sacks M., 2006. Biaxial stress-stretch behavior of themitral valve anterior leaflet at physiologic strain rates. Annals of Biomedical Engineering 34, 315–325.

Haitao Q., Mingyu X., 2007. Unsteady flow of viscoelastic fluid with fractional Maxwell model in a channel. Mechanics Research Communications 34, 210–212

Hayat T., Nadeem S., Asghar S., 2004. Periodic unidirectional flows of a viscoelastic fluidwith the fractional Maxwell model. Appl. Math. and Comp. 151, 153–161

Hayes S. et al., 2015.The structural and optical properties of type III human collagen biosynthetic corneal substitutes. Acta Biomaterialia 25, 121-130.

Hayes W.C., Mockros L.F., 1971. Viscoelastic constitutive relations for human articular cartilage. J. of Appl. Physiol. 18, 562–568.

Herna´ndez-Jime´nez A., Herna´ndez-Santiago J., Macias-Garcı´a A., Sa´nchez-Gonza´lez J., 2002.Relaxation modulus in PMMA and PTFE fitting by fractional Maxwell model. Polym. Test. 21, 325–331

Hu K.X., Zhu K.Q., 2011. A note on fractional Maxwell model for PMMA and PTFE. Polym. Testing 30, 797–799.

Ilic D., Moix T., Lambercy O., Sache L., Bleuler H., Ohta M., Augsburger L., 2005.Measurement of Elastic Properties of Blood Vessels. Proceedings of the IEEE Engineering in Medicine and Biology 27th Annual Conference

Jamil M., Fetecau C., Fetecau C., 2012. Unsteady flow ofviscoelastic fluid between two cylinders using fractional Maxwell model. Acta Mech. Sin. 28(2), 274–280

Jia J.H., Hua H.X., 2008. Study of oscillating flow of viscoelastic fluid with thefractional Maxwell method. ASME Trans. J. Fluids Eng. 130, 1-4.

Kampmeier J., Radt B., Birngruber R., Brinkmann R., 2000. Thermal and biomechanical parameters of porcine cornea. Cornea 19 (3), 355–363.

Levin A., Wyman J., 1927. The Viscous Elastic Properties of Muscle. Royal Society Publishingol. 101[709], 218-243

Lewandowski R., Chorázyczewski B., 2010. Identification of the parameters of the Kelvin–Voigt and the Maxwell fractional models, used to modeling of viscoelastic dampers. Computers and Structures 88, 1–17

Li L., Tighe B., 2006. The anisotropic material constitutive models for the human cornea. Journal of Structural Biology 153, 223–230

Li L., Tighe B., 2007. Nonlinear analysis of static axisymmetric deformation of the human cornea. Comp. Mater. Sc. 38, 618–624

Liu J., Xu M., Fractional Constitutive Equations Of Viscoelastic Materials Involving Three Different Parameters And Their Analytical Solutions. _Support By The National Natural Science Foundation Of China (10272067) And The Doctoral Program Foundation Of The Education Ministry Of China (20030422046).

Liu Y. et al., 2006. A Simple, Cross-linked Collagen Tissue Substitute for Corneal Implantation.Investigative Ophthalmology and Visual Science 47(5), 1869-1875.

Liu W.et al., 2008. Recombinant human collagen for tissue engineered corneal substitutes. Biomaterials 29, 1147-1158.

Lu L.Y., Lin G.L., Shih M.H., 2012. An experimental study on ageneralized Maxwell model for nonlinear viscoelastic dampers used in seismic isolation. Eng. Struc. 34,111–123

Makris N., 1991. Theoretical and experimental investigation of viscous dampers inapplications of seismic and vibration isolation. Ph.D. Thesis, State University of New York at Buffalo, Buffalo, N.Y.

Makris N., Constantinou M.C., 1991. Fractional-Derivative Maxwell Model forViscous Dampers.Journal of Structural Engineering, ISSN 0733-9445/91/0009-2708.

Miatello A., 2013. The Human Cornea: A New Comprehensive, BiomechanicalStructural Model. Principia Scientific International.

Ning X., Zhu Q., Lanir Y., Margulies S.S., 2006. A transversely isotropic viscoelasticconstitutive equation for brainstem undergoing finite deformation. ASME J. Biomech. Eng. 128, 925–933.

Nguyen T.D., Jones R.E., Boyce B.L., 2008. A Nonlinear Anisotropic Viscoelastic Model for the TensileBehavior of the Corneal Stroma. Journal of Biomechanical Engineering, DOI: 10.1115/1.2947399

Ostrander L.E., Lee B.Y., Testing Viscoelastic Properties of Biological SoftTissue.

Peña E., Peña J.A., Doblaré M., 2008. On modeling nonlinear viscoelastic effects inligaments. Journal of Biomechanics 41, 2659– 2666.

Phillips J.R., Khalaj M., McBrien N.A.,2000. Induced Myopia Associatedwith Increased Scleral Creep in Chick and Tree Shrew Eyes. Invest. Ophthalmol. Vis. Sci. 41,2028–2034

Qi H.T., Xu M.Y., 2007. Unsteady flow of viscoelastic fluid with fractional Maxwellmodel in a channel. Mech. Res. Commun. 34, 210-212.

Quaia C., Ying H.S., Nichols A.M., Optican L.M., 2009. TheViscoelastic Properties of Passive Eye Muscle in Primates. I: Static Forces and Step Responses. PLoS ONE 4(4), e4850. doi:10.1371/journal.pone.0004850

Quaia C., Ying H.S., Nichols A.M., Optican L.M., 2009. The ViscoelasticProperties of Passive Eye Muscle in Primates. II: Testing the Quasi-Linear Theory. PLoS ONE 4(8), e6480. doi:10.1371/journal.pone.0006480

Quaia C., Ying H.S., Nichols A.M., Optican L.M., 2010. The ViscoelasticProperties of Passive Eye Muscle in Primates. III: Force Elicited by Natural Elongations. PLoS ONE 5(3), e9595. doi:10.1371/journal.pone.0009595

Sacks M., 2000.Biaxial mechanical evaluation of planar biological materials.J.ofElas 61, 199–246.

Shin T.J., Vito R.P., Johnson L.W., McCarey B.E., 1997.The Distribution Of Strain In The Human Cornea. J. Biomech. 30(5), 497-503.

Suki B., Barabasi A.L., Lutchen K.R., 1994.Lung Tissue Viscoelasticity: a MathematicalFramework and its Molecular Basis .The American Physiological Society 0161-7565

Thurston G.B., Henderson N., Undar A., 1998. Blood Viscoelasticity Changes In CardiacSurgery. Southern Biomedical Engineering Conference

Tonsomboon K., Koh C.T., Oyen M.L., 2014. Time-dependentfracture toughness of cornea.J. of the Mech. Behav.of Biomed. Mater. 34, 116 – 123.

Tracy B.S., Gary D., 2000. Effect of Visco-elasticity on Chaos inCollapsible Blood Vessels.

Tripathy D., Pandey S.K., Das S., 2010. Peristaltic flow of viscoelastic fluid withfractional Maxwell model through a channel. Applied Mathematics and Computation 215,3645–3654

Tripathi D., 2011. Peristaltic transport of fractional Maxwell fluids in uniformtubes: Applications in endoscopy. Computers and Mathematics with Applications 62, 1116–1126

Wang H., Prendiville P.L., McDonnell P.J., Chang W.V., 1996.An Ultrasonic Technique For The Measurement Of The Elastic Moduli Of Human Cornea, J. Biomech 29[12], 1633-1636

Vasily E. T., 2008. Fractional vector calculus and fractional Maxwell's equations. Annals of Physics 323,2756–2778

Vieru D., Fetecau C., Fetecau C., 2008. Flow of a viscoelastic fluid with the fractionalMaxwell model between two side walls perpendicular to a plate. Appl.Math. Comp. 200,459–464

Wenchanga T., Wenxiao P., Mingyu X., 2003. A note on unsteady #ows of aviscoelastic fluid with the fractional Maxwell model between two parallel plates. Int. J. of Non-Linear Mech 38, 645 – 650

Yan B.H., Yu L., Yang Y.H., 2011. Study of oscillating flow in rolling motion with thefractional derivative Maxwell model.Progress in Nuclear Energy 53,132-138.

Yang D., Zhu K.Q., 2010. Start-up flow of a viscoelastic fluid in a pipe with afractional Maxwell's model. Computers and Mathematics with Applications 60, 2231–2238.

Yin Y.B., Zhu K.Q., 2006. Oscillating flow of a viscoelastic fluid in a pipe with thefractional derivative Maxwell model. Appl. Math. Comp. 173, 231-242.

Yin Y., Zhu K.Q., 2006.Oscillating flow of a viscoelastic fluid in a pipe withthe fractional Maxwell model. Appl. Math. and Comp. 173, 231–242.

Zeng Y., Yang J., Huang K., Lee Z., Lee X., 2001. A comparison ofbiomechanical properties between human and porcine cornea. J. of Biomech. 34, 533–537.

Zhang L., 2005. Evaluating the viscoelastic properties of biological tissues in a new way. J. Musculoskelet. Neuronal. Interact. 5(1), 85-90.

CHAPTER 3
NUMERICAL FOUNDATION

3.1 ELASTICITY

In physical science, elasticity is the inbuilt property of solid materials (called elastic materials) to return to their initial shape after being deformed. Solid objects will deform when forces are applied on them. If the material is elastic, the object will return to its original shape and size when the forces are removed. The loading and unloading stress-strain curves of a linear elastic material are identical implying no hysteresis. Additionally, the elastic nature of the deformation implies that there is no residual strain in the material upon complete unloading and that the stress-strain curve is not affected by the loading rate.

In engineering, the amount of elasticity of a material is determined by two types of material parameter. The first type of material parameter is called modulus which determines the amount of restoring force per unit area (i.e. stress) needed to produce a given amount of deformation. A higher modulus typically indicates that the material is harder to deform. The second type of parameter measures the elastic limit. The limit can be a stress beyond which the material no longer behaves elastic and permanent deformation of the material will take place. If the stress is released, the material will elastically return to a permanent deformed shape instead of the original shape.

3.1.1 Linear Elasticity

Linear elasticity accounts for the linear relationship between the stress and strain components of a solid material during small deformation (e.g. spring). Most elastic materials exhibit linear elasticity and can mathematically be described by a linear relation between the stress and strain (i.e. time independent equation). This relationship is given by Hooke's law. Which states that, within the elastic limit, of a deforming body, stress is directly proportional to strain, i.e., stress/strain = constant. This „constant" is the modulus of elasticity.
Mathematically, it can be expressed as:

$$\frac{\sigma}{\varepsilon} = E$$

$$Or, \sigma = E\varepsilon$$

3.1.2 Nonlinear Elasticity

Many a cases arises when the material remains elastic everywhere, but the stress strain relationship is nonlinear. As for example, a beam under simultaneous lateral and end loads.

3.2 HISTORY OF VISCOELASTICITY

In the late nineteenth century, physicists such as Maxwell, Boltzmann and Kelvin researched and experimented with creep and recovery of glasses, metals and rubbers (*McCrum et al., 2003*). In the late twentieth century, Viscoelasticity was further examined when synthetic polymers were engineered and used in a variety of applications. Depending on the relationship between rate of change of strain and stress applied inside a material, viscosity can be categorized as having either a linear, non-linear or even a plastic response. In case of a linear response the material is categorized as a Newtonian material, where the stress is linearly proportional to the strain rate. On the other hand, a Non-Newtonian material is categorized as those having a non-linear relationship between strain rate and stress applied. An interesting case appears when the viscosity decreases as the strain rate remains constant. Material exhibiting this type of behavioral properties is known as thixotropic (*Meyers and Chawla, 2009*). Plastic deformation occurs when the stress is independent of the strain rate. Practically none of the materials we see around us are purely Hookean. Materials do deviate from properties of being a pure elastic or viscous material, and possesses aspects of both. Thus the concept of Viscoelasticity has emerged as a practical case. Viscoelastic materials are those, for which the stress strain relationship is time dependent.

3.2.1 Viscoelasticity

Viscoelasticity is that property of materials which when undergone deformations exhibits both elastic and viscous characteristics. As for example, honey being a viscous material resists shear flow and strain linearly with time when deformation is applied. On the other hand elastic materials return to its original shape and size once strain is removed. Viscoelastic materials are such that exhibit properties of both these materials and have elements of both of these properties and as such show time-dependent deformation. Viscosity is the result of diffusion of atoms or molecules inside an amorphous material, whereas elasticity is usually the result of bond stretching along crystallographic planes in an ordered solid (*Meyers and Chawla, 2009*).

Almost all materials show some viscoelastic response. In common metals such as steel or aluminum, as well as in quartz, at room temperature and at small strain, the response does not deviate much from linear elasticity. Some of the human tissues also display significant viscoelastic characteristics in some respect or the other. Some examples of viscoelastic materials include amorphous polymers, semi-crystalline polymers, biopolymers, metals at very high temperatures and bitumen materials. When the strain is applied quickly and outside the elastic limit, then cracking occurs. Ligaments and tendons

are viscoelastic, so the extent of the potential damage to them depends both on the velocity of the change of their length as well as on the force applied. Here we will discuss and deal with Viscoelasticity of eye muscles or the corneal Viscoelasticity. Figure 3.1illustrates of the Linear Elastic Behavior with Full Energy Recovery, & Non-Linear rate-dependent Viscoelastic Behavior.

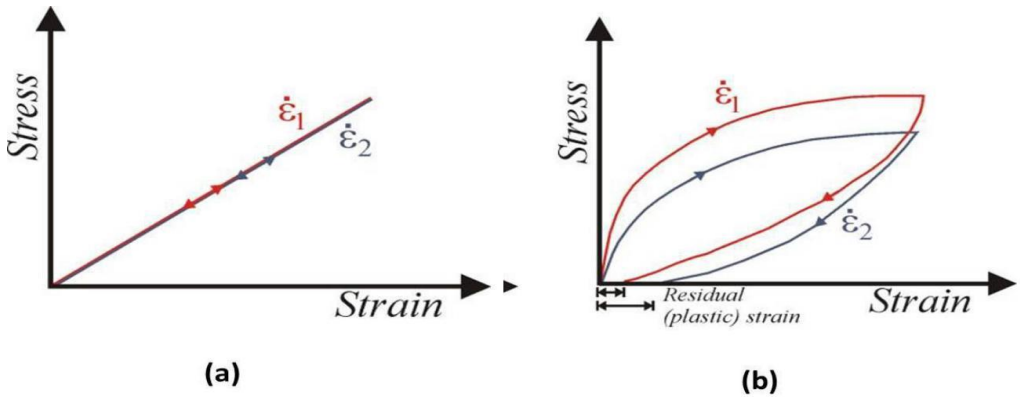

Fig.3.1: *(a) Illustration of the Linear Elastic Behavior with Full Energy Recovery, (b) Non-Linear rate-dependent Viscoelastic Behavior*

3.2.2 Few Viscoelastic Soft Tissues

Mechanical properties of few soft tissues of human body need to be discussed about in this respect and also state few viscoelastic property showing soft tissues. The stretch and time-dependent behavior of biological tissues has been widely investigated by means of number of experimental tests. For example, *Hingorani et al., 2004*, *Bonifasi-Lista et al. ,2005* and *Peña et al., 2008* found that ligaments exhibit a clear nonlinear viscoelasticresponse. They also found that the creep rate depends on the applied stress and that the relaxation rate depends on the applied stress. *Silver et al., 2003* found a rate dependent mechanical behavior of the porcine aorta, vena cava and carotid artery. Other authors found time-dependent material behavior of blood vessels (*Humphrey, 1995*), cornea (*Pinsky and Datye, 1991*), brainstem (*Ning et al., 2006*), aortic valves (*Grashow et al., 2006*), pericardium (*Sacks, 2000*) and articular cartilage (*Hayes and Mockros, 1971*). Hence it can be concluded from their works that soft tissue behavior of human body actually describes a time dependent response and hence to some extent or the other is viscoelastic. A review article on Mechanical Properties of Human Body Soft Tissues by *Mukherjee et al.* focuses on the soft tissues located mainly in the head, neck and spine.The tissues studied include brain tissues, scalp tissues, ligaments in cervical spine, neck muscles and spinal soft tissues. They also concluded that, non-linear Viscoelasticity,

anisotropy & also rate dependency needed to be kept in mind and hence well characterised while modeling the mechanical nature of the tissues.
An experimental work to assess instrumentation and methods for measuring the pressure and deformation of soft body tissues, mainly points to the rate dependent viscoelastic anisotropic properties of biological soft tissues and hence design and testing of a viscoelastic testing instrument consisting of a centre indenter. This determination and study of the Viscoelasticity of the soft tissues helped in evaluation of skin and other soft tissue damage from mechanical causes including edema, ulceration & necrosis.
Besides these few works, a number of works can be cited in this respect depicting the viscoelastic nature of bones (*Tara et al., 2011*), human fasciae under extension (*Chaudhry et al., 2007*) and even on the blood vessels.

3.2.3 Properties of Viscoelastic Materials

As mentioned earlier, viscoelastic materials exhibit both viscous and elastic characteristics when undergoing deformation (the viscous element being a dashpot and the elastic element being the spring). As the stress-strain relationship for a viscoelastic material is time dependent, there are three important and distinct properties of these types of materials: stress relaxation, creep and hysteresis.

3.2.3.1 Stress Relaxation

Let a constant strain ε_0 is given as an input to a material starting from time t_0. As the stress strain relation is time-dependent, the resulting time-dependent stress $\sigma(t)$ gradually decreases until a plateau is reached at some other point of time. The stress function G(t) resulting from unit step strain ($\varepsilon_0=1$) is referred to as the Relaxation Modulus (Fig.3.2).
This property is mostly seen in viscoelastic solids, which gradually relax and reach an equilibrium stress greater than zero, i.e,

$$\mathrm{Lim}_{t\to\alpha}\, G\,(t) = G\alpha > 0$$

On the other hand for viscoelastic fluids, the stress vanishes to zero, i.e,

$$\mathrm{Lim}_{t\to\alpha}\, G\,(t) = 0$$

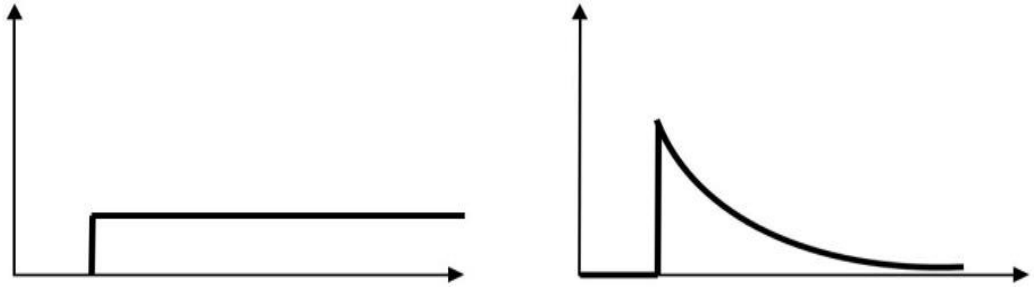

Fig.3.2: *(a) Unit Strain$\varepsilon_0$applied at an instant of time $t=t_0$, (b) Decreasing Stress nature Resulting from unit strain which is time dependent σ (t) and initiates too from $t=t_0$ thus showing Relaxation*

3.2.3.2 Creep Compliance

For a constant stress σ_0 as input to the material from time t_0, the resultant time-dependent strain is a gradual increasing one. The resultant strain function J(t) from unit step stress (σ_0=1) is referred to as the Creep Compliance (Fig.3.3).

For a viscoelastic solid, the resultant strain increases until it reaches a non zero value equilibrium value, i.e, $\text{Lim}_{t\to\alpha}$ J(t) = Jα > 0 For viscoelastic fluids, the resulting strain increases continuously, without bound as time increases.

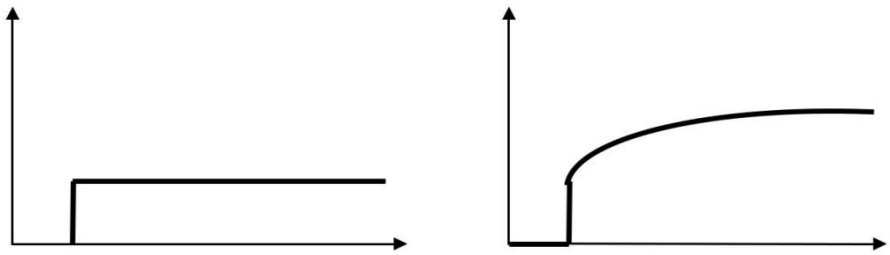

(a) ***(b)***

Fig.3.3: *(a) Unit Stress$\sigma_0$applied at $t=t_0$, (b) Strain Behavior Resulting from unit Stress which is increasing in nature showing creep*

3.2.3.3 Hysteresis

For a viscoelastic material, in the stress strain curve, loading process differs from that of unloading. For a purely Hookean elastic solid, loading and unloading path does not vary and hence follows a straight line path in the stress strain curve as shown in Fig.3.4 (a). On the other hand, for any viscoelastic solid (a Kelvin-Voigt solid as shown in Fig.3.4 (b)) the loading and unloading path can be well differentiated. This property is known as hysteresis of the material and a viscoelastic solid exhibits this characteristic property.

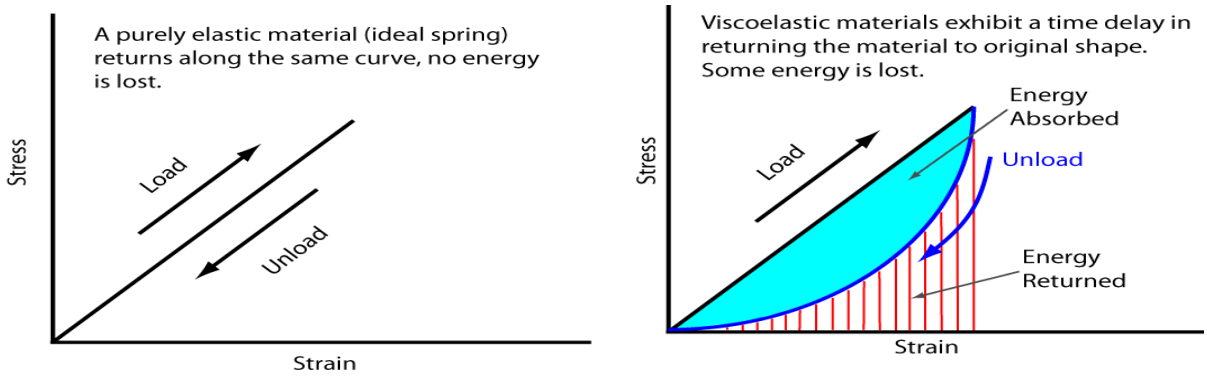

Fig 3.4: *Curves or elastic Model and Viscoelastic Model*

Study of the field of continuum mechanics is important in understanding the behavioral nature of materials which acts as a continuous medium and fills an occupied space completely. Continuum mechanics branch of mechanics deals with the analysis of the kinematics and the mechanical behavior of materials which are modeled as a continuous mass rather than as discrete particles. There are a number of interesting applications where modeling of elastic and viscoelastic materials is fundamental.

3.2.4 Modeling of Viscoelastic Properties

In order to mathematically simulate the viscoelastic behavior materials, rheological models comprising of springs and dashpots can be constructed as shown in Fig. 3.5. In linear viscosity analysis, parameters associated with the various elements are considered to be constant. However, for more complex materials, they may also be formulated as non-linear functions.

Fig. 3.5: *(a) Spring Element (Elastic) & (b) Dashpot Element (Viscous)*

The linear spring is an elastic element with a constant of proportionality of μ (co-efficient of elasticity) between the stress and strain. The linear dashpot is a purely viscous element with a proportionality constant 1/η (η= coefficient of viscosity) between the rates of strain to the applied stress.

Spring Element: The behavior of linear elastic solid can be represented by a linearspring having stiffness μ described by the following constitutive relationship:

$$\sigma = \mu \varepsilon$$

$$\text{Or,} \quad \varepsilon = J\sigma$$

Where, J is the compliance of the material.

Dashpot Element: The linear viscous behavior of solid/fluid is represented by linear dashpot, representing a piston moving in a viscous fluid having a particular viscosity (in this case say, η), which again follows the following constitutive relationship:

$$\frac{d\varepsilon}{dt} = \frac{1}{\eta}\sigma$$

There are various models describing the viscoelastic behavior of a material. But, there are two basic conventional models that can be used to describe Viscoelasticity in terms of simplicity, efficiency and ease in mathematical modeling. Various other viscoelastic

models are mostly derived from these two basic traditional models either applying a fractional calculus approach or by various other series-series, series-parallel or even parallel-parallel arrangement of K-V or Maxwell element with each other or with the individual spring or dashpot elements.

3.2.5 Kelvin-Voigt Model

The Kelvin-Voigt or simply Kelvin or the K-V model consists of a spring having modulus μ and a dash- pot with viscosity η, coupled in parallel, as shown in Fig.3.6.
Another very significant name of it is that it is an Iso-strain model. The name itself explains the strain distribution in the model. The deformation (ε) is equal in both the arms of the model, however high stress (σ) is applied. The reason behind this type of strain distribution is the parallel connection of the arms and hence the name.

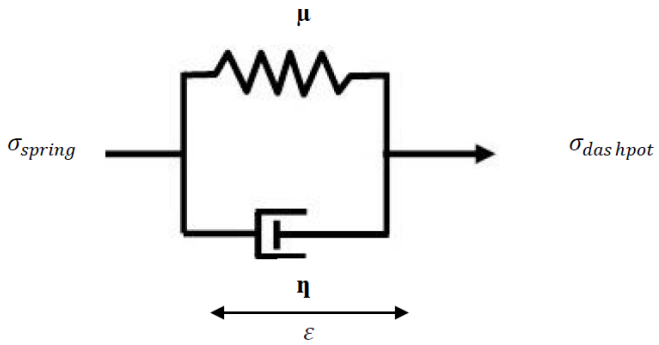

Fig. 3.6: *Kelvin Voigt Viscoelastic Model*

As the strain experienced by both the elastic and the viscous element is same, it can be written that:

$$\varepsilon_{spring} = \varepsilon_{dashpot} = \varepsilon$$

The governing differential equation for the Kelvin Voigt model can be thus constructed as:

$$\sigma = \sigma_{spring} + \sigma_{dashpot}$$

$$\sigma_{spring} = \mu\varepsilon_{spring}$$

$$\sigma_{dashpot} = \eta\frac{d\varepsilon_{dashpot}}{dt}$$

$$\therefore \sigma = \mu\varepsilon + \eta\frac{d\varepsilon}{dt}$$

In this case the deformation of the viscous element is restricted by the deformation in the spring & hence the dashpot cannot undergo a continuous deformation & for this reason this model describes the nature of a viscoelastic solid.

3.2.6 Maxwell Model

The Maxwell model consists of a spring of modulus μ and a dashpot with viscosity η,coupled in series, as shown in Fig.3.7. This model is also known by the name Iso-stress model. Similarly as in K-V Model where the strain is uniform, in this model it is the force or the stress which is uniform in the arm of the model being series in connection.
As the stress applied remains same, it can be written that:

$$\sigma_{spring} = \sigma_{dashpot} = \sigma$$

The governing equations can be constructed as:

$$\varepsilon = \varepsilon_{spring} + \varepsilon_{dashpot}$$

$$\sigma_{spring} = \mu\varepsilon_{spring}$$

$$\sigma_{dashpot} = \eta\frac{d\varepsilon_{dashpot}}{dt}$$

$$\therefore \frac{d\varepsilon}{dt} = \frac{1}{\mu}\frac{d\sigma}{dt} + \frac{\sigma}{\eta}$$

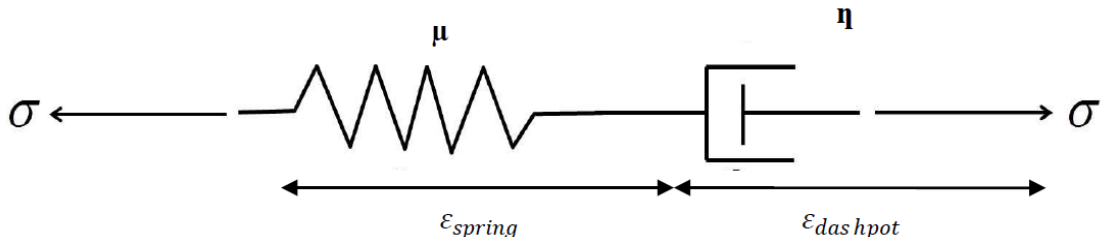

Fig. 3.7: *Fractional Maxwell Model*

As the K-V Model describes the nature of a viscoelastic solid, similarly in case of the Maxwell Model, the dashpot keeps on deforming as long as the force exists. Thus, this model behavior is more like a fluid than solid & hence named as the viscoelastic solid model.

3.3 FRACTIONAL CALCULUS

In the recent years, fractional calculus has appeared as an important tool to deal with a number of mathematical problems associated with different fields such as physical, chemical or even mechanical modeling of various aspects including biological and even aerospace fields.

Fractional calculus is a branch of mathematical analysis that studies the possibility of taking real number powers or complex number powers of the differentiation operator D, and the integration operator J. Fractional Calculus was born in 1695. It was G.F.A. de L'Hôspital (1661–1704) who 1st raised the question as to what the consequences and solution would be if the order of a differential equation be n=1/2. An important point is that the fractional derivative at a point x is a local property only when a is an integer; in non-integer cases we cannot say that the fractional derivative at x of a function f depends only on values of very near x, in the way that integer-power derivatives certainly do. Therefore it is expected that the theory involves some sort of boundary conditions, involving information on the function further out. To use a metaphor, the fractional derivative requires some peripheral vision. As far as the existence of such a theory is concerned, the foundations of the subject were laid by Liouvillein a paper from 1832. The fractional derivative of a function defined by the Riemann-Liouville Fractional Differential Operator to order α is often now defined by means of the Fourier or Mellin integral transforms.

Let us assume f(x) is a monomial of the form:

$$f(x) = x^k$$

The 1st derivative is as usual:

$$f'(x) = \frac{d}{dx} f(x) = kx^{k-1}$$

Repeating this gives the more generalized form:

$$\frac{d^a}{dx^a} x^k = \frac{\Gamma(k+1)}{\Gamma(k-a+1)} x^{k-a}, k \geq 0$$

For k=1 and a= ½, we obtain the half derivative of the function x as

$$\frac{d^{1/2}}{dx^{1/2}} x = \frac{\Gamma(2)}{\Gamma\left(\frac{3}{2}\right)} x^{1/2} = \frac{1}{\sqrt{\pi}/2} x^{1/2}$$

Repeating the process:

$$\frac{d^{1/2}\ 2x^{1/2}}{dx^{1/2}\ \sqrt{\pi}} = \frac{2\ \Gamma(\frac{3}{2})}{\sqrt{\pi}\Gamma(1)}x^0 = \frac{2\frac{\sqrt{\pi}}{2}x^0}{\sqrt{\pi}0!} = 1$$

Now this result is the predicted result of

$$\left(\frac{d^{1/2}\ d^{1/2}}{dx^{1/2}dx^{1/2}}\right)x = \frac{d}{dx}(x) = 1$$

For a general function f(x) and 0<α<1, the complete fractional derivative is,

$$D^{\alpha}f(x) = \frac{1}{\Gamma(1-\alpha)}\frac{d}{dx}\int_0^x \frac{f(t)}{(x-t)^{\alpha}}dt$$

For arbitrary α, since the gamma function is undefined for arguments whose real part is a negative integer and whose imaginary part is zero, it is necessary to apply the fractional derivative after the integer derivative has been performed. For example,

$$D^{\frac{3}{2}}f(x) = D^{\frac{1}{2}}D^1 f(x) = D^{\frac{1}{2}}\frac{d}{dx}f(x)$$

3.3.1 Fractional Maxwell Model (FMM)

In the field of fluid biomechanics, the non-Newtonian fluids are being considered more important and appropriate in technological applications as compared with the Newtonian fluids. In many fields, such as food industry, drilling operations and bio-engineering, the fluids, either synthetic or natural, are mixtures of different stuffs such as water, particle, oils, red cells and other long chain molecules; this combination imparts strong non-Newtonian characteristics to the resulting liquids; where the viscosity function varies non-linearly with the shear rate; elasticity is felt through elongation and time-dependent effects. Large classes of real fluids do not follow the linear relationship between stress and the rate of strain. Because of the non-linear dependence, it is much more difficult to obtain the exact analytic solutions for the flows of the non-Newtonian fluids. In these cases, the fluids have been treated as viscoelastic fluids. Because of the difficulty to suggest a single model which exhibits all properties of viscoelastic fluids, they cannot be described as simply as Newtonian fluids. For this reason, many models or constitutive equations have been proposed and most of them are empirical or semi empirical. One of the simplest types of models to account for the rheological effects of viscoelastic fluid is the Maxwell model.

Due to the recent popularity and success of fractional calculus, it has successfully been used in the description of the complex dynamics. Surprisingly, it has been proved to be a valuable tool to handle viscoelastic properties in particular. The starting point of the fractional derivative model of non-Newtonian fluid is usually a classical differential equation being modified by replacing the time derivative of an integer order by the so-called Riemann–Liouville fractional calculus operator. Hence the success of using the fractional calculus and hence the Riemann-Liouville fractional operator has been also proved in the study of flows of a viscoelastic fluid between two co-axial cylinders by using Weber Transform and Inverse Laplace Transform to obtain the exact solutions (*Haitao and Hui, 2006*). Work by *Tan et al., 2003*established exact solutions for a class of unsteady flows of a viscoelastic fluid with this fractional derivative Maxwell Model between two infinite parallel plates. Fractional-derivative Maxwell model has also been proposed for viscous dampers, which are used for vibration isolation of piping systems, forging hammers, and other industrial equipment, as well as for vibration and seismic isolation of building structures (*Markis and Constantinou, 1991*).

The constitutive governing equation of Fractional Derivative Maxwell Model (FDMM) or the Fractional Maxwell Model (FMM) is given by (*Hayat et al., 2004; Tripathy et al.,2010; Yan et al., 2011; Haitao and Mingyu, 2007*):

$$\sigma(t) + \lambda^{\alpha}\frac{d^{\alpha}\sigma(t)}{dt^{\alpha}} = \mu\lambda^{\beta}\frac{d^{\beta}\varepsilon(t)}{dt^{\beta}}$$

Where $\sigma(t)$ is the time dependent stress, μ is the sheer modulus, λ is the relaxation time, given by

$$\lambda = \frac{\eta}{\mu} = \frac{viscosity\ coefficient}{sheer\ modulus}$$

And α β are the fractional calculus parameters such that $0 \leq \alpha \leq \beta \leq 1$. For $\alpha > \beta$ relaxation function is increasing, which is, in general, not reasonable. While $\alpha = \beta = 1$, it may be simplified as the ordinary Maxwell model & for $\alpha = 0$; $\beta = 1$, it may be simplified as the classical Newtonian fluid. A further modeling of FMM and the physics behind it has been made in the Mathematical Modeling chapter.

3.3.2 Fractional Maxwell Model

Flourishing of fractional calculus in research has been noticed recently as there are lots of positive aspects behind the invention. Similarly fractional Maxwell Model has also emerged as a promising scope in the fields such as mechanics, biology and a lot more. In this paper the human corneal viscoelastic nature has been also tried to be modeled using this specific mathematical method. Most of the works in the history of researches on the nature and behavior of human eye and the associated tissues are either experimental or

simulation based. Not much work has been studied where the biological soft tissues of human eye have been tried to give a mathematical design and specially using the fractional calculus. The immediate question that arises in this context is that why the Fractional Calculus in this especially over the other conventional and particularly viscoelastic models have been chosen? A clear clarification to this curiosity can be described by two main points, viz.:

A. *Drawbacks of Conventional Methods:* The 1st section deals with the drawbacks of the conventional viscoelastic models. It needs to be mentioned in this regard that the two initial models, the Kelvin-Voigt Model and the Maxwell Model shows some limitations while describing a purely anisotropic, non-linear, time dependent viscoelastic behavior. As already mentioned, K-V Model realizes more of a viscoelastic solid behavior than liquid, whereas Maxwell Model depicts more of a viscoelastic fluid nature. The foremost reason behind this nature discrimination of the models is due to the parallel and series arrangement of the elastic and viscous components in the model design. This behavioral property of the models restricts it to define the soft tissue of human cornea as it shows properties of both solid and fluid Viscoelasticity. Besides the K-V Model is unable to show any instantaneous deformation due to the absence of a purely elastic element and the change in length of the spring element remains a function of the movement of the viscous element being an Iso-strain model. In spite of these limitations a purely K-V Model element describes the corneal Viscoelasticity to some extent and realizes the predicted nature of curve that needs to be obtained ideally. This section has been included and proved right in this paper by performing a simulation based derivative equation solving in a 2-D cornea structure in COMSOL MULTIPHYSICS 4.3.The Standard Linear Solid (SLS) models on the other hand comprises of either a series or parallel coupling of either of the two models with either of the spring or the dashpot element as shown in Fig.3.8. These models somehow cannot facilitate a clear demarcation between a purely elastic and a purely viscous element thus lacking the ability to describe our desired nature.

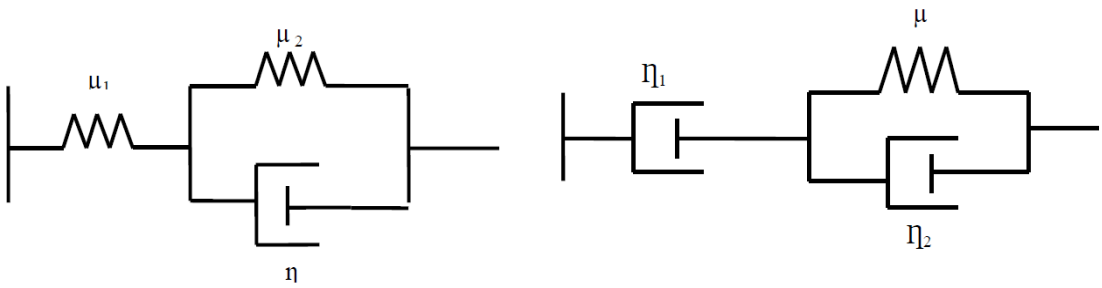

Fig. 3.8: *Standard Solid Models: (a) Elastic Element in series with K-V element, (b) Viscous Element in Series with K-V element*

As moving on to the so called Maxwell Viscoelastic Model, a lot of limitations on the way have been noticed. Firstly, the Maxwell Model is a series combination of a spring and a dashpot, as a result when a stress is applied, the deformation of the spring occurs instantaneously and thus overcomes the limitation of the K-V Model, but as far as the dashpot is concerned, the deformation takes place in a very sloth manner due to the viscosity of the dashpot fluid. As a result, the creep in the system is continuous. It takes a prolonged time span the system to attain stability. Another vital disadvantage with this model is hysteresis which is a highly undesired error of any system. After the force is released, the Maxwell element cannot fully regain from its point of deformation and hence a small degree of deformation retains in the body. Thus the path of loading and unloading is different for the system. These two drawbacks cannot be overcome in case of human eye as it has a specific value of elastic limit, viscosity and also relative density and the viscous element cannot be chosen to have a high co-efficient of viscosity in the model. That the Maxwell Model does not clearly mimics the nature of human eye stress-strain behavior and carries a large demarcation with the practical case, is further computed and shown in the following chapters.

B. *Advantages of Fractional Maxwell Model:* Fractional calculus as already discussed is preferred over other mechanical models due to its simplicity and also lesser number of parameters. While defining nature of corneal muscles this model has been preferred in this work as well due to its versatility. Corneal elastic and viscous properties cannot be isolated and hence shows a combinational behavior. The degree of elasticity and viscosity provides the strength of viscoelastic or plastic nature in the eye muscles. This degree can be well identified by the fractional model by a proper selection of the fractional order parameters α & β.

References:

Bonifasi-Lista C., Lake S.P., Small M.S., Weiss J.A., 2005. Viscoelastic properties of the human medial collateral ligament under longitudinal, transverse and shear loading. J. Ortho. Res. 23, 67–76.

Grashow J.S., Yoganathan A.P., Sacks M., 2006. Biaxial stress-stretch behavior of the mitral valve anterior leaflet at physiologic strain rates. Annals of Biomedical Engineering 34, 315–325.

Haitao Q., Hui J., 2006. Unsteady Rotating Flows of a Viscoelastic Fluid with the Fractional Maxwell Model between coaxial cylinders. Springer, ActaMechanicaSinica 22, 301-305

Haitio Q., Mingyu X., 2007. Unsteady flow of viscoelastic fluid with fractional Maxwell model in a channel. Mech. Res. Communications 34, 210–212

Hayat T., Nadeem S., Asghar S., 2004. Periodic unidirectional flows of a viscoelastic fluid with the fractional Maxwell model. Applied Mathematics and Computation 151, 153–161

Hayes W.C., Mockros L.F., 1971. Viscoelastic constitutive relations for human articular cartilage. Journal of Applied Physiology 18, 562–568.

Hingorani R.V., Provenzano P.P., Lakes R.S., Escarcega A., Vanderby Jr. R., 2004.Nonlinear viscoelasticity in rabbit medial collateral ligament. Annals of Biomedical Engineering 32, 306–312.

Humphrey J.D., 1995. Mechanics of the arterial wall: review and directions. Critical Reviews in Biomedical Engineering 23, 1–162.

Markis N., Constantinou M.C., 1991. Fractional Derivative Maxwel Model for Viscous Damper. Journal of Structural Engineering 119(7),

McCrum N.G., Buckley C.P., Bucknell C.B., (2003): "Principles of Polymer Engineering," 117-176.

Meyers M.A., Chawla K.K., 2009. Mechanical Behavior of Materials, Cambridge University Press, 978-0-521-86675-0

Ning X., Zhu Q., Lanir Y., Margulies S.S., 2006. A transversely isotropic viscoelastic constitutive equation for brainstem undergoing finite deformation. ASME, J. BiomechEng 128, 925–933.

Pinsky P.M., Datye V., 1991.A microstructurally-based finite element model of the incised human cornea.J. of Biomech. 10, 907–922.

Sacks M., 2000.Biaxial mechanical evaluation of planar biological materials. Journal of Elasticity 61, 199–246.
Mukherjee S., Chawla1 A., Karthikeyan B., Review of Mechanical Properties of Human Body Soft Tissues in the Head, neck and spine

Silver, F.H., Snowhill, P.B., Foran, D.J., 2003. Mechanical behavior of vessel wall: a comparative study of aorta, vena cava, and carotid artery. Annals of Biomedical Engineering 31, 793–803.

Tan Wenchang , Pan Wenxiao, XuMingyu., 2003. Anote on unsteady fows of a viscoelastic fuid with the fractional Maxwell model between two parallel plates. International Journal of Non-Linear Mechanics 38 645 – 650

Tara N. Shepherd, Jingzhou Zhang, Timothy C. Ovaert, Ryan K. Roeder, Glen L. Niebur, 2011. Direct Comparison OfNanoindentation And Macroscopic Measurements Of Bone Viscoelasticity, Journal Of The Mechanical Behavior Of Biomedical Materials 42055 – 2062

Tripathy, S.K.Pandey, S.Das, 2010. Peristaltic flow of viscoelastic fluid with fractional Maxwell model through a channel. Applied Mathematics and Computation 215 3645–3654

Yan, L. Yu, Y.H.Yang, 2011. Study of oscillating flow in rolling motion with the fractional derivative Maxwell model. Progress in Nuclear Energy 53 132e138

CHAPTER 4
IMPACT ANALYSIS

4.1 IMPACT MECHANICS

Impact is defined as a sudden contact of a moving body with a motionless barrier, or a body of much larger size *(Gregory, 2010).* It is concerned with the reaction forces that develop during a collision and the dynamic responses of the structures to these reaction forces *(Strong, 2004).*
The dynamic energy in a moving object, like falling ball or dust particles can be expressed as

$$E = \frac{1}{2}mv^2$$

Where, E is dynamic energy in joules, m is the mass in kg and v is the velocity in m/s.
Work done by an impact force in slowing down the object can be expressed as

$$W = F.s$$

where W is the work done in joules, F is the slowdown force in newton and s is the slowdown distance in metre. In an impact like a crash, the dynamic energy from the object is converted to work done. The equation can be expressed as,

$$F.s = \frac{1}{2}mv^2$$

$$or, F = \frac{1}{2s}mv^2$$

The slowdown distance (s) is very important and a key to limit the impact forces acting in crashes.

4.2 IMPORTANCE OF IMPACT TESTING

Impact testing is testing an object's ability to resist high-rate loading. An impact test is a test for determining the energy absorbed in fracturing a test piece at high velocity. Most of us think of it as one object striking another object at a relatively high speed.

Impact resistance is one of the most important properties for a part designer to consider, and without question, the most difficult to quantify. The impact resistance of a part is, in many applications, a critical measure of service life. More importantly these days, it involves the perplexing problem of product safety and liability. Impact test determines the amount of energy absorbed by a material during fracture. This absorbed energy is a measure of a given material's toughness and acts as a tool to study temperature-dependent brittle-ductile transition. It is to determine whether the material is brittle or ductile in nature.

A nail is pounded with a series of impacts, each by a single hammer blow. These high velocity impacts overcome the static friction between the nail and the substrate. A pile driver achieves the same end, although on a much larger scale, the method is commonly used during civil construction projects to make building and bridge foundations. An impact wrench is a device designed to impart torque impacts to bolts to tighten or loosen them. At normal speeds, the forces applied to the bolt would be dispersed, via friction, to

the mating threads. However, at impact speeds, the forces act on the bolt to move it before they can be dispersed. In ballistics, bullets utilize impact forces to puncture surfaces that could otherwise resist substantial forces. A rubber sheet, for example, behaves more like glass at typical bullet speeds. That is, it fractures, and does not stretch or vibrate. Road traffic accidents usually involve impact loading, such as when a car hits a traffic bollard, water hydrant or tree, the damage being localized to the impact zone. When vehicles collide, the damage is proportionate to the relative velocity of the vehicles, the damage increasing as the square of the velocity since it is the impact kinetic energy ($1/2\ mv^2$) which is the variable of importance. Much design effort is made to improve the impact resistance of cars so as to minimize user injury. It can be achieved in several ways: by enclosing the driver and passengers in a safety cell for example. The cell is reinforced so will survive in high speed crashes, and so protect the users. Parts of the body shell outside the cell are designed to crumple progressively, absorbing most of the kinetic energy which must be dissipated by the impact. Various impact tests are used to assess the effects of high loading, both on products and standard slabs of material. Ball or projectile drop tests are used for assessing product impacts. The Columbia disaster was caused by impact damage when a chunk of polyurethane foam impacted the carbon fibre composite wing of the space shuttle. Although tests had been conducted before the disaster, the size of the chunks was much smaller than that which fell away from the booster rocket and hit the exposed wing.

4.3 CRASH SIMULATION

A crash simulation is a virtual recreation of destructive crash test of a car or highway guard rail system using a computer simulation in order to examine the level of safety of cars and its occupants. During a crash simulation, the kinetic energy of the body in motion, that the body has before the impact is transformed into deformation energy, mostly by plastic deformation (plasticity) of the body material at the end of the impact. Modeling of human body and its dynamic problems, particularly in crash or high acceleration environments, has been the interests of researchers for many years. There are four reasons for this interest, (a) a growing number of vehicle accidents; (b) an increase in severity of injuries; (c) modeling of crash-victim system by surrogates (i.e. dummies and cadavers), is still very expensive; (d) improvements in computer hardware and software have increased the opportunities for crash-victim simulation *(Huang, 1995).*
Crash simulations use finite element method to solve complex problems by dividing a surface into a large but finite number of elements and determining the motion of those elements over a small interval of time.

***4.3.1 Structural analysis*:** In a typical crash simulation, the car body structure is analyzed using spatial discretization, i.e., breaking up the continuous movement of the body in real time into smaller changes in position over small, discrete time steps. The discretization

involves subdividing the surface of the constituent into a large number of quadrilaterals and triangular regions, each of which spans the area between 'nodes' to which its corners are fixed. The spatial co-ordinates (*x*), displacement (*u*), velocity (*v*) and acceleration (*a*) of each node is mostly expressed in a three-dimensional Cartesian co-ordinate system with axis X, Y, Z. If the nodes move during a crash simulation, the connected elements move, stretch, bend with their nodes, which cause them to impart forces and moments to their nodal connections. The forces and moments at the nodes correspond to the inertia forces and moments, caused by their translational and angular accelerations and to the forces and moments transmitted by the resistance of their structural material of the connected material as they deform.

4.3.2 Time Analysis:A crash simulation also uses time discretization as well to separate the continuous changes in time into very small, usable segments. According to the explicit finite time difference time integration method used by most crash codes, the acceleration, velocities and displacements of the body are related by the following equations:

$$a_n = M^{-1}(F_{ext} - F_{int})$$

$$v_{n+1/2} = v_{n-1/2} + a_n \Delta t_n$$

$$u_{n+1} = u_n + v_{n+1/2} \Delta t_{n+1/2}$$

In these equations subscripts $n \pm \frac{1}{2}$, *n*, *n+1* denotes past, present and future times, *t*, at half and full time intervals with time steps Δt_n and $\Delta t_{n+1/2}$, respectively.

4.3.3 Solution:The above system of equations is solved for acceleration, an, velocities, $v_{n+1/2}$ and displacements, u_{n+1} at each discrete point of time, *t*, during the crash duration.

4.4 OCULAR INJURY

From literature, various classification of eye or ocular trauma has been known. *Kuhn (1996)* categorized eye injury into closed globe injury and open globe injury.

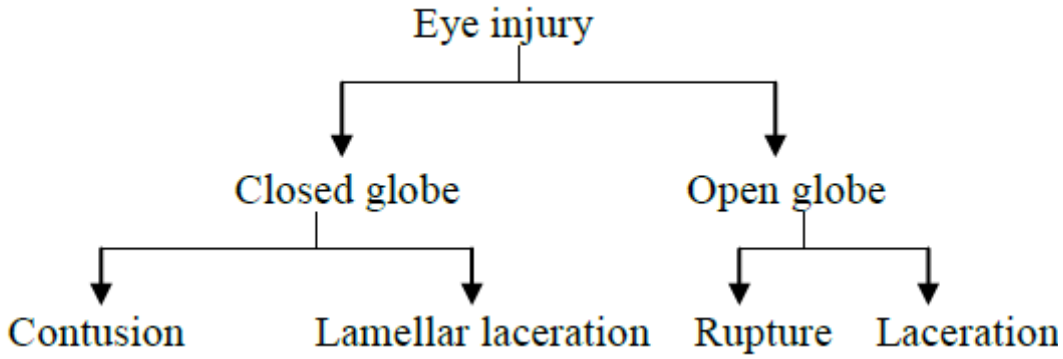

Laceration in open globe injury includes penetrating injuries, perforating injuries and Intra-Ocular Foreign Body (IOFB) injuries.

Vinger in 1994 categorizes the mechanism of blunt ocular trauma into four major classes: Class 1: It is the penetration of the globe by a sharp object such as glass.

Class 2: The second class involves ocular injuries caused by blunt objects smaller than the orbital opening, such as paintball

Class 3: It is identical to class 2, except that the blunt object is larger than the orbital opening, such as baseballs.

There are three theories that describe the injury mechanism of blunt ocular trauma: coup, contrecoup, and equatorial expansion *(Giovinazzo, 1987).* Any single mechanism or any combinations of these three mechanisms can cause eye injury.

(i) With coup injury, all the kinetic energy is directly absorbed at the site of impact, which is where the localized injury occurs (Fig 4.1a). Coup injuries can range from mild corneal abrasions to severe retinal detachments.

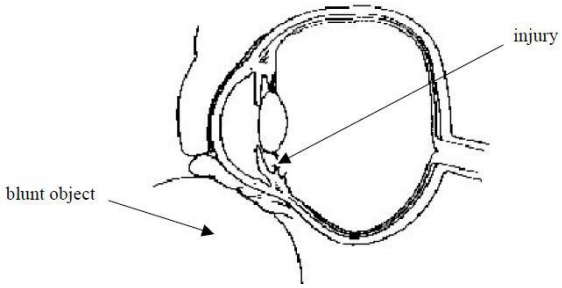

Fig 4.1a*: Coup Injury*

(ii) The second theory, contrecoup injury, explains instances of tissue damage away from the site of blunt impact. An impact produces a line of force that propagates along this line, travelling across the entire globe (Fig 4.1b). Injuries can occur at tissue boundaries, thus the damage can occur on the optic nerve due to contrecoup.

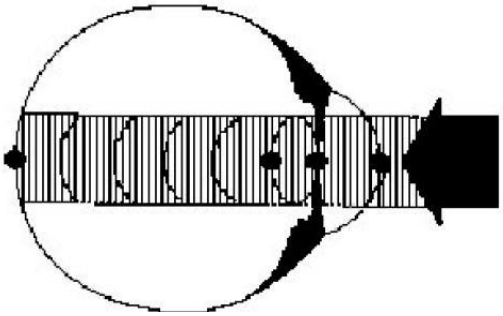

Fig 4.1b:*Contrecoup resulting in a force propagating across the globe (Giovinazzo, 1987)*

(iii)The third and the final theory, equatorial expansion, are most widely believed to produce retinal tears. The globe compresses along the line of impact and expands

perpendicular to the line of impact (Fig 4.1c). As the sclera expands, tension is produced, which can cause tearing of retina from sclera. The choroid (a layer between the retina and sclera) is also susceptible to separation as a result of this expansion.

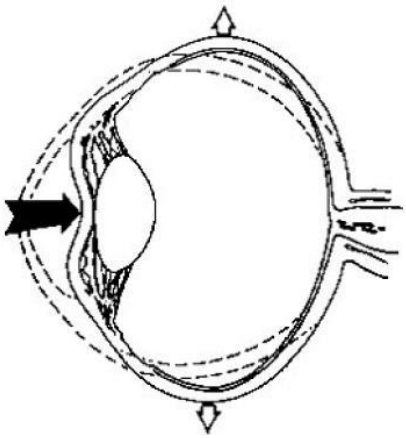

Fig 4.1c: *Equatorial expansion occurring perpendicular to the line of impact (Giovinazzo, 1987)*

From the previous works on simulation of foreign body on cornea, it has been noticed that the simulation is done by either altering the size and velocity of the missile particle or varying the velocities of the missile particle and set to impact on cornea undergone PRK and LASIK surgery.

The scope of the present work is to study the strain and Von-Misses stress behavior on the cornea of normal eye by impacting different blunt foreign bodies on the cornea surface using Altair Hyperworks v11.0. A simulation model of eye was set up based on the information of cadaver eyes done in earlier works in this domain. A three-dimensional Finite Element Analysis (FEA) was applied for understanding and analyzing the impact of foreign body causing Intra Ocular Foreign Body (IOFB) injuries. Using the physiological parameters of human eye and data available from previous works, the model is constructed in AutoCAD and using the modules of Hypermesh (Altair Engineering, Tokyo, Japan) solid mapped mesh is created and entire preprocessing was done. Blunt shaped missiles were also constructed in AutoCAD. The projectile missile was a decahedron and was set to impact on the surface of the eye cornea with variable velocities to see the results of impact and plastic strains on cornea. The simulation is solved in RADIOSS Block 90 Format. The axial strain graphs on cornea correspondent to various material properties of the projectile are analyzed.

4.5 MATERIAL PROPERTIES

Cornea exhibits unique properties of stiffness, mechanical strength and optical transparency which enable it to provide protective barrier to the inner components of the

globe and also the primary refractive medium of the eye. The fibrous microstructure of the stromal layer of cornea, which in humans constitutes 90% of the corneal thickness, results in this unique nature of the tissue.The stromal thickness is composed of around 200 lamellar sheets of collagen myofibrils implanted in hydrated matrix of glycoproteins, keratocyte cells and proteoglycans*(Maurice, 1957).* Cornea exhibits complex microstructure strongly regulated by the human body itself. After death, the cornea swells and its optical clarity and tear film is lost. Thus the biomechanical properties of the eye changes due to the combined effect of these biomechanical changes along with tissue degradation and alteration in temperatures *(Hjortdal, 1995).*In addition, *Kobayashi et al*. (1973) explained that the cornea is not purely elastic but rather is viscoelastic, which means the loading rate applied on the tissue alters the calculated value of the Young modulus. Due to the combination of all these factors, previous literatures has reported large range of Young's Modulus ranging from 0.159 MPa to 57 MPa*(Elsheikh, 2007 and Andreassen, 1980).*Under loading condition, cornea shows instantaneous deformation which demonstrates purely elastic response followed by gradual and progressive deformation which signifies its viscoelastic nature *(Kobayashi, 1973 and Edmund, 1989).*These behaviors could be modeled fairly with a Hookian spring system for pure elastic nature and with a spring-dashpot system for the viscoelastic nature as shown in figure 4.2, where the dashpot represents time-dependent viscous resistance to an applied force. Here one spring-mass system is in series with a spring-mass damping system where the damping is parallel to the spring system.

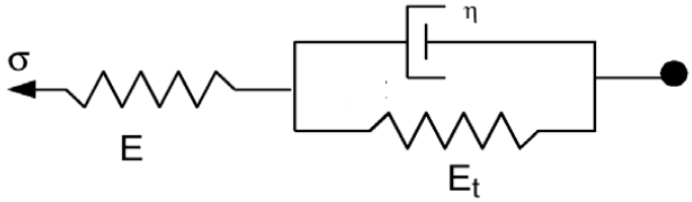

Fig 4.2: *Generalized KV model*

For viscoelastic model, generalized Fractional Kelvin-Voigt Deravativehas been selected as other model (e.g. Maxwell model) continually to creeps indefinitely under load. In the cornea, creep approaches asymptotically *(Jue, 1986).* Another limitation of Maxwell model is that it does not regain its original form after the load cease to act. The pure Kelvin-Voigt model was not selected because it does not possess a purely elastic component and thus no instantaneous deformation occurs. A simple graphical model has been developed in MATLAB for a corneal model with Young's modulus in the above mentioned range and viscosity of 9.02 KPa-s, which shows time-dependency of the deformation for a particular load. Figure 4.3 shows that the steepness of the curve increases as the stress increases and after the elastic limit it experiences no further deformation.

The elastic nature of the model is assumed to be an isotropic, linear elastic model obeying Hook's law and represents a linear relation between stress and strain. The stress-strain relationship could be presented as:

$$e_{ij} = \frac{1+\vartheta}{E}\sigma_{ij} - \frac{\vartheta}{E}\sigma_{kk}\delta_{ij}.$$

$$\sigma_{ij} = 2Ge_{ij} + \lambda e_{kk}\delta_{ij}.$$

Where, e_{ij} represents the Eulerian strain tensor and σ_{ij} represents Cauchy stress tensor's component *(Material Laws. Large Displacement Finite element analysis-Part2.RADIOSS Theory Manual v10.0., 2009).*

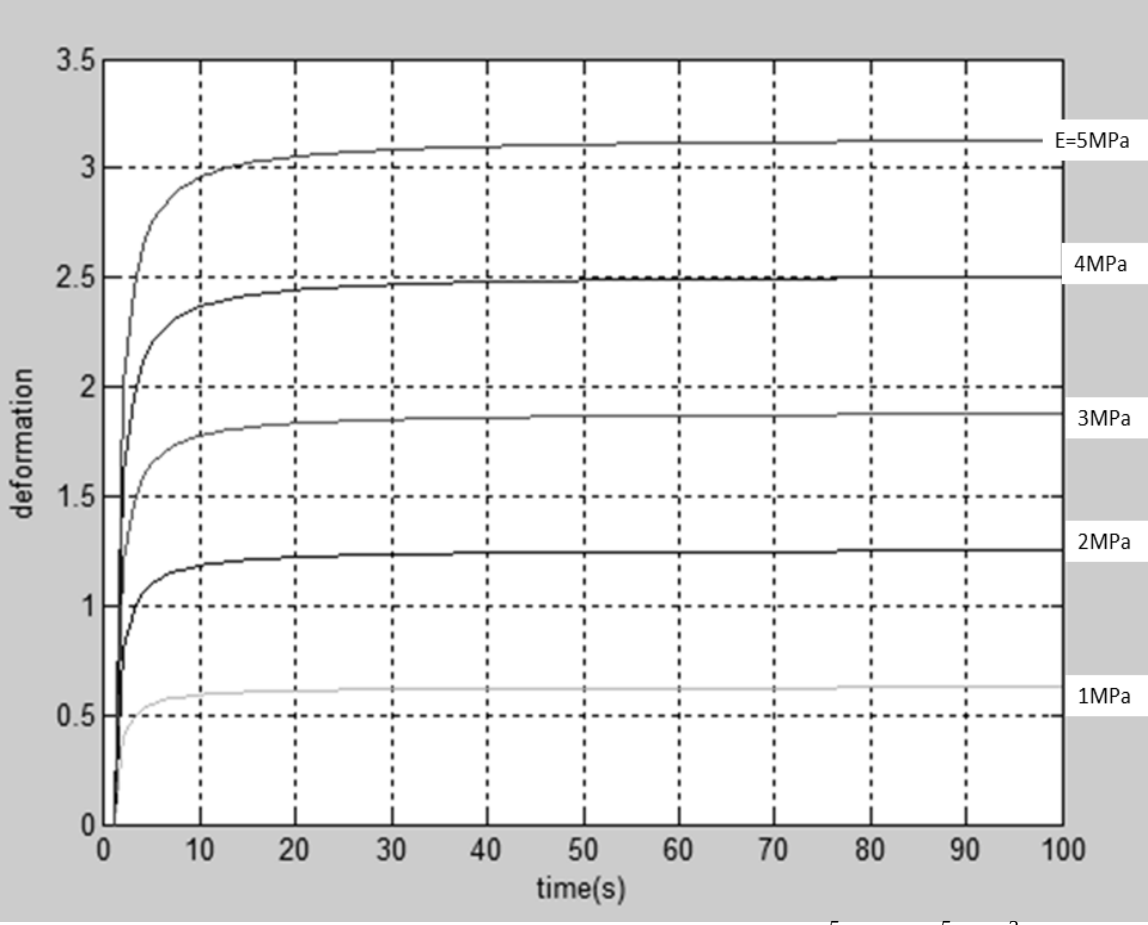

Fig 4.3: *Strain versus time for load varying from 1x10^5 to 5x10^5 Nm^{-2}*

KVFD governing equation arises out of the conventional governing equationof the K-V Model by replacing the ordinary integral derivatives with a fractional order. Order of the derivative of strain with respect to time is thus assumed to be a fraction and the corresponding stress-strain plot has been obtained. Stress has been varied between 1MPa-9MPa and the corneal tissue has a co-efficient of viscosity of 9.02KPa.sand elastic limit of 11.05MPa *(Uchio, 2003; Glass, 2008; Wua, 2013).* These data have been incorporated into the governing equation of KVFD to obtain the characteristic plots. The fractional order α takes up values such as 1/3, 2/3, 1/2, 1/4 and 3/4. When α=1, KVFD reduces to the conventional K-V Model. The conventional KV equation and KVFD equation thus can be written as:

$$\sigma(t) = E\varepsilon(t) + \eta \frac{d\varepsilon}{dt}$$

$$\sigma(t) = E\varepsilon(t) + \eta \frac{d^{\alpha}\varepsilon}{dt^{\alpha}}$$

Stress relaxation and Creep Compliance response for a KVFD model are obtained by taking a Heaviside function of the deformation and stress respectively.In the standard Kelvin-Voight model α=1, and the stress relaxation is equal to a delta function at time zero with a constant response after. No real material follows this function. In the KVFD model, where 0<α<1 the stress relaxation has the form $t^{-\alpha}$, where t is time. The creep compliance, J(t), and stress relaxation, G(t), functions, for the KVFD model are *(Lawrence, 2002).*

$$J(t) = \frac{1}{E}\left[1 - E_{\alpha}\left\{-\left(\frac{Et}{\eta}\right)^{\alpha}\right\}\right]$$

Where, E_{α} is the Mittag-Leffler function and is given by:

$$E_{\alpha}(x) = 1 + \sum_{n=0}^{\infty} \frac{x^{n}}{\Gamma(\alpha n + 1)}$$

And,

$$G(t) = E \ + \eta \frac{(1-\alpha)t^{-\alpha}}{\Gamma(2-\alpha)}$$

Figure 4.4, shows that KVFD depicts predicted nature of plot for deformation against time, where the deformation is increasing exponentially for the first 0.06 sec and then converges within a very short interval of time for various α values: 1/3, 2/3, ½ and 1. For α=1 the deformation is constant, for α=1/3 and α=2/3 he deformation is gradual with increasing time but for α=1/2 the slope is steep and the deformation increases within a very short interval of time.

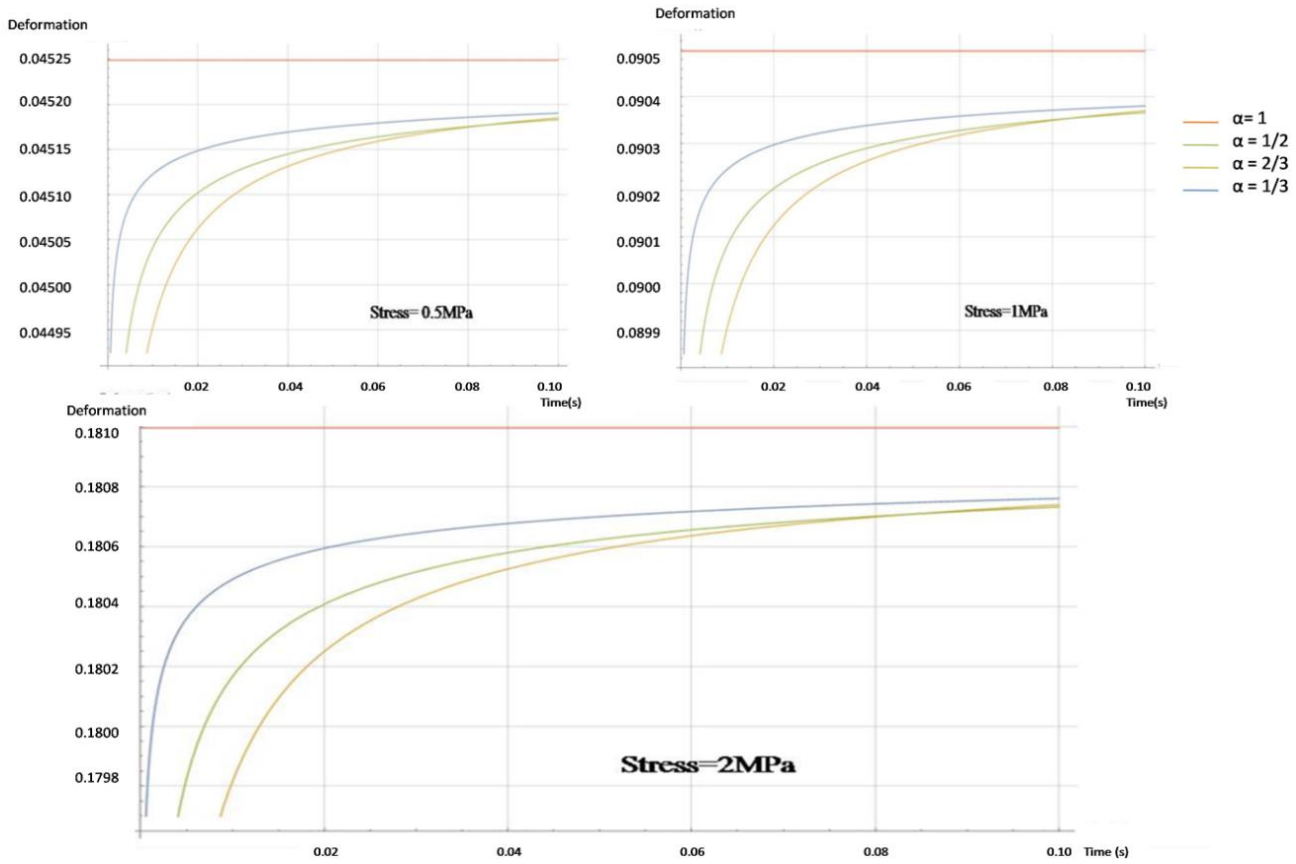

Fig 4.4: *KVFD Response for Deformation (mm/mm) vs Time(s) for four different values of α for (1.1) Stress = 0.5MPa, (1.2) Stress = 1MPa, (1.3) Stress = 2MPa*

*Nguyen et al. (2008)*suggested the development of a constitutive model based on the tissue microstructure for the nonlinear anisotropic viscoelastic tensile behavior of the stroma layer that comprise an explanation of fully nonlinear viscoelastic response of the lamellar level. The model is based on a newly developed general nonlinear constitutive framework for soft fiber-reinforced composites *(Nguyen, 2007).*The model represents the stroma as a continuum mixture consisting of collagen fibrils structured into lamellae characterized by an in plane orientation angle and embedded in a soft isotropic matrix.

The geometric model for the present work is based on the size, structure and dimensions of a generic human eye model. The model has been derived from previous work which is a three-dimensional geometry of eye cornea that has been developed and imported in Altair Hyperworks 10.0 suite in Block 90 format and linear hexahedral volume mesh is generated throughout the thickness of the cornea and is constituted of eight nodes hexahedral element called hex8 element in Altair Hypermesh environment, containing total 3095 elements comprising off 3960 nodes shown in figure 4.5.

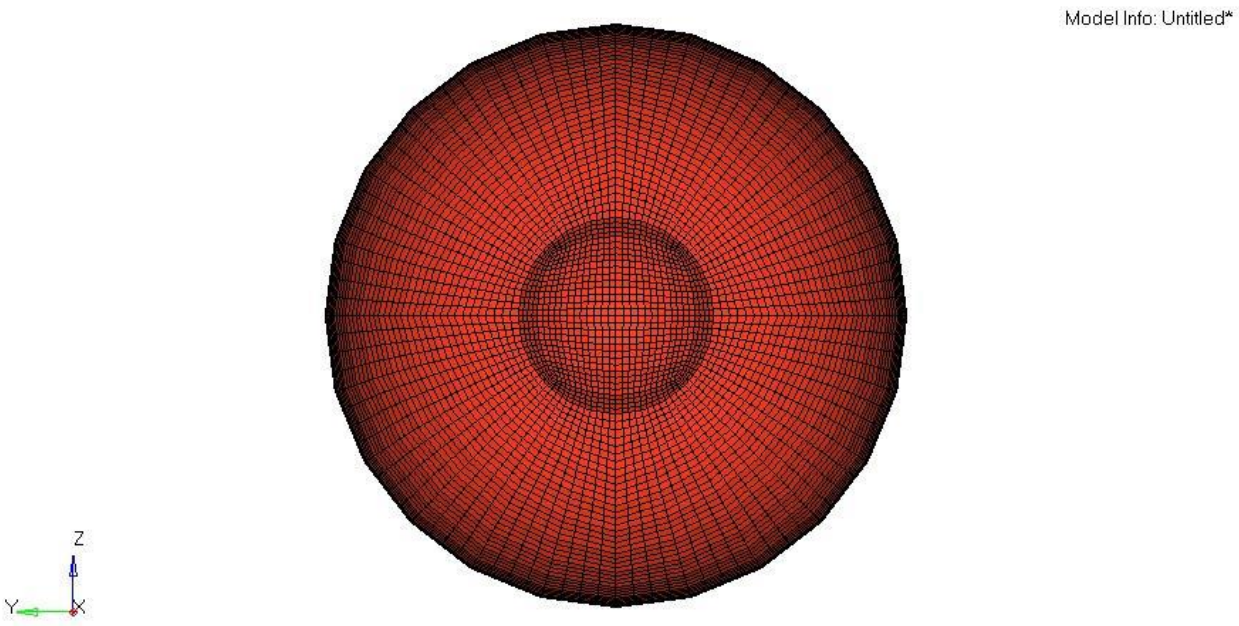

Fig 4.5: *Meshed Cornea geometry (Front View)*

From the experiment report of *Uchio et al.* (1999) it was found that Poisson's ratio for cornea is 0.420 and it was assumed that rupture occurs at a strain of 18% in cornea, and at a stress of 9.4 MPa. The blunt decahedron projectile, shown in figure 4b, is generated based on previous work of *Uchio et al.* (1999) and *Mousavi et al* (2012). Three different materials were considered for projectile i.e. Aluminum, bone and stainless steel with corresponding material properties. The bullet projectile has been meshed with linear hexahedral brick element mesh comprising of total 980 elements with 1124 nodes as shown in figure 4.6.

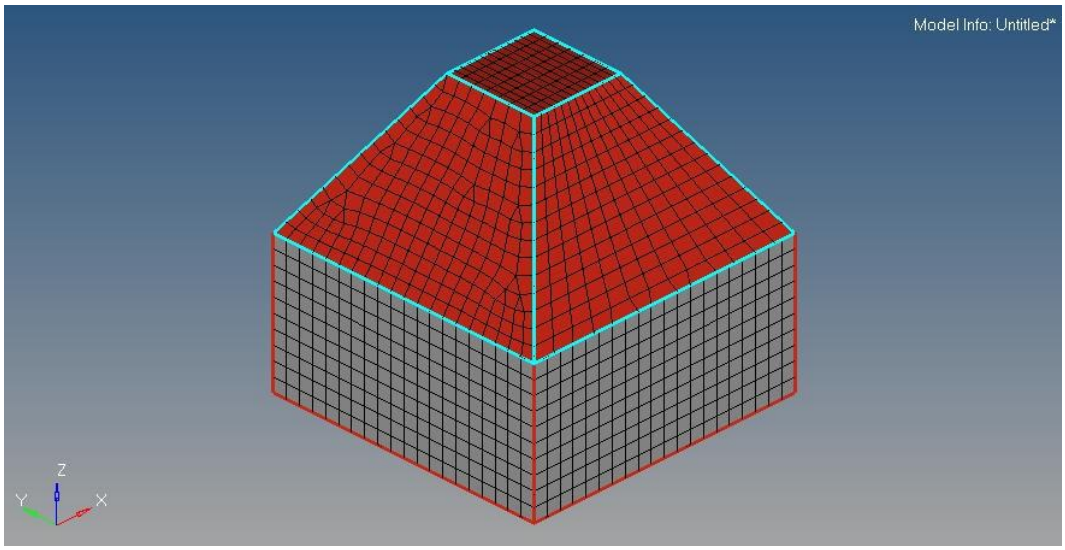

Fig 4.6: *Solid Map meshing of blunt projectile*

The mechanical properties used for various materials are enumerated in Table 4.1 *(Rupin, 2008 and Geringer, 2008).* The base area of the projectile is 0.25mm^{2}whose mass varies depending on the material. The cornea geometry is constrained about all axes to prevent any linear or rotational movement in any directions and the projectile material is set to impact on the surface at variable speed of 25ms^{-1}, 50 ms^{-1}, 75 ms^{-1} and 100ms^{-1}. The computation has been performed in Z230 HP workstation.

Table 4.1:*Mechanical properties of various materials considered to be as the foreign body*

Material	Density (gm/cm^3)	Young's Modulus (Mpa)	Poisson's Ratio
Bone	1.9	9000	0.30
Aluminium	2.7	69000	0.35
Steel	3.0	197000	0.29

4.6 OBSERVATIONS AND DISCUSSIONS

It has been observed through the simulation result that when the corneal tissue is considered as viscoelastic in nature it offers better resistance to the impacting object. The magnitude of the von-Misses stress generated on the surface of the elastic nature cornea almost gets double compared to the viscoelastic nature of the tissue. In the case of strain rate it has been observed that the localized straining is more on the surface of the elastic tissue. The variation in the strain effect on the cornea surface for both the material behavior range in the order $10^{-2} \pm 0.002$. It is mainly observed how the strain behavior and von Misses stress behavior varies on the surface of the cornea when crashed with projectiles of such varied mechanical properties. Human cortical bone has the lowest range of Young's modulus and density among the three materials used, the other two being Aluminum and stainless steel of grade AISI 316. The results are plotted for both plastic strains and Von Misses stresses of the cornea for all the three impacting material and for both the mechanical nature of cornea. From the plots it could be easily said that the value of the result parameters increases with increase in velocities. The plots also depicts that the value of both the result parameters sharply varies with the mechanical properties of the impacting material used for given set of velocities as shown in figure 4.7a and b.

The higher the Young's Modulus and density of the material higher is the value of plastic strain and von Misses stress at a particular velocity. Stress and strain are generated and transient behavior plot of the strain and stress on the tissue surface are developed which is shown in figure 4.8 for the case of an aluminum projectile with a velocity of 50 ms^{-1}. From the transient response of the stress and strain, it is observed that the stress generated and strain effect on the tissue surface due to high velocity blunt body impact is comparably less for the viscoelastic nature of cornea than that of the elastic nature for

similar test conditions. This leads to better energy absorption in the model constituted with viscoelastic nature thus it could provide better and long term resistance to the impacting body before failure.

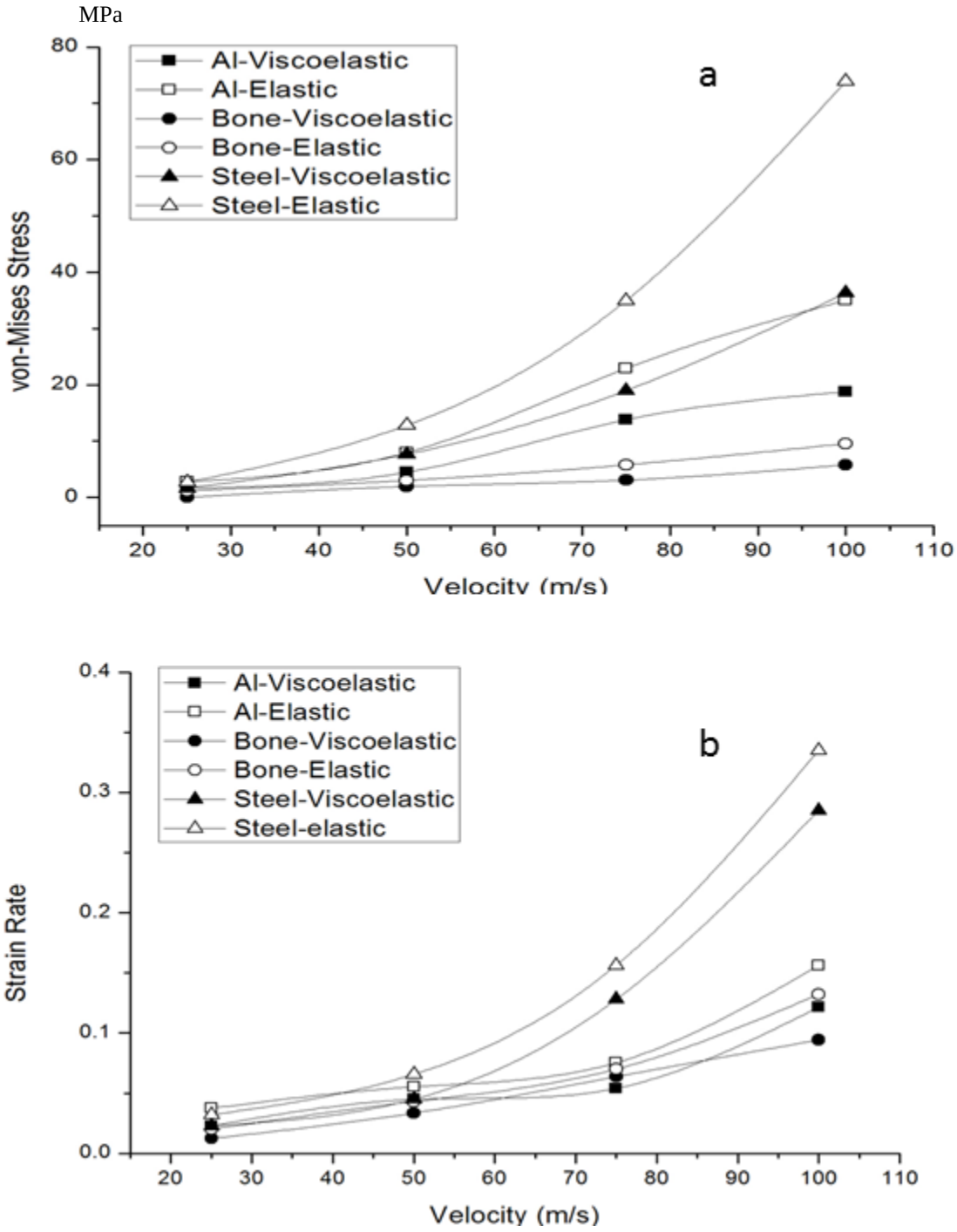

Fig 4.7 a: *Stress versus velocity curve,* ***b:*** *Strain rate versus velocity curve*

In this study the displacement of the surface of the cornea is also studied. The transient response of the displacement is shown in figure 4.8 where it is clearly explained that elastic nature shows instantaneous deformation and is short termed but viscoelastic nature shows prolonged and progressive deformation.

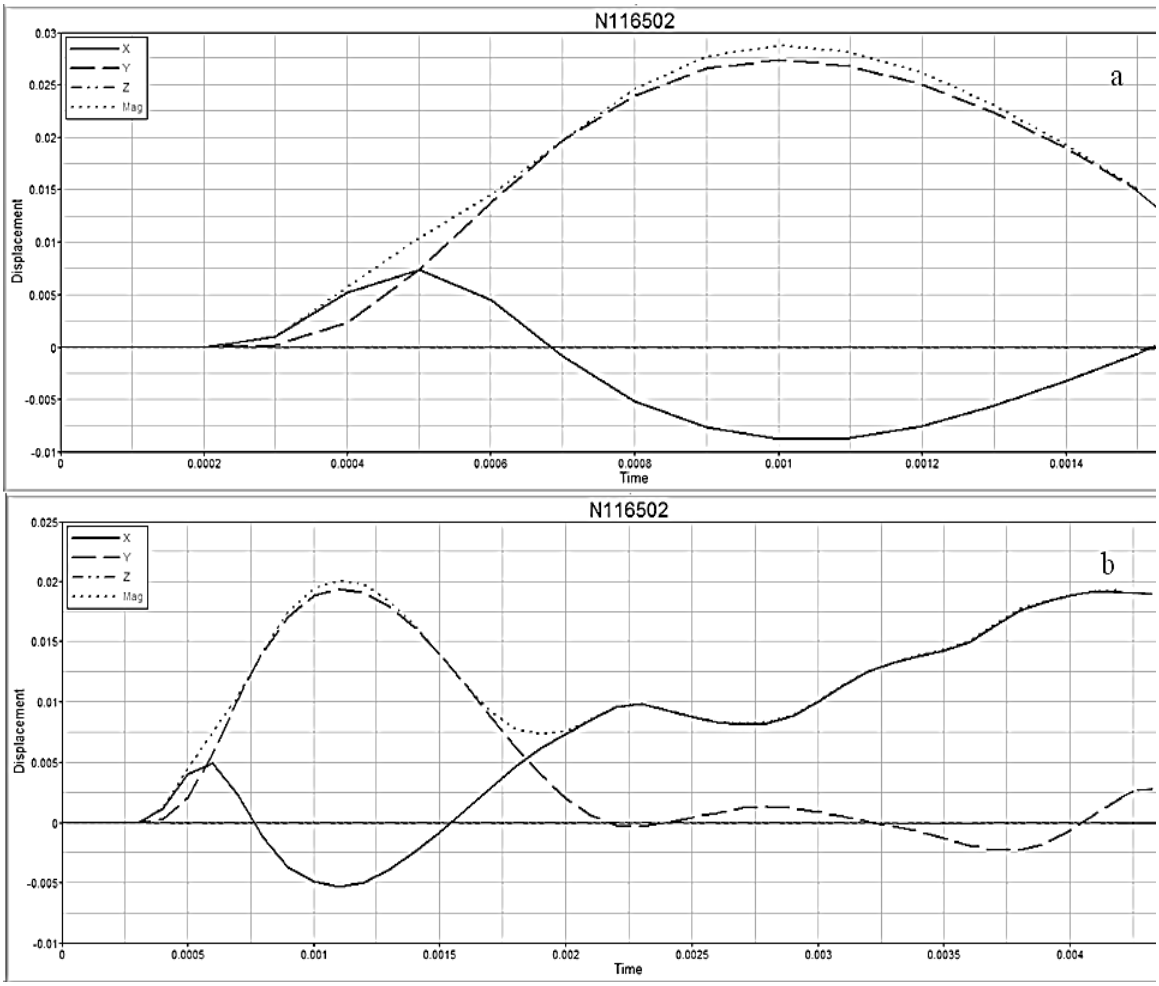

Fig 4.8: *Transient responses of the displacement (a) for elastic model, (b) viscoelastic model*

Table 4.2 shows the duration of deformation for different material and projectile velocity combination. There in all the cases we can observe that for viscoelastic model the deformation is much gradual than the elastic model.

Table 4.2: *Duration of deformation for different cornea material behavior and projectile velocity combination; E: Elastic model of cornea, VE: Viscoelastic model of cornea*

Velocities (ms^{-1})	**25**		**50**		**75**		**100**		**Projectile Material**
Duration of Deformation (sec)	***E***	***VE***	***E***	***VE***	***E***	***VE***	***E***	***VE***	
	0.0007	0.0028	0.0010	0.0037	0.0016	0.0045	0.0021	0.0051	**Bone**
	0.0011	0.0035	0.0015	0.0043	0.0019	0.0051	0.0025	0.0056	**Aluminum**
	0.0016	0.0043	0.0022	0.0052	0.0026	0.0059	0.0031	0.0066	**Steel**

In our range of maximum velocities, it has been observed that maximum duration for energy absorption is around 5.0, 5.5 and 6.5 milli-second respectively for each of the projectile material. However, the transient response time increases as the elastic moduli and density of the projectile increases. For example the duration of deformation for bone projectile impact is about 5.0 milli-seconds whereas for that of steel is around 6.5 milli-second. Due to this prolonged deformation stage in viscoelastic model which is not an instantaneous shock to the material rather it follows a gradual deformation with respect to the force applied, this model could be used for further research in this area. Figure 4.9 shows the contour for strain on the tissue surface with time along with the strain versus time plot for a particular element.

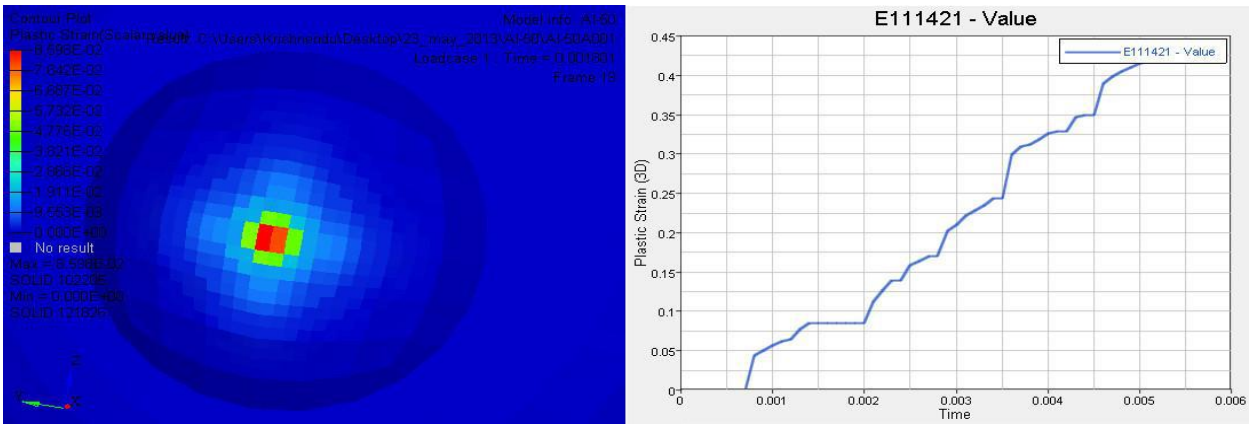

Fig 4.9: *Animation of the simulation on hyperview along with plastic strain on element E111421*

While studying the transient response of stress and strain it has been noticed that strain for viscoeslastic model is much low with respect to elastic model for same time interval and for the same force on the same element. It also holds true while analyzing the strain responses, the energy absorption in viscoelastic model is quiet prompter than that for elastic model. This nature has been depicted in figure 4.10.

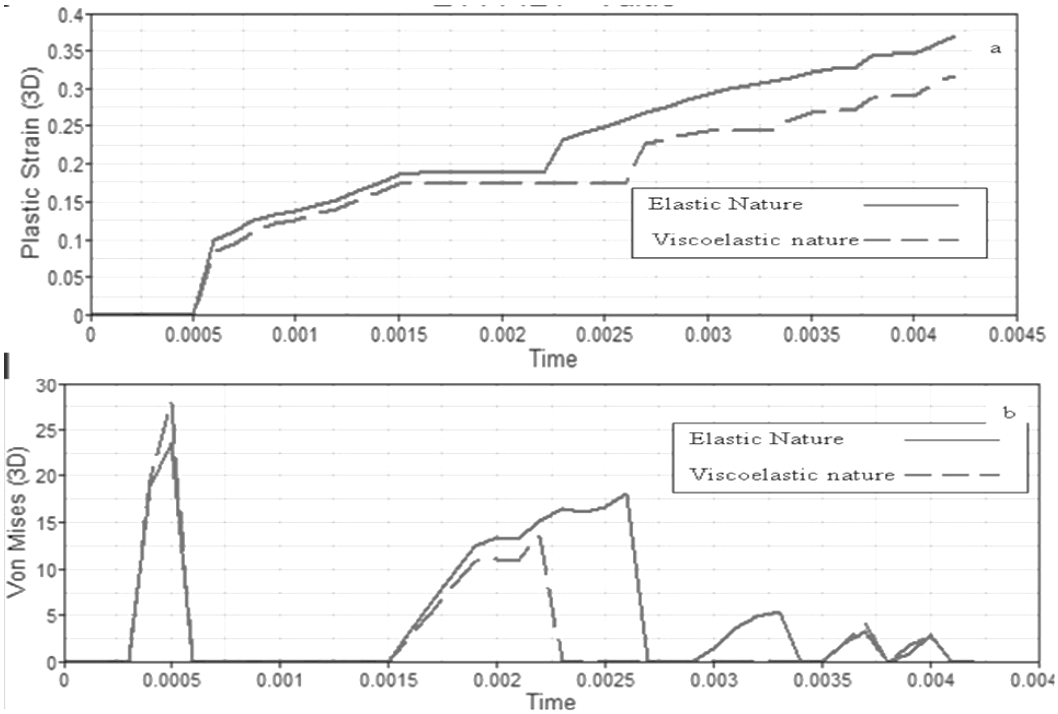

Fig 4.10: *Transient response of strain and stress with time* ***(a)*** *transient response of strain with time,* ***(b)****Transient response of stress with time.*

Cadaver eye cornea transplant reported several issues of donor graft rejection, biocompatibility and such other issues and anti-rejection drugs are commonly administered which could lead to infections. The Generalized Kelvin-Voigt Model that has been used in this study could provide a better alternative for donor cadaver cornea as this model with conjunction to the silica composite synthetic cornea can provide a far better viscoelastic barrier similar to collagen tissues. This behavior of material properties could also be used in artificial soft contact lenses to resist any damage to the prosthesis from crash injuries or environmental hazards.

References

Alvi N.P., Donohue E.K., Curnyn K., Sugar J. 1995, Rupture of radial keratotomy sites after presumed blunt trauma. Ophthalmic Surg Lasers, 26(6), 574-575.

Andreassen T.T., Simonsen A.H., OxlundH. 1980, Biomechanical properties of keratoconous and normal corneas. Exp Eye Res 31,435-441.

Artola A., Ayala M.J., Ruiz-Moreno J.M., De La Hoz F., Alio J.L. 2003, Rupture of radial keratotomy incisions by blunt trauma 6 years after combined photorefractive keratectomy/radial keratotomy. J. Refract Surg. 19(4), 460-462.

Behr M., Arnoux P.J., Serre T., Bidal S., Khang H.S., Thollon L., Cavallero C., Kayvantash K., Brunet C. 2003, A human model for road safety: from geometrical acquisition to model validation with radioss. Comput Methods Biomech Biomed Eng 6, 263–273

Binder P.S., Waring G.O. III, Arrowsmith P.N., Wang C. 1988, Histopathology of traumatic corneal rupture after radial keratotomy. Arch Ophthalmol.;106(11), 1584-1590.

Bryant M.R., Szerenyi K., Schmotzer H., McDonnell P.J. 1994 Corneal tensile strength in fully healed radial keratotomy wounds. Invest Ophthalmol Vis Sci.;35(7), 3022-3031.

Burnstein Y., Klapper D., Hersh P.S. 1995, Experimental globe rupture after excimer laser photorefractive keratectomy.ArchOphthalmol. 113(8), 1056-1059.

Campos M., Lee M., McDonnell P.J. 1992, Ocular integrity after refractive surgery: effects of photorefractive keratectomy, phototherapeutic keratectomy, and radial keratotomy. Ophthalmic Surg, 23(9), 598-602.

Cappon H., Mordaka J., van Rooij L., Adamec J., Praxl N., Muggenthaler H. 2007. A computational human model with stabilizing spine: a step towards active safety. SAE Technical Paper no. 2007-01-1171.Warrendale, PA, USA: SAE International.

Dar F.H., Meakin J.R., Aspden R.M. 2002, Statistical methods in finite element analysis. J. Biomech., 35, 1155– 1161

Delotte J., Behr M., Baque P., Bourgeon A., Peretti F., Brunet C. 2006, Modeling the pregnant woman in driving position, SurgRadiolAnat, 28, 359-363.

Edmund C. 1989, Corneal topography and elasticity in normal and keratotonic eyes: a methodological study concerning the pathogenesis of keratoconus. ActaOphthalmolSuppl 193,1-36.

Elsheikh A., Wang D., Brown M., Rama P., Campanelli M., PyeD. 2007, Assessment of corneal biomechanical properties and their variation with age.Curr Eye Res 32,11-19.

Fisher R.F. 1969, Elastic constants of the human lens capsule, The J. of Physiology, 201, 1-19.

Fraga F., van Rooj L., Symeonidis I., Peldschus S., Happee R., Wismans J. 2009. Development and preliminary validation of a motorcycle rider model with focus on head and neck biofidelity, recurring to line element muscle models and feedback control. Paper presented at: 21st International Technical Conference on the Enhanced Safety of Vehicles; Jun 15–18; Stuttgart, Germany.

Geringer J., Atmani F., Forest B. 2008, Friction Corrosion of AISI 316L/Bone Cement and AISI 316L/PMMA contacts: ionic strength on tribological behavior 267(5-8), 763-769.

Giovinazo V.J. 1987, The ocular sequelai of blunt trauma, Adv Ophthalmic Plast Reconstruct Surg, 6, 107

Glasgow B.J., Brown H.H., Aizuss D.H., Mondino B.J., Foos R.Y. 1988,Traumatic dehiscence of incisions seven years after radial keratotomy. Am J. Ophthalmol. 106(6), 703-707.

Glass D.H., Roberts C.J., Litsky A.S., Weber P.A. 2008, A Viscoelastic Biomechanical Model of the Cornea Describing the Effect of Viscosity and Elasticity on Hysteresis. Invest Ophthalmol Vis Sci49, 3919–3926

Goldberg M.A., Valluri S., Pepose J.S. 1995, Air bag-related corneal rupture after radial keratotomy. Am J. Ophthalmol. 120(6), 800-802.

Gregory S. 2010, Formulas for Mechanical and Structural SHOCK and IMPACT, CRC Press.

Gupta O.P. 2000, Finite and Boundary Element Methods in Engineering, Oxford and IBH Publishing Co. Pvt. Ltd.

HjortdalJ.O. 1995, Extensibility of the normo-hydrated human cornea.ActaOphthalmolScand 723, 12-17.

Huang S.C. 1995, Biomechanical Modeling and Simulations of Automobile Crash Victims, Computers &Strucrures , 57(3), 541-549

Ivarsson B., Kerrigan J., Lessley D., Drinkwater D., Kam C., Murphy D., Crandall J., Kent R. 2005. Dynamic response corridors of the human thigh and leg in non-midpoint three-point bending.2005 SAE World Congress, Detroit, MI, USA.Paper No. 2005-01-0305.

Jingwen et al, 2011, A Stochastic Visco-hyperelastic Model of Human Placenta Tissue for Finite Element Crash Simulations, Annals of Biomedical Engineering, 39(3), 1074-1083.

Jue B., Maurice D.M. 1986, The mechanical properties of rabbit and human cornea. J Biomech 19,847-853.

Kerrigan J., Drinkwater D., Kam C., Murphy D., Ivarsson B., Crandall J., Patrie J. 2004. Tolerance of the human leg and thigh in dynamic latero-medial bending. International J. Crashworthiness, 9 (6), 607–623.

Kuhn F., Morris R., Witherspoon C.D., et al., 1996, A standardized classification of ocular trauma. Ophthalmology, 103, 240–243.

Kung J.S., Lucca J.A., Santamaria J. II.1996; Incision depth vs. incision number in the rupture strength of pig eyes following radial keratotomy. J. Refract Surg. 12(2 Suppl):S294-S296.

Larson B.C., Kremer F.B., Eller A.W., Bernardino V.B. Jr. 1983, Quantitated trauma following radial keratotomy in rabbits. Ophthalmology, 90(6), 660-667.

Lawrence S.T., Amy L.L., Deborah J.R., Kevin J.P. 2002, A Kelvin-Voigt Fractional Derivative Model for Viscoelastic Characterization of Liver Tissue. ASME IntMechEngg Congress and Exposition 32605.

Lee B.L., Manche E.E., Glasgow B.J. 1995, Rupture of radial and arcuate keratotomy scars by blunt trauma 91 months after incisional keratotomy.Am J. Ophthalmol. 120(1), 108-110.

Luttrull J.K., Jester J.V., Smith R.E. 1982, The effect of radial keratotomy on ocular integrity in an animal model. Arch Ophthalmol, 100(2), 319-320.

Material Laws.Large Displacement Finite element analysis-Part2.RADIOSS Theory Manual v10.0.,2009.

Maurice D.M. 1957, The Structure and Transparency of the Cornea. J Physiol (London) 136, 263-286.

McKnight S.J., Fitz J., Giangiacomo J. 1988, Corneal rupture following radial keratotomy in cats subjected to BB gun injury. Ophthalmic Surg., 19(3), 165-167.

Mo F., Arnoux P.J., Jure J.J., Masson. C. 2012, Injury tolerance of tibia for car-pedestrian impact, Accident Analysis and Prevention, 46, 18-25.

Moussavi et al., 2012, Finite Element analysis of blunt foreign body impact on the cornea after PRK and LASIK, J. of Refractory Surgery, 28(1), 59 – 64.

Mukherjee S., Chawla A., Karthikeyan B., Soni A. 2007, Finite element crash simulations of the human body: Passive and active muscle modelling, Sadhana, 32(4), 409-426.

Nyquist G.W., Cheng R., Ei-Bohy A., King A. 1985. Tibia bending: strength and response. In: SAE World Congress, Paper No. 851728.

Nguyen T.D., Jones R..E, Boyce B.L. 2007, Modelling the Anisotropic Finite – Deformation Viscoelastic Behavior of Soft Fiber-Reinforced Composites. Int J Solids Struct 44,8366-8389.

Nguyen T.D., Jones R.E., Boyce B.L. 2008, A Nonlinear Anisotropic Viscoelastic Model for the Tensile Behavior of Corneal Stroma. J BiomechEng 130,041020/1-10.

Östh J., Brolin K., Happee R. 2012, Active muscle response using feedback control of a finite element human arm model, Computer Methods in Biomechanics and Biomedical Engineering, 15(4), 347-361

Panda A., Sharma N., Kumar A. Ruptured globe 10 years after radial keratotomy. 1999, J. Refract Surg. 15(1), 64-65.

Peacock L.W., Slade S.G., Martiz J., Chuang A., Yee R.W. 1997, Ocular integrity after refractive procedures.Ophthalmology. 104(7), 1079-1083.

Pearlman M.D., Klinich K.D., Schneider L.W., Rupp J., Moss S., Ashton-Miller J. 2000, A comprehensive program to improve safety for pregnant women and fetuses in motor vehicle crashes: a preliminary report. Am J ObstetGynecol 182, 1554–1564

Pearlstein E.S., Agapitos P.J., Cantrill H.L., Holland E.J., Williams P., Lindstrom R.L. 1988, Ruptured globe after radial keratotomy. Am J. Ophthalmol. 106(6), 755-756.

Pinheiro M.N.Jr, Bryant M.R., Tayyanipour R., Nassaralla B.A., Wee W.R., McDonnell P.J. 1995, Corneal integrity after refractive surgery. Effects of radial keratotomy and mini-radial keratotomy.Ophthalmology.; 102(2), 297-301.

Rupin F., Amena S., Dolmas D 2008, .Experimental determination of Young's Modulus and Poisson ratio in cortical bone tissue using high resolution Scanning Acoustic Microscopy and Nanoindentation 123(5),3785-3795.

Rylander H.G., Welch A.J., Fremming B. 1983, The effect of radial keratotomy in the rupture strength of pig eyes. Ophthalmic Surg.; 14(9), 744-749.

Schmitt-Bernard C.F., Villain M., Beaufrere L., Arnaud B. 1997, Trauma after radial keratotomy and photorefractive keratectomy. J. Cataract Refract Surg. 23(5), 803-804.
Serre T., Brunet C., Bidal S., Behr M., Ghannouchi S.E., Chabert L., Durand F., Cavallero C., Bonnoit J. 2002, The seated man: geometry acquisition and three-dimensional reconstruction. SurgRadiolAnat 24, 382–387.

Strong W.J. 2004, Impact Mechanics, Cambridge University Press (CUP).

Tropiano P., Thollon L., Arnoux P.J., Huang R.C., Kayvantash K., Poitout D.G., Brunet C. 2004, Using a finite element model to evaluate human injuries application to the HUMOS model in whiplash situation. Spine 29, 1709–1716.

Uchio E., Ohno S., Kudoh J., Aoki K., Kisielewicz L.T. 1999, Simulation model of eyeball based on finite element analysis on a supercomputer, Br. J. Opthalmol, 83, 1106 – 1111.

Uchio E., Watanbe Y., Kaonosono K., Matsuako Y., Goto S. 2003, Simulation of airbag imoact on eyes after photorefractive keratectomy by finite element analysis method, Graefe's Arch ClinExpOphthalmol, 241, 497-504.

Vinger P.F. 1994, The eye & sports medicine, In Duane's Clinical Ophthalmology, 1-94
Vinger P.F., Mieler W.F., Oestreicher J.H., Easterbrook M. 1996, Ruptured globes following radial and hexagonal keratotomy surgery. Arch Ophthalmol. 114(2), 129-134.

Weaver A.A., Kenedy E.A., Duma S.M., Stitzel J.A. 2011, Evaluation of Different Projectiles in Matched Experimental Eye Impact Simulations, J. of Biomechanical Engineering, 133, 031002-1- 031002-10.

Wua J., Nasseri M.A., Eder M., Gavaldon M.A., Lohmann C.P., Knoll A. 2013, The 3D Eyeball FEA Model with Needle Rotation. APCBEE Procedia 7, 4 –10

CHAPTER 5
FRACTIONAL CALCULUS MODEL

5.1 MATHEMATICAL MODEL

Fractional viscoelastic spring-dashpot models are becoming more and more popular presently because their ability of describing the behavior of viscoelastic dampers using a small number of parameters. The use of fractional constitutive models is motivated in large part by the fact that fewer parameters are required to represent material viscoelastic behavior than are required when using traditional models, so such models enable one to vary the rheological parameters in a broad fashion. Additionally, the fractional models are open to analysis using Fourier or Laplace transforms. We note also that experimental results have suggested that the rheological properties that give rise to Viscoelasticity may have a fundamental behavior based on fractional rather than integer calculus .An important difficulty, connected with these models, is the estimation of model parameters. In this paper we consider two standard solid models and comment on their existence and also we consider the fractional order Maxwell model and a combination of both fractional order Maxwell and K-V models

5.1.1 Standard Solid Models Estimation of two such standard solid models has been performed in this work and as a result their creep and stress relaxation has also been studied. Let us consider the following standard solid models: the one having a spring element in series with the K-V element (Fig.5.1) and the other having a viscous dashpot in series with the K-V element (Fig.5.2).

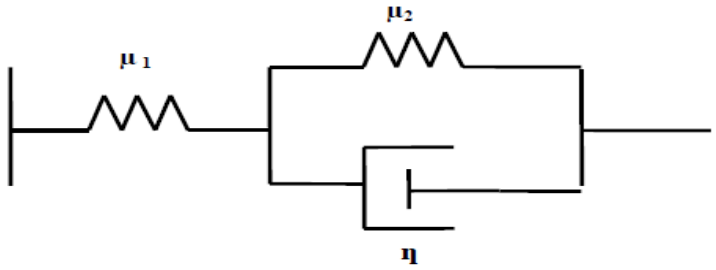

Fig.5.1: *SLS Model with an Elastic Spring Element in series with a KV Element*

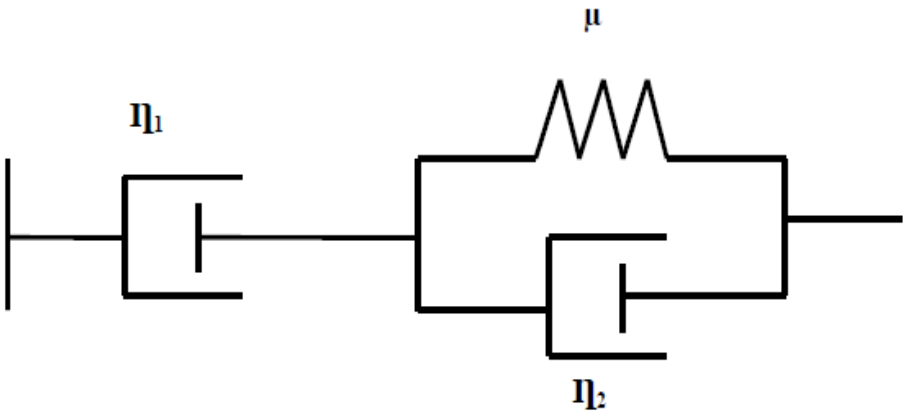

Fig.5.2: *SLS Model with a Dashpot Viscous Element in series with a KV Element*

For the 1st type of standard solid model (as in Fig.5.1) a spring with a varying stiffness is connected in series across a K-V element (a parallel arrangement of the viscoelastic spring-damper system). The 2nd system (Fig.5.2) of solid structure modelling, a viscous fluid in a dashpot arrangement is also connected in series with a K-V element. For both the models, the complete arrangement experiences the same magnitude of stress in both the blocks resembling to that of an Iso-stress model. But, the deformation or the rate of change in strain is not same for both the blocks as the second block comprises of a parallel arrangement of a spring-dashpot system. The 1st model (Fig.5.1) is segregated into the two following blocks (Fig.5.3 (a) & Fig.5.3 (b)) and the governing equations for the complete model are thus deduced:

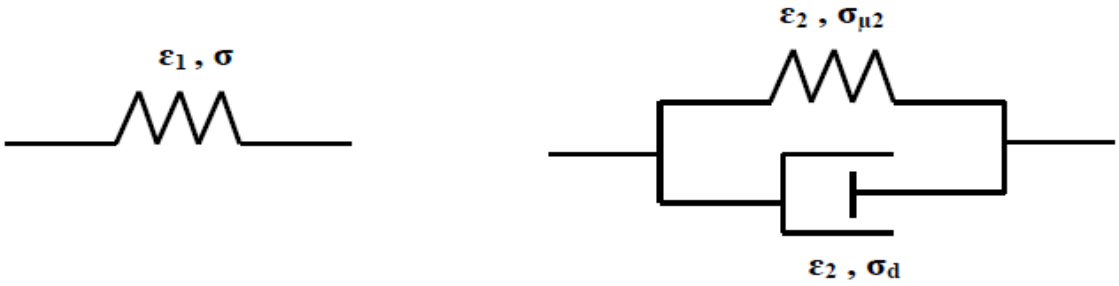

(a) ***(b)***

Fig 5.3: *(a) Spring (elastic) element of the SLS Model, (b) K-V Element of the SLS Model*

From Fig.5.3 (a), there exists only an elastic component having elasticity as μ_1, so a linear relationship between the stress σ and strain ε_1 exists as following:

$$\varepsilon_1 + \varepsilon_2 = \varepsilon$$

$$\varepsilon_1 = \frac{\sigma}{\mu_1}$$

Now, for Fig.5.3 (b), it is a parallel system of a spring with an elastic limit say μ_2 and a dashpot system with a viscous fluid in between having a viscosity of let η. In this particular system, deformation is same in both the components but the total stress is distributed in both the components.

$$\sigma = \sigma_d + \sigma_2^{\mu}$$

$$\sigma_2^{\mu} = \mu_2 \varepsilon_2$$

$$\sigma_d = \eta \frac{d\varepsilon_2}{dt}$$

$$\therefore \sigma = \eta\frac{d\varepsilon_2}{dt} + \mu_2\varepsilon_2$$

Change in strain takes place as a function of time for the viscous model as because as time increases by the virtue of the property of a viscous element, deformation increases as we have seen for the creep nature of a perfectly viscous element. Thus, solving for ε_2 and replacing the values in the first equation, we obtain:

$$\varepsilon\mu_1\mu_2 + \varepsilon\mu_1\eta = \sigma t\mu_2 + \sigma\eta + \mu_1\sigma t$$

Now if we consider the dashpot section of the Figure 5.3(b), then the governing equations can be obtained as:

$$\varepsilon\eta_1 t\mu + \varepsilon\eta_2\eta_1 = t^2\mu\sigma + t\eta_2\sigma + t\eta_1\sigma$$

Hence, the stress relaxation and creep responses for the models are programmed and studied and a time dependent plot for the same is obtained.

5.1.2 Fractional Maxwell Model

The fractional calculus has a long history from 30 September 1695, when the derivative of order α=1/2 has been described by Leibniz (*Oldham & Spanier, 1974; Samko et al., 1993*). There are many interesting books about fractional calculus and fractional differential equations. Derivatives and integrals of fractional order, and fractional integral-differential equations have found many applications in recent studies in physics (*Vasily, 2008*). The non-Newtonian fluids are increasing being considered more important and appropriate in technological applications in comparison with the Newtonian fluids. A large class of real fluids does not exhibit the linear relationship between stress and the rate of strain. Because of the non-linear dependence, the analysis of the behavior of the fluid motion of the non-Newtonian fluids tends to be much more complicated and subtle in comparison with that of the Newtonian fluids.

In recent years there have been several studies (*Rajagopal 1982; Rajagopal& Gupta, 1984; Rajagopal & Bhatnagar, 1995; Rajagopal 1984; Siddiqui et al., 1999; Hayat et al., 1999, Hayat et al., 2000, Hayat et al., 2004*) on flows of non-Newtonian fluids, not only because of their technological significance but also in the interesting mathematical features presented by the equations governing the flow. On the other hand, it is well known that the rheological properties of many fluids are not well modelled by the Navier–Stokes equations. One of the simplest types of model to account for rheological effects of viscoelastic fluid is the Maxwell model. Recently, fractional calculus has encountered much success in the description of Viscoelasticity (*Veliev & Engheta,Naqvi& Abbas, 2004; Hussain & Naqvi, 2006; Naqvi et al., 2006*). In this

present work, we used Laplace transform of fractional derivative, to construct the exact solutions of the viscoelastic nature of human cornea.

Previously, various works have been done considering human cornea as a perfectly viscoelastic mechanical model of three or two components in either series or a parallel combination. As for example, a three-component spring and dashpot model was created in Simulink in MATLAB to represent the purely elastic and viscoelastic behavior of the cornea during a measurement using device called an Ocular Response Analyzer (ORA) (*Dianne et al., 2008*). Works have also dealt with fluids, such as blood, oil, and polymer solution, which not only have the viscosity of the fluid, but also exhibit the elasticity of the solid. These kinds of fluids are often treated as viscoelastic fluids. Because of the difficulty to suggest a single model which exhibits all characteristic of viscoelastic fluids, there exist many viscoelastic models and constitutive equations. Among those the Maxwell model is the simplest one. It is constructed by the series of the spring and dashpot and can qualitatively reflect some properties of the viscoelastic fluid, such as stress relaxation. However, the Maxwell model is a linear model for viscoelastic fluids and it is proper only under the condition that non-linear effects are negligible, such as very low strain and stress. The model also leads to an exponential stress relaxation modulus; for real materials, however, the stress relaxation obeys an algebraic decay (*Hilfer, 2000*).Recently, fractional calculus has encountered much success in the description of Viscoelasticity (*Hernández et al., 2002; Dao & Ti, 1998; Rossikhin & Shitikova, 2001; Palade et al., 1999*). The fractional derivative models with the algebraic stress decay can be easily constructed. And the fractional Maxwell model is one among these fractional models. Experimental research has shown that a better agreement of the experimental data could be achieved with the fractional Maxwell model than the ordinary Maxwell model (*Hernández et al., 2002*).

The fractional Maxwell model can be constructed through the replacement of:

$$\sigma + \lambda^{\alpha} \frac{d^{\alpha}\sigma}{dt^{\alpha}} = \mu\lambda^{\beta} \frac{d^{\beta}\varepsilon}{dt^{\beta}}$$

Where, σ is the shear stress, ε is the shear strain, μ is a shear modulus, λ = η /μ is a relaxation time, η is the constant viscosity coefficient, and α, β are fractional parameters which satisfy

$$0 < \alpha < \beta < 1.$$

First, we introduce the stress–strain relation with fractional-order derivative (*Blare, 1947*):

$$\sigma(t) = \mu\lambda^{\gamma}(d^{\gamma}\varepsilon/dt^{\gamma}), (0 < \nu < 1)$$

A special case of this model is deduced by $\gamma = 0$ as Hooke's Law, which shows the behavior of a perfectly elastic element. Whereas, by placing $\gamma = 1$ we obtain the case of a perfectly viscous element described as the Newtonian Law. Hence, the aforesaid model

can be interpreted as a model interpolated between these two cases. In order to construct the fractional model, we introduce the fractional element defined as the mechanical elements which obey the above equation. A fractional element is determined by three parameters (γ, μ, λ) and is symbolized by a triangle, as shown in Fig.5.4 (c). In the following, we will treat a fractional element as the same status as a spring and a dashpot which are shown in Fig.5.5 (a) and (b) to construct the viscoelastic models.

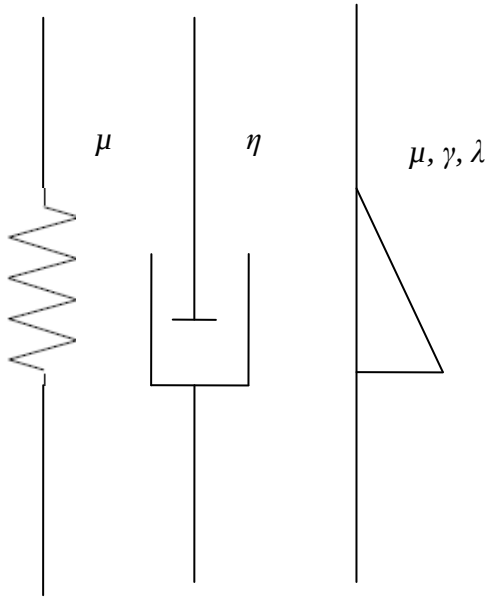

Fig 5.4: *Single Elements (a) Elastic Element, (b) Viscous Element, (c) Fractional Element*

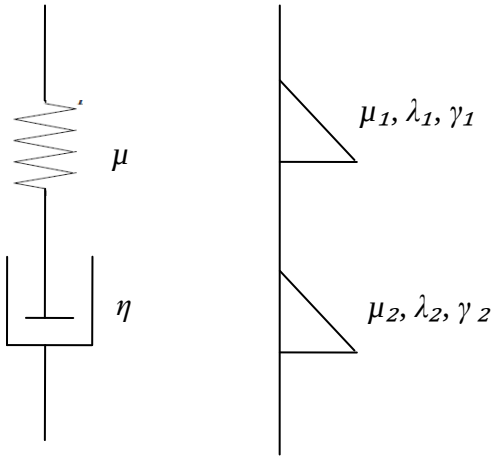

Fig 5.5: *(a) The Classical Maxwell Model, (b) The Fractional Maxwell Model*

Due to series connection of the elements, we obtain (*Youbing& Zhu, 2006*):

$$\sigma(t) + \lambda^{\gamma_1 - \gamma_2} \frac{d^{\gamma_1 - \gamma_2} \varepsilon(t)}{dt^{\gamma_1 - \gamma_2}} = \mu \lambda^{\gamma_1} \frac{d^{\gamma_1} \varepsilon(t)}{dt^{\gamma_1}}$$

This equation is hence the constitutive equation of the fractional Maxwell model.
If we replace $\gamma_1 - \gamma_2$ and γ_1 with α, β respectively, where the above equation is reduced to

$$\sigma + \lambda^{\alpha} \frac{d^{\alpha} \sigma}{dt^{\alpha}} = \mu \lambda^{\beta} \frac{d^{\beta} \varepsilon}{dt^{\beta}}$$

where the two fractional parameters can be written in the form of:

$$\alpha = |\gamma_1 - \gamma_2| \text{ and } \beta = \max\{\gamma_1, \gamma_2\}$$

The procedure is much easier to understand through a generalization of the classical viscoelastic model. With the similar procedure, we can construct other fractional models, such as the fractional Voigt model and so on. It can be seen that this model includes the classical Maxwell model as a special case for $\alpha = \beta = 1$ and the Newtonian fluid model when $\alpha = 0, \beta = 1$.

Taking Laplace Transform of:

$$L\{\sigma + \lambda^{\alpha} \frac{d^{\alpha} \sigma}{dt^{\alpha}}\} = L\{\lambda^{\beta} \frac{d^{\beta} \varepsilon}{dt^{\beta}}\}$$

$$\sigma(s) + \lambda^{\alpha} s^{\alpha} \sigma(s) - \lambda \sum_{k=1}^{\alpha} s^{\alpha-1} \sigma^{(k-1)}(0) = \mu s^{\beta} \varepsilon(s) - \mu \sum_{k=1}^{\beta} s^{\beta-1} \varepsilon^{(k-1)}(0)$$

$$\sigma(s) + \lambda^{\alpha} s^{\alpha} \sigma(s) = \mu s^{\beta} \varepsilon(s)$$

$$\sigma(s)[1 + \lambda^{\alpha} s^{\alpha}] = \mu s^{\beta} \varepsilon(s)$$

$$\sigma(s) = \frac{\mu s^{\beta}}{1 + \lambda^{\alpha} s^{\alpha}} \varepsilon(s)$$

Where, s is the transform parameter, L{f(t)} = F(s) , is the Laplace Transform of the function f(t).

5.1.2.1 Relaxation Modulus of FMM: Assuming $\varepsilon(t) = \varepsilon_0 H(t)$, where, H (t) is the Heaviside unit step function (*Jiagui & Mingyu*), from the last equation derived it can be deduced as:

$$G(s) = \frac{\sigma(s)}{\varepsilon_0} = \frac{\mu s^{\beta}}{s(1 + \lambda^{\alpha} s^{\alpha})}$$

$$G(s) = \frac{\mu}{\lambda^{\alpha}}\left[\frac{s^{\beta-1}}{s^{\alpha} + (1/\lambda)^{\alpha}}\right]$$

Taking the Fractional Parameters as unity and considering the case of an ideal Maxwell viscoelastic equation, i.e. α = β = 1,

$$G(s) = \frac{\mu}{\lambda}\left[\frac{1}{s + 1/\lambda}\right]$$

Hence taking Inverse Laplace Transform of G(s)

$$G(t) = \mu e^{\left(\frac{-t}{\lambda}\right)} \Big/ \lambda$$

5.1.2.2 Creep Compliance of FMM: H(t) being the Heaviside unit step function, and assuming

$$(t) = \sigma_0(t)$$

$$J(s) = \frac{\varepsilon(s)}{\sigma_0} = \frac{1 + \lambda^{\alpha} s^{\alpha}}{\mu s^{\beta+1}}$$

$$J(s) = \frac{1}{\mu}\left\{\frac{1}{s^{\beta-1}} + \frac{\lambda^{\alpha}}{s^{\beta+1-\alpha}}\right\}$$

Replacing the fractional parameter values α = β = 1 and taking Inverse Laplace Transform of the function

$$J(s) = \frac{1}{\mu}\left\{1 + \frac{\lambda}{s}\right\}$$

$$J(t) = t + \lambda \Big/ \mu$$

To compute the stress-strain plot for particular values of the fractional parameters α &β

$\sigma(s) = \frac{\mu s^{\beta}}{1 + \lambda^{\alpha} s^{\alpha}} \varepsilon(s)$, has been simplified according to the corresponding values of the parameters. As for example, at different fractional Brownian motion the values of α is taken as at 1/3, 2/3, 1/2 and at a standard motion at α=1(*Tripathi et al., 2010*). Besides these values two other random fractional values of 1/4 and 3/4 have been taken and simplified for the study to tally with the real time experimental values of human sclera and choroidal strips. As a result the closeness of the points and the nature has been under the consideration.

$$\sigma(s) = \varepsilon(s)\frac{\mu s^{\beta}}{(1+\lambda^{\alpha}s^{\alpha})}$$

$$\varepsilon(s) = \sigma(s) \Big/ \mu[\frac{1}{s^{\beta}} + (\lambda^{\alpha}s^{\alpha-\beta})]$$

5.1.2. 3 Results obtained from FMM

As discussed earlier, constitutive equations involving Fractional Calculus for viscoelastic materials incorporates lesser number of parameters in describing viscoelastic behaviour than any traditional integer models. The work done here is mainly based on reducing the Conventional Maxwell Model to obtain the Fractional Maxwell Model (FMM) in describing the viscous and elastic properties of cornea by replacing the ordinary derivatives of stress-strain by derivatives of fractional order. Here we have made use of Laplace Transform of fractional derivatives to construct the exact solutions of the governing equations and apply Inverse Laplace Transform to compute the graph nature. A number of experimental researches have shown that a better agreement of the experimental data could be achieved with FMM that the ordinary traditional method by a proper selection of the fractional parameters. Solving such Fractional approach equation in order to obtain a plot in Laplace or Fourier Domain has much of mention in a number of literatures. One such mathematical work performed by J.Liu&M.Xu mentions the Fractional model is amenable to analysis using these two methods of transforms.

The strain observed for each set of α & β for values 1/3, 2/3, 1/2, 1, 1/4 & 3/4 have been computed by replacing the fractional parameters in the governing equation of FMM in Laplace domain and a consequent Inverse Laplace Transform of the deduced equation. The values of the fractional parameters have been derived from those of a peristaltic flow of a viscoelastic fluid as in the survey done by *Tripathi et al., 2010.* This section has already covered in the Mathematical Modelling chapter. The computation of this section has been performed by the software WOLFRAM MATHEMATICA 10.2.00 and the corresponding plots have been segregated in Microsoft Excel for the different observations. The list of deformations for the fractional parameter values for stress ranging from 1-5 N/m^2x10^5 have been listed below as in Table5.1.

Table.5.1: *Strain (mm/mm) obtained for α & β of values 1/3, 2/3, 1/2, 1, 1/4 &3/4 for Stress(A)1, (B)1.5, (C)2, (D)2.5, (E)3, (F)3.5, (G)4, (H)4.5, (I)5x10^5 N/m^2*

	α=1/3	α=2/3	α=1/2	α=1	α=1/4	α=3/4
(A) Stress=1*10^5 N/m^2						
β=1/3	0.021	0.023	0.025	0.021	0.023	0.02
β=2/3	0.0195	0.0175	0.018	0.0175	0.021	0.018
β=1/2	0.023	0.023	0.0215	0.022	0.025	0.022
β=1	0.0107	0.00923	0.0097	0.008	0.01175	0.00914
β=1/4	0.019	0.018	0.017	0.02	0.018	0.018
β=3/4	0.018	0.016	0.0165	0.016	0.019	0.016
(B) Stress=1.5*10^5 N/m^2						
β=1/3	0.031	0.034	0.037	0.03	0.035	0.03
β=2/3	0.029	0.027	0.027	0.026	0.032	0.027
β=1/2	0.035	0.035	0.033	0.033	0.038	0.032
β=1	0.016	0.01385	0.0145	0.0135	0.0176	0.01371
β=1/4	0.029	0.028	0.026	0.028	0.028	0.028
β=3/4	0.027	0.024	0.0245	0.024	0.029	0.024
(C) Stress=2*10^5 N/m^2						
β=1/3	0.042	0.038	0.05	0.044	0.046	0.042
β=2/3	0.039	0.175	0.036	0.036	0.042	0.035
β=1/2	0.046	0.046	0.044	0.044	0.05	0.044
β=1	0.0214	0.01845	0.01935	0.018	0.0235	0.01828
β=1/4	0.039	0.036	0.034	0.038	0.031	0.036
β=3/4	0.035	0.032	0.033	0.032	0.038	0.032
(D) Stress=2.5*10^5 N/m^2						
β=1/3	0.062	0.068	0.074	0.062	0.058	0.05
β=2/3	0.058	0.055	0.055	0.054	0.053	0.044
β=1/2	0.07	0.068	0.066	0.066	0.064	0.054
β=1	0.0321	0.0277	0.029	0.028	0.0294	0.02285
β=1/4	0.048	0.046	0.044	0.046	0.046	0.046
β=3/4	0.044	0.04	0.041	0.04	0.048	0.04
(E) Stress=3*10^5 N/m^2						
β=1/3	0.062	0.068	0.074	0.062	0.07	0.06
β=2/3	0.058	0.055	0.055	0.054	0.064	0.052
β=1/2	0.07	0.068	0.066	0.066	0.076	0.065
β=1	0.0321	0.0277	0.029	0.028	0.0352	0.02744
β=1/4	0.058	0.055	0.052	0.055	0.056	0.055

β=3/4	0.053	0.048	0.049	0.048	0.058	0.048
(F) Stress=3.5*10^5 N/m^2						
β=1/3	0.074	0.08	0.09	0.074	0.08	0.075
β=2/3	0.068	0.062	0.065	0.062	0.074	0.062
β=1/2	0.08	0.08	0.076	0.076	0.09	0.075
β=1	0.0374	0.0323	0.0339	0.032	0.041	0.03199
β=1/4	0.068	0.065	0.06	0.065	0.064	0.065
β=3/4	0.062	0.056	0.057	0.056	0.068	0.055
(G) Stress=4*10^5 N/m^2						
β=1/3	0.074	0.08	0.09	0.074	0.08	0.075
β=2/3	0.068	0.062	0.065	0.062	0.074	0.062
β=1/2	0.08	0.08	0.076	0.076	0.09	0.075
β=1	0.0374	0.0323	0.0339	0.032	0.041	0.03199
β=1/4	0.068	0.065	0.06	0.065	0.064	0.065
β=3/4	0.062	0.056	0.057	0.056	0.068	0.055
(H) Stress=4.5*10^5 N/m^2						
β=1/3	0.095	0.1	0.115	0.095	0.105	0.095
β=2/3	0.088	0.08	0.082	0.08	0.096	0.08
β=1/2	0.105	0.105	0.1	0.1	0.115	0.095
β=1	0.0482	0.04156	0.0435	0.04	0.053	0.04113
β=1/4	0.085	0.08	0.08	0.085	0.084	0.08
β=3/4	0.08	0.072	0.074	0.072	0.086	0.072
(I) Stress=5*10^5 N/m^2						
β=1/3	0.105	0.11	0.125	0.105	0.115	0.1
β=2/3	0.1	0.088	0.09	0.09	0.106	0.09
β=1/2	0.115	0.115	0.11	0.11	0.125	0.11
β=1	0.0536	0.0462	0.0484	0.045	0.0586	0.0457
β=1/4	0.095	0.09	0.09	0.095	0.09	0.09
β=3/4	0.088	0.08	0.082	0.08	0.096	0.08

5.1.2.3.1 Observation Made On Nature of Deformation

The 1st set of observation made from the data as in Table.5.1 has been done based on the deformation obtained for each set of the fractional parameter values for each stress.

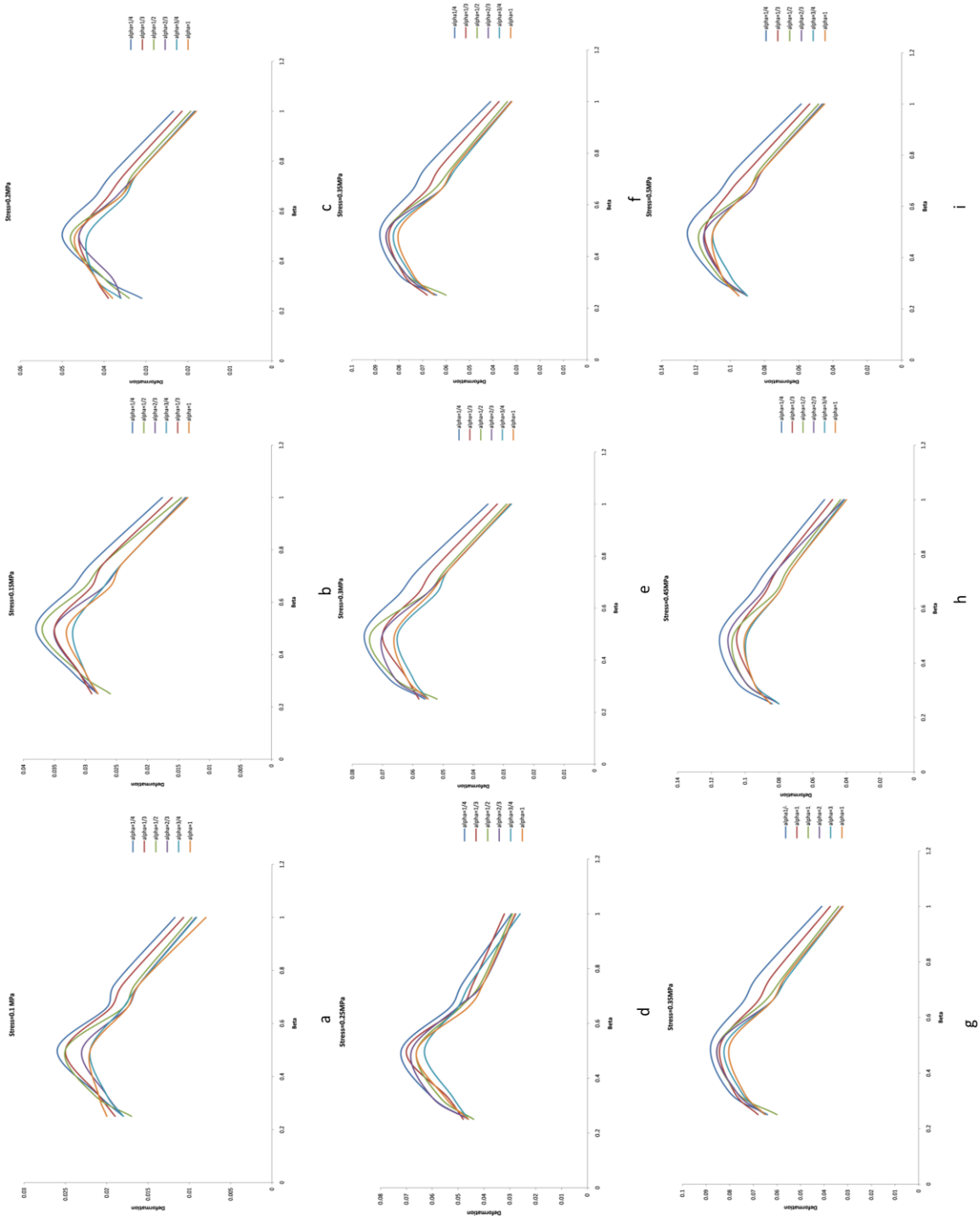

Fig.5.6: *Deformation plots for each set of fractional parameters α & β for (a) Stress=1N/m^2*10^5, (b)Stress=1.5N/m^2*10^5, (c) Stress=2N/m^2*10^5, (d) Stress=2.5N/m^2*10^5, (e) Stress=3N/m^2*10^5, (f) Stress=3.5N/m^2*10^5, (g) Stress=4N/m^2*10^5, (h) Stress=4.5N/m^2*10^5, (i) Stress=5N/m^2*10^5*

A complete observation of the type and range of deformation can be approximated from the plots as in Fig.5.6 (a) to (i) and an idea of the deformations that can be achieved when human cornea is modeled by the Fractional Calculus approach can be concluded.
The maximum deformation achieved has been noticed to be concentrated mostly around β=1/2 & α=1/4. Average value of the maximum deformations is 0.1mm/mm. A table showing the maximum deformations for each stress is shown in Table.5.2.

Table.5.2. *Maximum Deformation Fractional Parameter Combination for Each Stress*

Stress(N/m^2)	**1**	**1.5**	**2**	**2.5**	**3**	**3.5**	**4**	**4.5**	**5**
α	1/4	1/4	1/4	1/2	1/4	1/4	1/4	1/4	1/4
β	1/2	1/2	1/2	1/3	1/2	1/2	1/2	1/2	1/2
Maximum deformation	0.026	0.038	0.05	0.072	0.076	0.088	0.091	0.115	0.125

5.1.2.3.2 Observation Made On Stress-Strain Curve

Before moving on the next section which deals with the stress-strain nature of the corneal Viscoelasticity, it is very much essential to refer to few works done in this context. Two such works referred here have been performed by *Uchio et al., 1999* and *Friberg& Lace, 1988*. Based on these two experimental works, a comparative studyhas been made with that of these theoretically computed points and closeness with the values predicts the almost exact values of the fractional parameters which are to be taken to model the cornea completely. A few comments can be done for these two works for the modelling to complete.
According to the works of *Uchio et al., 1999*, stress strain curve has been plotted as obtained from 12 corneal and scleral samples. 3 pairs of human cadaver eyes were enucleated between 8 and 24 hours after death and stored in a refrigerator at 4°C, and experiments were conducted within 48 hours of enucleation. The ages of the patients from whom the eyes were taken were 64, 78, and 81 years. The main objectives of the work was determination of the Poisson's ratio of the strips and in that context, develop a Finite Element Analysis (FEA) to determine the physical and mechanical conditions of impacting foreign bodies causing Intraocular Foreign body (IOFB) injuries. But for the fulfillment of the objective of the work a stress-strain curve for corneal and scleral samples were presented graphically as shown by the referred Fig.5.7. Increasing levels of stress produce larger amounts of strain. Rupture hence occurred at a mean strain of 18% at mean stress of 9.45 MPa in the cornea and similar values for sclera were 6.8% mean strain for mean stress of 9.49MPa.

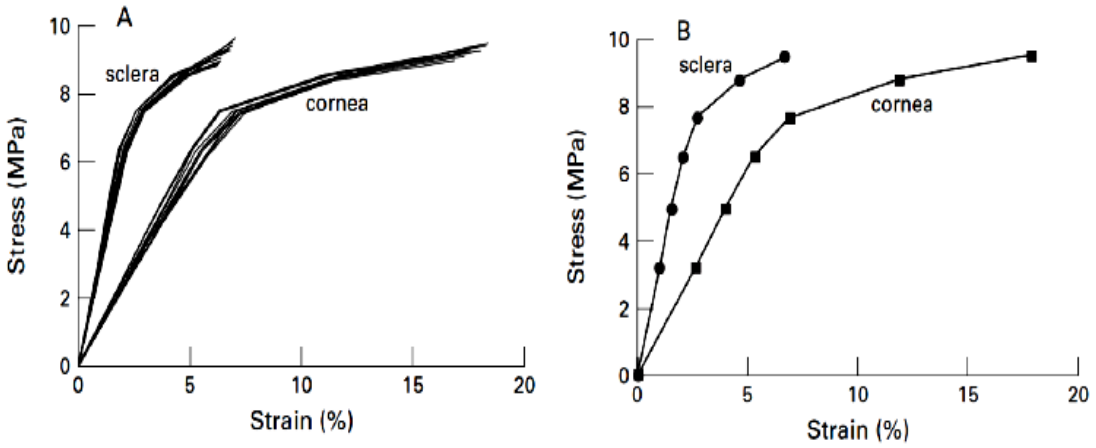

Fig.5.7: *Stress-Strain Curves For Sclera and Cornea both experimentally & by Simulation by the Works of Uchio et al.1999*

The next work to be discussed about in this respect is the work done by *Friberg & Lace, 1988*. The main objective of their work was to determine the rigidity and hence the modulus of elasticity of multiple strips of choroid and sclera by subjecting them to simple tension in a test apparatus. In their experiment, a total of 16 eyes from eight donors were tested. Choroidal data were obtained from 28 strips from each of right and left eye. The same eyes provided 64 scleral strips from various locations including circumferential and radial strips. For every 5s, a strain of 0.5mm/mm was applied in order to obtain the breakage point and hence derive the elastic modulus of the respective strips. In the way of the fulfillment of their aim, they obtained the stress-strain curve nature for the strips which helped to show both the elastic and viscous nature of the tissues hence showing the breakage. In this perspective the nature shown was almost linear with rupturing at a stress of about $6x10^5$ N/m^2 with an average deformation of 0.25 in the sclera and 0.35 in the choroidal tissue. This range of stress has been used in this particular work to tally with the rupturing deformation and also predict the nature of curve and model it mathematically.

The experimental plots of stress-strain for the choroid and sclera have been referred to in Fig.5.8. The plots are done for the strips for the various locations, for sclera the strips are taken from (A) anterior circumferential, (B) radial inferotemporal, (C) radial superonasal and (D) posterior circumferential. Similarly for the choroid strips the locations are (A) radial inferotemporal, (B) radial superonasal and (C) radial superotemporal.

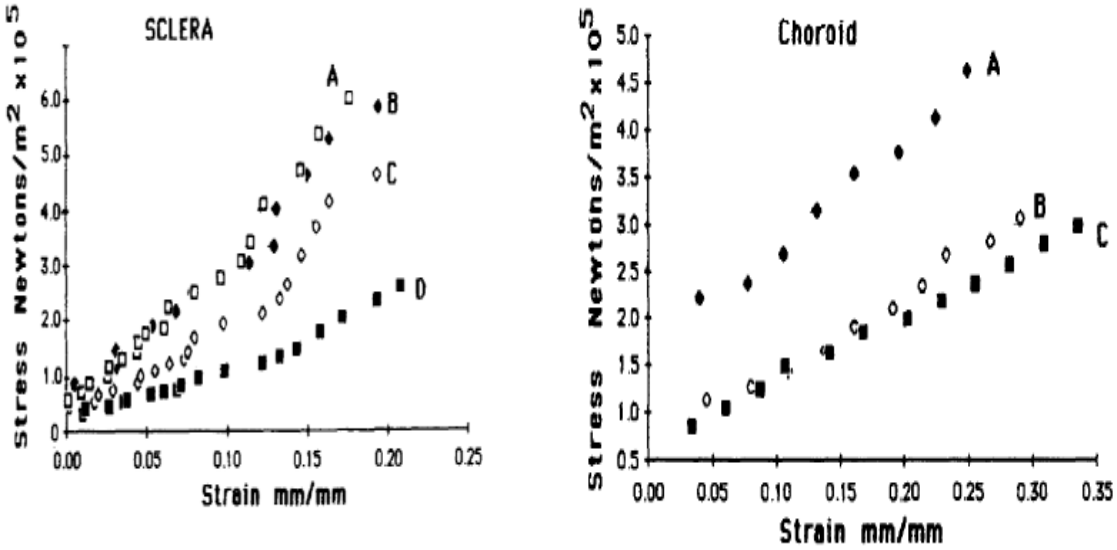

Fig.5.8: *Stress Strain Curve for Choroid and Sclera from the Experimental Works of Thomas R. Friberg & John W. Lace, 1988*

After attaining a conception on the range and nature of deformation, the next observation which needs to be made is the behavior of the stress-strain plot for the same. The stress-strain curve for the aforementioned Fractional Parameter combinations have been obtained and a comparative study to that of the various experimental data obtained from works done by several people on human cornea and sclera has been drawn.

Based on the fractional parameter values, stress-strain plot has been obtained after computation of the values by Inverse Laplace Transform of the governing equation. The plots thus obtained have been compared with the real time experimental results of the works done by *Friberg& Lace in 1988*. The average breakage points experimentally obtained have been tallied with the breakage and nature of the plot for the parameter values.

The stress-strain plots have been arranged for specific values of β in Fig.5.9 (a) to (f) and a comparison plot with the works of Friberg & Lace have been shown in the same plots.

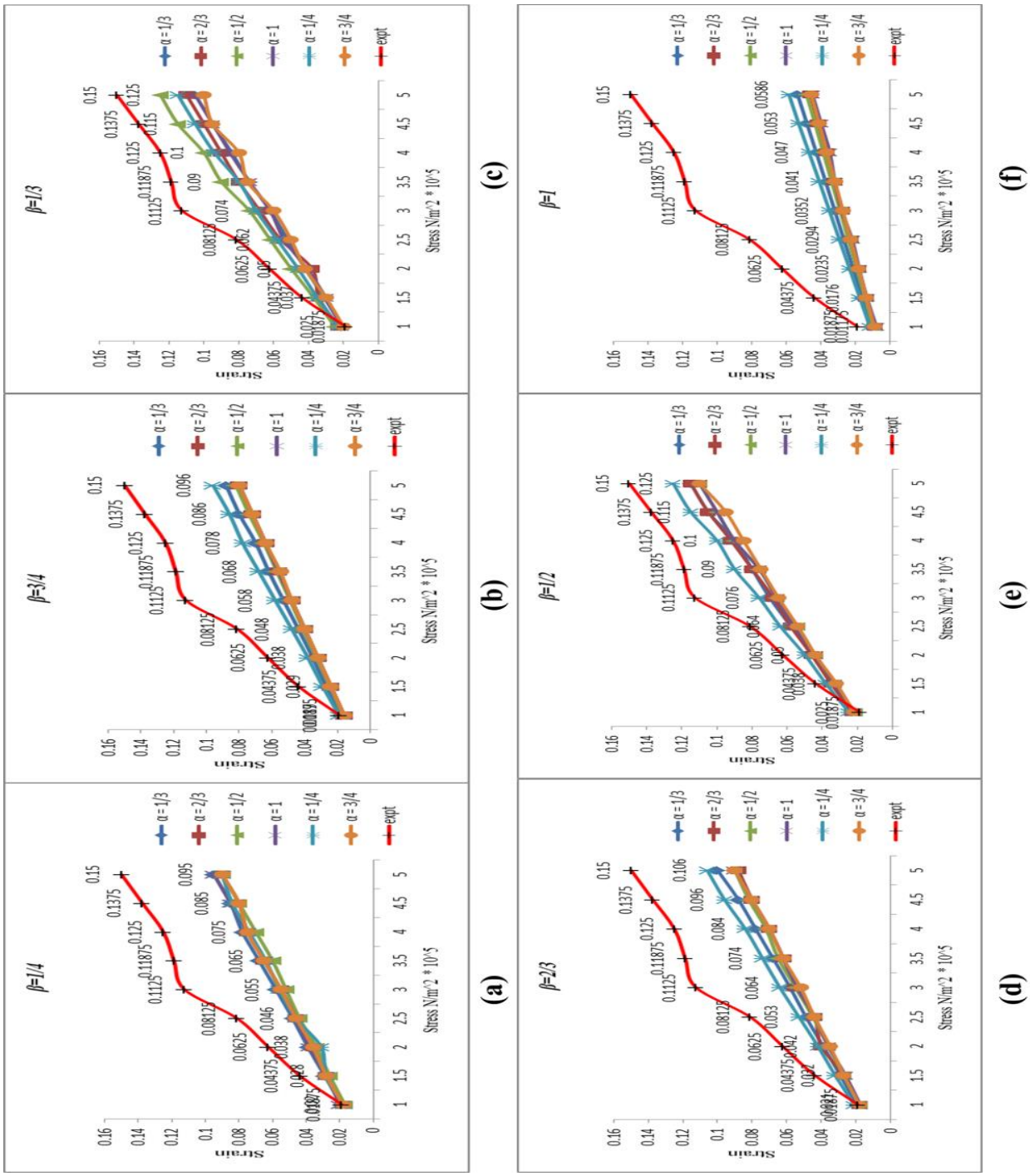

Fig.5.9: *Stress ($10^5 N/m^2$) versus Strain (mm/mm) for Different Values of α With the Discrepancy with Experimental Data by Friberg & Lace for (a) β=1/4, (b) β=3/4, (c) β=1/3, (d) β=2/3, (e) β=1/2, (f) β=1*

It is clearly noted from Fig.5.9 (a) to (f) that the difference between the experimental and theoretical results is minimum for the range of data for β=1/2. The average maximum deformation as already mentioned is said to be lying in the range of values for α=1/4 and

β=1/2. Fig.5.10 shows the complete stress-strain plot for this closely resembled range of the fractional parameters. For this particular set of values of stain the theoretically computed values of deformation closely resembles that of the experimental data obtained from the literatures. As already mentioned, the rupture of the corneal tissues occurs at 18% strain (0.18mm/mm) and 6.8% strain (0.068mm/mm) for the scleral tissues as mentioned by *Uchio et.al, 1999* for MN/m^2 range of force applied at an average stress of 9.4MPa. Similarly *Friberg* at a lower order stress says that for the radial superotemporal strips of cornea, breakage occurs at a deformation of 0.35mm/mm and 0.25mm/mm for the scleral strips approximated at an average stress of $6x10^5 N/m^2$.

It can be summarized that the mathematically computed theoretical values thus obtained shows close similarity with both the obtained experimental results tracing an average deformation of 12.5% or 0.125mm/mm. For such an average value, both the corneal and scleral tissues can be modeled by this Fractional Calculus approach of the Maxwell Model where the originality of the behavior of the curve is retained. A mathematical modeling of the human cornea and sclera nature thus can be obtained by a proper selection of the fractional parameters for the Maxwell Model and not by the conventional one.

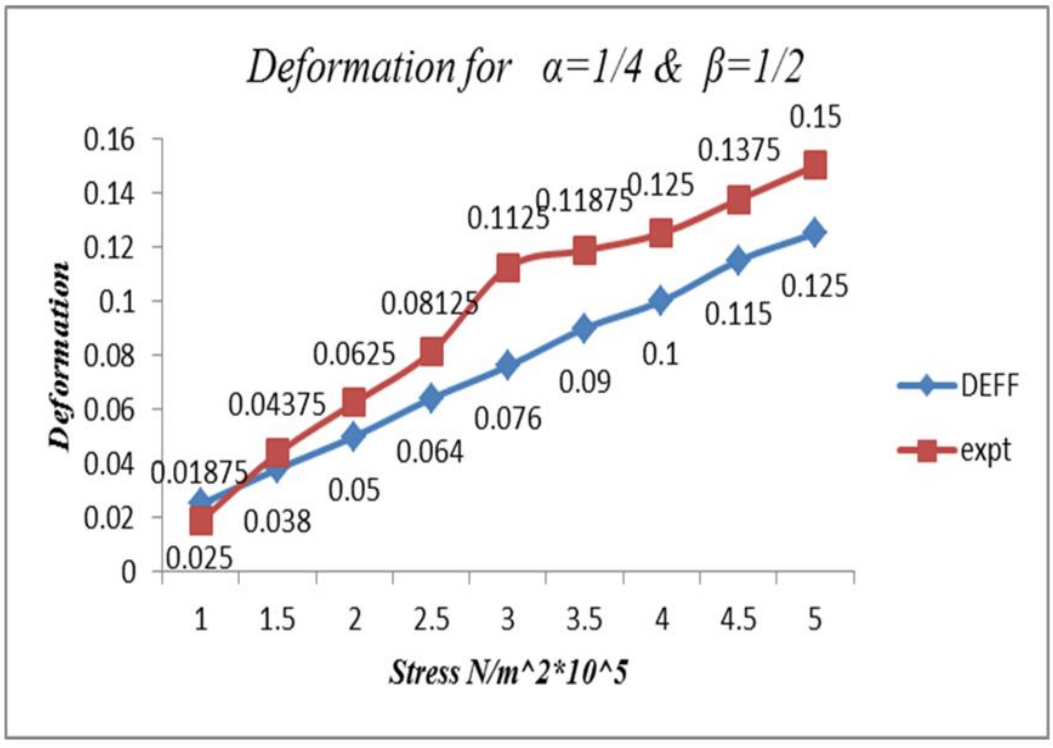

Fig.5.10: *Stress (N/m^2x10^5) versus Deformation (mm/mm) Plot for α=1/4 & β=1/2Showing closely Predicted Nature*

5.1.2.3.3 Violation with the Conventional Maxwell Model

Figure 5.11 shows the stress-strain curve nature for a conventional Maxwell Model which can be well derived by placing the two fractional parameters as unity, i.e. α=β=1. In the

governing equation of FMM, when α & β are put as unity, it takes the nature of the Maxwell Model Equation both mathematically and theoretically.

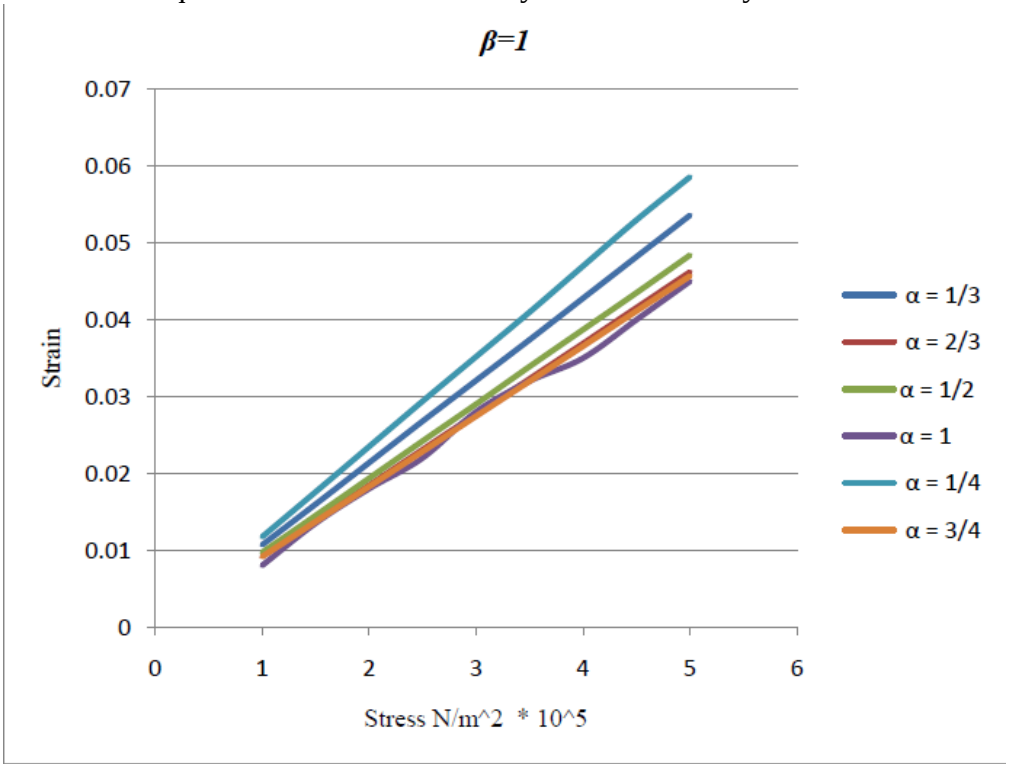

Fig.5.11: *Strain (mm/mm) For Different Fractional Values of α for β=1 Showing the Conventional Maxwell Model Curve for cornea*

Figure 5.12 shows a vast discrepancy between the mathematically obtained nature and the experimentally obtained nature by Friberg & Lace in the stress-strain curve. The maximum deformation obtained for the conventional model lies somewhere between 0.05 and 0.04. From the plot it is evident that the human corneal & scleral tissue viscoelastic nature simply disobeys the form of viscoelastic nature described by the traditional Maxwell Model when either of the parameter attains unit value. Thus the drawback of the Maxwell Model of showing an infinite creep response actually takes place due to the series arrangement of the elastic and viscous components and the human eye nature in this very context does not show any such similarity. The deformation range is much beyond the hold of the theoretically modeled nature and a corresponding change in the viscosity and elastic modulus needs to be changed to attain the desired range of strain. Figure 5.13 shows the difference in the Stress Strain Curve between the Works of Friberg & Lace and Ideal Maxwell Viscoelastic Model with α=β=1.

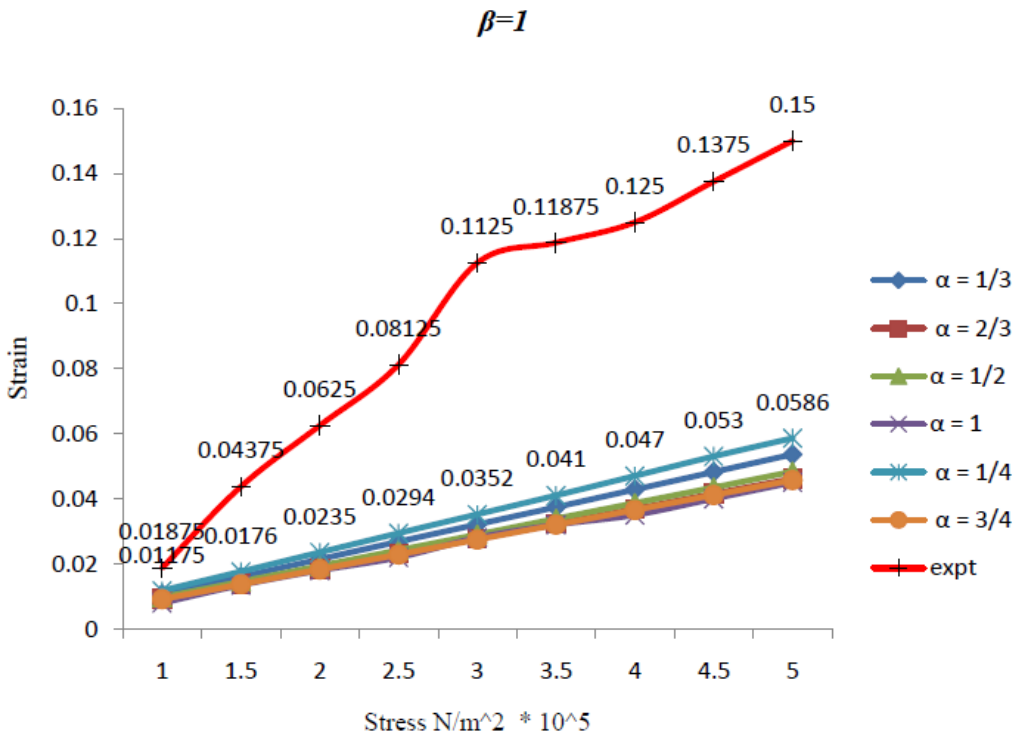

Fig.5.12: *Discrepancy between Experimental Data by Friberg& Lace with the Condition of Fractional Parameter β=1 & α with Several Fractional Values in Order*

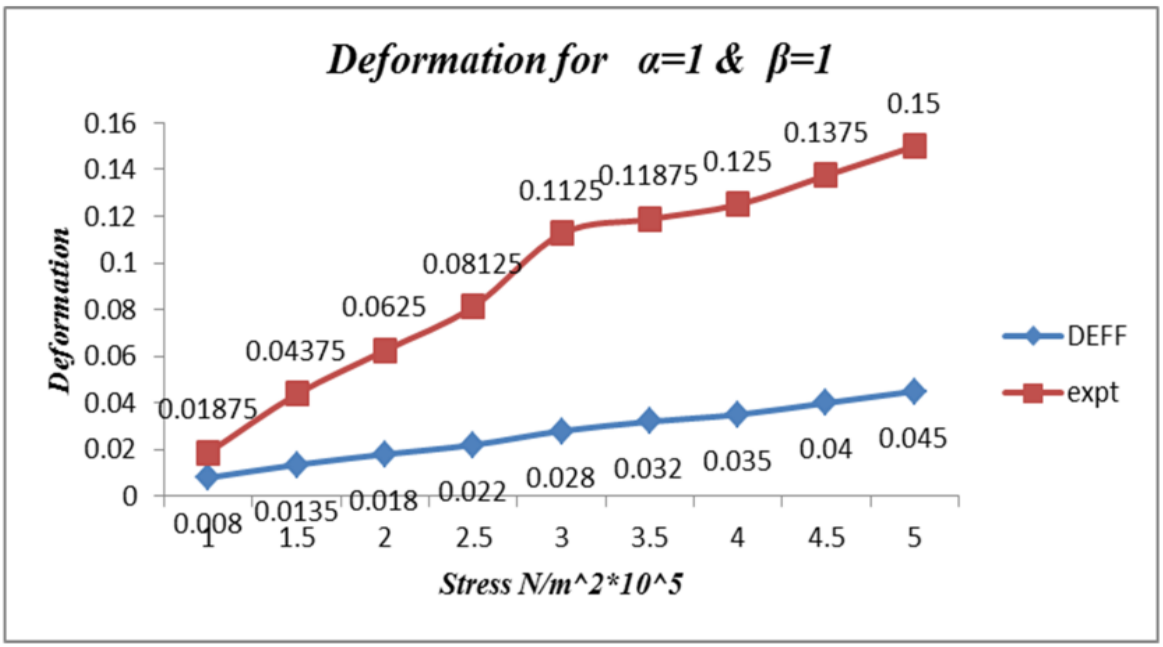

Fig.5.13: *Difference in the Stress-Strain Curve between the Works of Friberg & Lace and Ideal Maxwell Viscoelastic Model with α=β=1*

5.1.3 FMM & KVFD

Results show a vast discrepancy between the nature of plots for FMM and KVFD for the same values of the fractional parameter (Fig.5.14). FMM showing closer approximation with the experimental plots imply KVFD not being a correct choice for a mathematical or simulative study.

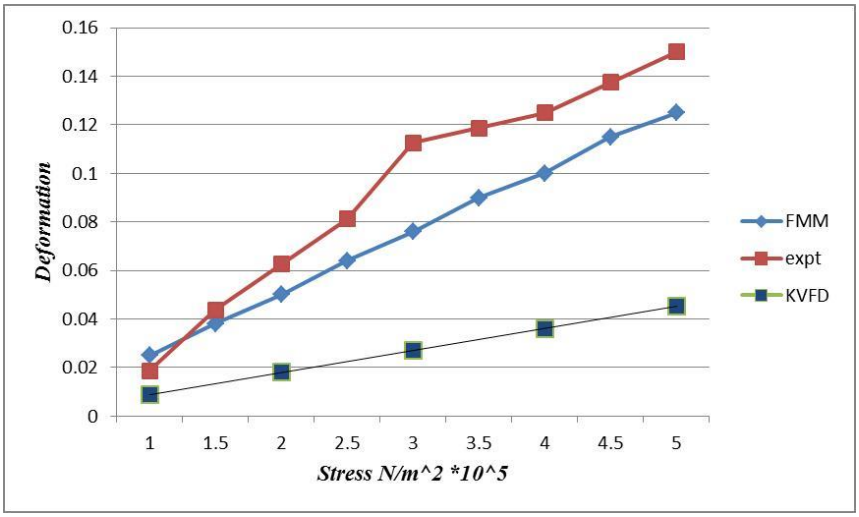

Fig. 5.14: *Difference between the Stress-Strain Nature of FMM and KVFD and Their Discrepancy with Experimental Data*

Change in the nature of the plot for KVFD for different values of the fractional parameter on the other hand is almost negligible as in Fig.5.15, and tabulated in table 5.3 implying the fact that a fractional order implementation on the Kelvin Voigt Model does not help much in improvising the drawbacks of the conventional model and give much detailed study.

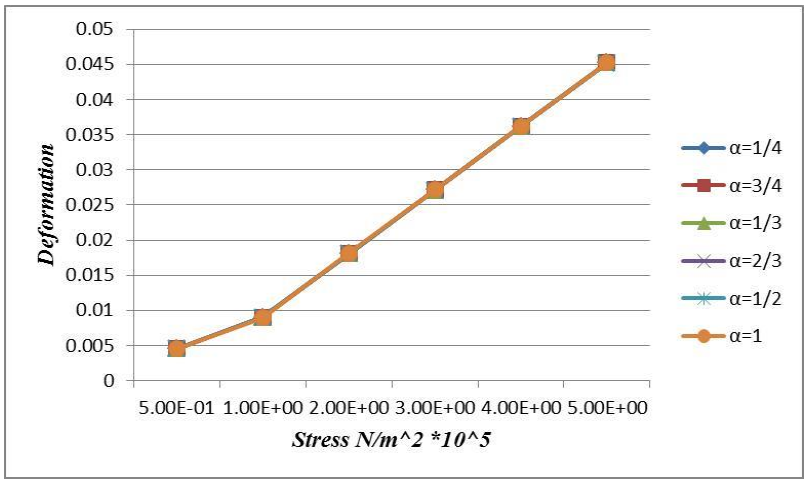

Fig. 5.15: *Stress-Strain Plot for KVFD for Different Values of Fractional Parameter α*

Table 5.3: *Maximum deformation for various stresses for various α values of KFVD model*

Stress	α=1/4	α=3/4	α=1/3	α=2/3	α=1/2	α=1
5.00E-01	0.004519	0.004519	0.004519	0.004518	0.004518	0.004525
1.00E+00	0.009039	0.009038	0.009038	0.009037	0.009036	0.008954
2.00E+00	0.01808	0.01808	0.01808	0.01807	0.01807	0.01809
3.00E+00	0.02712	0.02712	0.02711	0.02711	0.02711	0.02715
4.00E+00	0.03616	0.03615	0.03615	0.03615	0.03615	0.03619
5.00E+00	0.04519	0.04519	0.04519	0.04518	0.04518	0.04525
6.00E+00	0.05423	0.05423	0.05423	0.05422	0.054222	0.05429

5.2 CONCLUSION

A few conclusions that can be drawn from the nature &behavior of the plots so observed and studied for both the KVFD and FMM thus approaching the conventional Models can be summarized as follows.

The human eye thus resembles the Maxwell Model only under the Fractional Calculus where the degree of elasticity and viscosity can be aforementioned.The final values approximation of the fractional parameters as α=1/4 &β=1/2 means: β = max{γ_1,γ_2} = 1/2 &α = |γ_1-γ_2| = ¼. Hence values of the fractional elements γ_1&γ_2 are either 1/4 or 1/2.We know for a perfectly viscous element γ=0 & for a perfectly elastic element γ=1. Figure 5.16 is the graphical abstract of this chapter.

As a conclusion it can be said that the human cornea exhibits viscoelastic tissue behavior with the fractional element lying between the values of perfectly elastic and viscous values with a cling towards elasticity, i.e., the elasticity retains its nature more with a tendency of being viscous. Thus a human cornea actually mimics a viscoelastic soft tissue and can be modeled with fractional parameters. It can also be concluded from this study that the human cornea does not actually behaves a Maxwell viscoelastic tissue and thus does not obey the parameters that to be maintained for a fractional model to be a Maxwell Model i.e., α = β = 1. As mentioned this particular case shows a large demarcation with the experimental data observed in literature works. Study from nature of deformation for both FMM and KVFD on the other hand gives clear views of the validation of the two models. As far as experimental works are considered, KVFD depicts a very small change in deformation for the same range of stress applied thus giving out very less energy losses. As a result KVFD can be preferred to Fractional order Maxwell Model in case of implant design or synthesis for drug delivery related purposes. FMM on the other hand shows more close approximation with experimentally obtained data from cadaver cells.

The results are more realistic as for the similar range of force; deformation is high and attains rupture within a shorter range of stress.

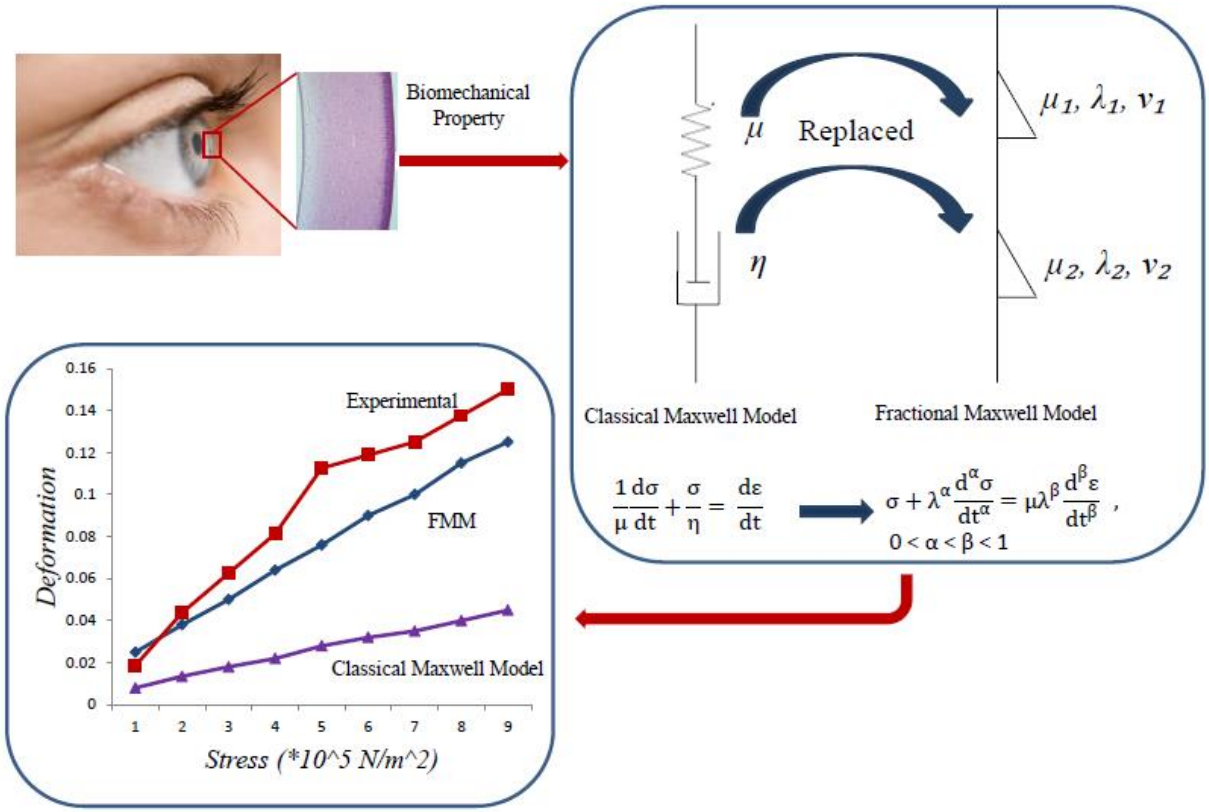

Fig 5.16: *Graphical Abstract*

References

Andreassen T.T., Simonsen A.H., Oxlund H. 1980.Biomechanical Properties of Keratoconous and Normal Corneas. Exp. Eye Res. 31,435-441

Blair G.S. 1947.The role of psychophysics in Rheology. J. Colloid Sci. 1, 21-33

Boyce B.L., Jones R.E., Nguyen T.D., Grazie rJ.M. 2007.Stress controlled viscoelastic tensile response of bovine cornea.40,2367-2376

Charles W., Harald S., Criag B., Keith M.M., Ahmed E. 2015.Biomechanical model of the human cornea: Considering shear stiffness and regional variation of collagen anisotropy and density., J Mech. Behavior of Biomedical Materials 42,76-87

Chen Y.C., Jiang C.J., Yang T.H., Sun C.C. 2012. Development of a human eye model incorporated with intraocular scattering for visual performance assessment. Jour.Of Biomed. Optics 17,075-009

Dianne H.G., Cynthia J.R., Alan S.L., Paul A.W. 2008. A viscoelastic biomechanical model of the cornea describing the effects of viscosity and elasticity on hysteresis. IOVS 49, 3919-3926

Di Y., KeQ.Z. 2010.Start-up flow of a viscoelastic fluid in a pipe with a fractional Maxwell's Model.Computers and Math. With Applications 60 ,2231-2238

Eiichi U., Shigeaki O., Joju K., Koki A., Lech T.K. 1999.Simulation model of an eyeball based on finite element analysis on a supercomputer. Br. J. Opthalmol 83, 1106-1111

Friberg T.R., Lace J.W. 1988. A comparison of the elastic properties of human choroid andsclera. Exp. Eye Res. 47, 429-436

Haitao Q., Mingyu X. 2007.Unsteady flow of viscoelastic fluid with fractional Maxwell Model in a channel.Mech. Res. Comm. 34, 210-212

Hayat T., Nadeem S., Asghar S. 2004. Periodic Unidirectional flows of a viscoelastic fluid with the fractional Maxwell Model. App. Math. And Comp. 151, 153-161

Henk A.W., Gabi E., Fritz S., Cartsen H.M., Wolfgang P., van der H. Rob G.L. 2005.Dynamic mechanical properties of human lenses. Exp. Eye Res. 80, 425-434

Hjortdal J.O.1996. Regional elastic performance of the human cornea. J. Biomech 29, 931-942

Hoeltzel D.A., Altman P., Buzard K., Choe K.I. 1992. Strip Extensiometry for comparison of the mechanical response of bovine, rabbit and human corneas. ASME J. Biomech. Engg. 114, 202-215

Hsichun W., Paul L.P., McD.Peter J.,Wenji V.C.1996. An ultrasonic technique for the measurement of the elastic moduli of human cornea.J. Biomech. 1633-1636

Jue W., Maurice D.M. 1991.The mechanical properties of the rabbit and human cornea", Journal of Biomech. 24, 907-922

Kampmeier J., Radt B., Birngruber R., Brinkmann R.2000. Thermal and biomechanical parameters of porcine cornea.Cornea 19,355-363

Lago M.A., Rupérez M.J., Martínez-Martínez F., Monsserrat C., Larra E., Güell J.L., PerisMartínez C.2015.A new methodology for in vivo estimation of the elastic constants that characterize the patient-specific biomechanical behavior of the human cornea.J. Biomech. 48, 38-43

Liu J., Xu M. Fractional constitutive equations of viscoelastic materials involving three different parameters and their analytical solutions

Maurice D.M.1957.The structure and transparency of the cornea.J.Physiol 136, 263-286

Nathan G.C., Karen B.R., Harry A.Q. 2006.Central corneal thickness and corneal hysteresis associated with glaucoma damage. J. Opthalmol 141,868-873

Nguyen T.D., Jones R.E., Boyce B.L. 2008. A nonlinear anisotropic viscoelastic model for the tensile behavior of the corneal stroma. J. Of Biomech. Engg. 041-020-1

Nyquist G.W. 1968. Rheology of the Cornea: Experimental techniques and results", Exp. Eye Res. 7, 183-188

Shin T.J., Vito R.P., Johnson L., McCarey B.E..1997.The distribution of strain in the human cornea. J. Biomech 30, 497-503

Thomas R.F., John W.L. 1988.A comparison of the elastic properties of human choroid and sclera.Exp. Eye Res. 47, 429-436

Thomas J.S., Raymond P.V., Lindsay W.J., McCarey Bernard E. 1997.The distribution of strain in the human cornea. J. Biomech. 497-503

Tripathi D., Pandey S.K., Das S. 2010.Peristaltic flow of viscoelastic fluid with fractional Maxwell Model through a channel. App. Mathematics and Comp. 215, 3645-3654

Vieru D., Feteau C.2008.Flow of a viscoelastic fluid with the fractional Maxwell Model between two sidewalls perpendicular to a plate.App. Math. And Comp. 200, 459-464

William J.D.Jr., Steven E.W.2006.Biomechanics and wound healing in the cornea.Exp. Eye Res. 83,709-720

Wollensak G., Spoerl E., Seiler T. 2003.Strain-stress measurements of human and porcine corneas after riboflavin-ultraviolet-a-induced cross linking .J. Cataract Refractive Surg., 29, 1780-1785

Woo S.L.Y., Kobayashi A.S., Schlegel W.A., Lawrence C. 1972.Nonlinear material properties of intact cornea and sclera. Exp. Eye Res. 14, 29-39

Youbing Y., Ke-Q.Z. 2006. Oscillating flow of a viscoelastic fluid in a pipe with the fractional Maxwell Model. App.Math. And Comp. 173 ,231-242

Yuan Li L., Brian T. 2006. The anisotropic material constitutive models for the human cornea. J. Structural Biology 153, 223-230

CHAPTER 6

EXPERIMENTAL STUDY ON SYNTHETIC MATERIAL TOWARDS DEVELOPMENT OF SILICA COLLAGEN COMPOSITE

This chapter deals with the development of collagen hybrids and derivation of native collagen from fish skin. The chapter has been divided into two major subparts, they are as follows:

6.1 DEVELOPMENT OF NOVEL SILICA-COLLAGEN COMPOSITE AS CORNEAL SUBSTITUTE

The human cornea is made out of five layers, an overlying epithelium underneath which is a stringy meshwork called Bowman's layer. The greater part of the tissue is constituted by the stroma, a collagen-rich central layer that contains almost 90% of the thickness of the cornea, and underneath this lies Descemet's film which supports the single layer of endothelial cells covering the posterior cornea. In ordinary corneas the greater part of these are thin to the point that light scattering is negligible. For instance, in people, Bowman's layer and Descemet's film, both collagenous tissues like the stroma, together contribute under 4% to the aggregate corneal thickness. The corneal epithelium, on the other hand, is about 53 mm deep (*Reinstein et al., 2008*) and thus constitutes about 10% of the corneal thickness. Its transparency is due to the homogeneity of the refractive index of all its constituent cells (*Dohlman, 1971*). The intrinsic properties of the healthy cornea, namely its strength, transparency and precise curvature enable it to withstand external damage and resist intraocular pressure, whilst also allowing it transmit over 95% of incoming light (*Beems, 1990*) and provide 70% of the focussing power of the eye. These properties are to a great extent represented by the one of a kind engineering of the corneal stroma, which measures around 500 lm in thickness and involves 90% of the aggregate corneal thickness. The physiologically hydrated stroma comprises fundamentally of water (78%) and the protein collagen (15%) (*Maurice, 1984*). Collagen in the corneal stroma is transcendently write I, with littler measures of sorts V, VI, XII, XIII, XIV and XXIV; the presence of sort III collagen in the solid, unwounded corneal stroma is still bantered about (*Ihanamaki, 2004*). Corneal transparency is subject to the particular arrangement of collagen inside the stroma, whereby slender (˜32 nm *Boote, 2003*), equitably dispersed collagen fibrils lie parallel to each other in cross-orientated stacked layers (lamellae). One of the fundamental ultra-basic highlights of 'local' collagen fibrils is the nearness of substituting hole and cover areas along the fibril (D-periodicity), emerging from the amazed relationship of neighboring collagen particles (*Meek, 1983*). This D-intermittent course of action is basic for the development of heterotypic structures comprising of fibrillar collagens and non-collagenous macromolecules. Proteoglycans tie at particular locales along the fibrils (*Scott, 1988 and Meek, 1986*) and assume a part in fibril gathering, framework association and at last corneal transparency (*Maurice, 1957*). Small angle X-beam dispersing designs created from corneal collagen deliver a progression of supposed "meridional" X-beam reflections originating from the D-periodicity and ordering on around 65 nm (*Meek, 1981*). The cornea, not at all like most connective tissues, additionally creates a small angle "equatorial" pattern which is caused

by the consistency of fibril breadths and the customary dispersing of collagen fibrils (over a short range), inside every lamella of the corneal stroma (*Goodfellow, 1978*). Further information about collagen association inside the cornea can be found out from wide point equatorial X-beam disseminating, which emerges from the parallel pressing of the atoms inside the collagen fibrils. Utilizing this strategy it has been demonstrated that human corneal collagen has a normal Bragg intermolecular dispersing of 15 A (*Daxer, 1998*) and that lamellae in the focal locale of the human cornea (in the more profound stromal layers (*Abahussin, 2009*)), are prevalently adjusted in the predominant superior-inferior and nasal-temporal bearings (*Boote, 2006 and Meek, 1987*). It is believed that this course of action, which isn't found in bring down visual keenness species (*Hayes, 2007*), might be important to oppose the powers of the four noteworthy extraocular muscles which embed into the sclera at contradicting positions along every meridian.

Collagen fibrils inside the cornea are smaller than in numerous other connective tissues and this is an essential factor for straightforwardness, which is an element of the measurement (*Hart and Farrell, 1969*). There are around 300 to 400 triple-helical molecules inside the cross-area of a fibril, contingent upon the species (*Meek and Leonard, 1993; Holmes and Kadler, 2005*), which are masterminded pivotally with the run of the mill 67 nm D-occasional stun (*Meek and Holmes, 1983*) with holes between the N-and C-ends of back to back particles (Fig. 6.1).

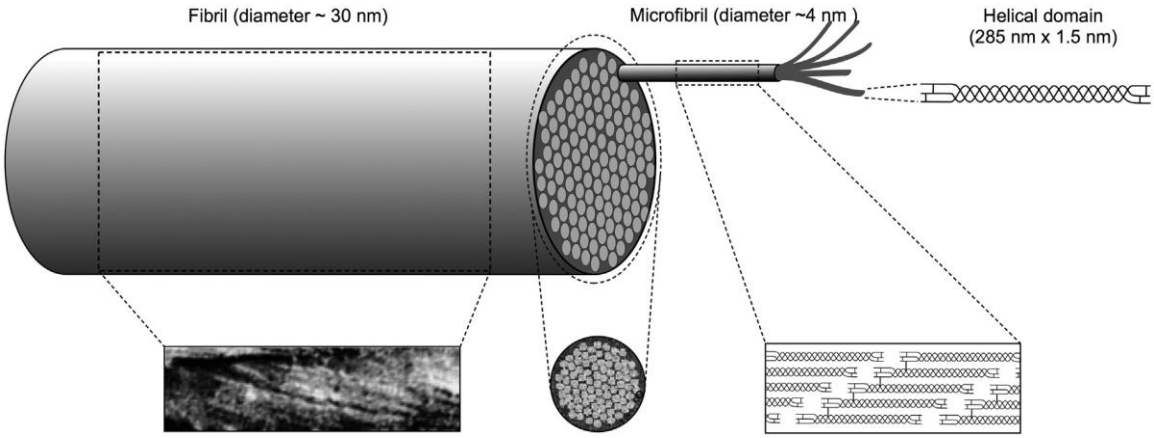

Fig. 6.1*: Structural hierarchy in corneal collagen (not to scale). Three helical alpha chains are supercoiled to produce the collagen triple helix molecule (top right). These molecules self-assemble in a staggered axial array (bottom right) to form microfibrils consisting of five molecules which in turn coil together to form the 30 nm diameter collagen fibrils seen in the electron microscope. The micrograph bottom left is reproduced from Ottani et al. (2002), and shows the coiled microfibrils within the collagen fibril; the micrograph bottom middle is reproduced from Baldock et al. (2002), and shows the microfibrils in cross-section within the collagen fibril.*

An expected 10 million individuals overall experience the ill effects of vision misfortune caused by corneal harm or ailment (*Whitcher, 2002*). For the most pessimistic scenarios,

the main accessible treatment is transplantation with human donor corneal tissue. In any case, there is a serious lack of sheltered, great quality corneal tissue, especially in the Third World and creating nations, prompting different endeavors to create tissue substitutes. Albeit various completely engineered materials have been produced as corneal prostheses, it has been demonstrated that materials in view of normally happening extracellular grid macromolecules have improved biocompatibility (*Carlsson, 2003*).

The experimental part of the research mainly focused on the synthesis and development of Silica-Collagen Hybrids that can substitute normal healthy cornea of human. The main issue that concerns the patients and doctors after a donor corneal transplant is Auto-Immune rejection by host body which may be due to biocompatibility, haemocompatibility or cytotoxicity. The research thrives for synthesis of a composite comprised of Collagen, the basic protein that can be abundantly found in human body and silica which is biosafe and biocompatible to physiological system and can act as a scaffold for tissue engineering and drug delivery.

6.1.1 Chemicals, Instruments and Materials:

The chemicals that had been used for the experiment are listed in table 6.1 below.

Table 6.1: *List of Chemicals required for the experiments*

Sl. No.	Chemicals	Company
1.	Collagen Type I 20ml Solution	Advanced Biomatrix, San Diego, CA
2.	Collagen Type III 10mg Lyophilized powder	Advanced Biomatrix, San Diego, CA
3.	Acetic Acid 99.9%	Sigma Aldrich, India
4.	3-Aminopropyl triethoxysilane (APTES)	Sigma Aldrich, India
5.	De-Ionized water	Merck Germany
6.	Phosphate Buffer Saline (PBS)	Merck Germany
7.	Ethanol	Merck Germany
8.	NaOH pellets	Sigma Aldrich, India

The instruments that was required for the experiments are

1. Magnetic Stirrer, 2 ltrs, 2MLH, Remi, 2016
2. Ultrasonic Bath Sonicator, Analab Scientific Instruments Pvt. Ltd., 2007
3. Centrifuge machine, Remi, 2004
4. Freeze Dryer, Bionics Scientific Technologies (P) Ltd., 2010
5. Incubator, Bioline Technologies, 2015

Along with these instruments other accessories were pH Meter, Laboratory thermometer.

6.1.2 Methodology:

6.1.2.1 Sol Gel Technique: In sol–gel technique, materials are produced through the gelation of solutions or sols. Accordingly, this process is characterized by the low-temperature processing. Additionally, it is noticed that the sol–gel items are basically nanomaterials. Sol– gel preparing can understand different sorts of microstructures, for example, thick, permeable, cross breed, organic– inorganic, undefined, crystalline microstructures, thus it covers an extensive variety of practical materials, for example, optical, electronic, mechanical, concoction and biochemical, and biomedical materials. This adaptability has prompted a considerable number of utilizations in both propelled innovation and novel propelled materials (*Sakka, 2013*).

Sol– gel science is a flexible tool that can be utilized to create natural and inorganic mixture materials that have properties that can be hard to get from just inorganic or natural manufactured methodologies. The engineered approach includes the polycondensation of sol–gel dynamic particles to shape a macromolecular system structure. The sol– gel procedure is utilized to create a porous structure made out of transition metal alkoxides. These structures most generally use a siloxane (Si−O) to frame the spine structure. The blend of these sol– gels includes a hydrolysis of a silicone monomer took after by the buildup of the silica into a porous structure with a three-dimensional arranged structure. The physical structures of these sol– gels can be customized to create structures with an extensive variety of valuable properties and the synthetic surface science can be adjusted to deliver different surface interactions (*Peterson, 2014*). Figure 6.2 illustrates a schematic overview of the technique.

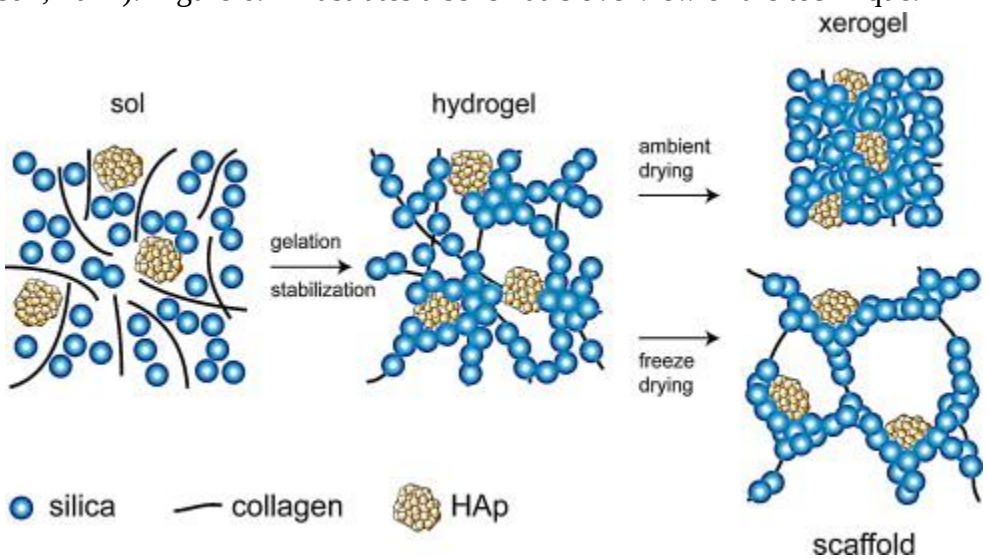

Fig 6.2: *Schematic of Sol Gel method for synthesis of Hap Collagen Scaffold and Xerogel*

***6.1.2.2 Procedure*:** The starting material of the synthesis is a silica precursor, 3-Aminopropyl triethoxysilane (APTES) which had been further diluted with acetic acid in a magnetic stirrer. 600µl of APTES had been diluted with 2.4ml of Acetic acid in an ice

bath ultrasonicator to prevent the elevation of temperature beyond 4°C. Type I collagen solution have a concentration of 3mg/ml. The type III collagen powder had been solubilized with 10ml of Acetic acid to a final concentration of 1mg/ml in a sonicator.
Silica collagen (%w/w) has been maintained at 3:1 and the ration of collagen type I and III has been maintained 7:1 (%w/w). Now 6.8 ml of type I collagen is mixed 3.2 ml of the type III solution earlier formed and thoroughly sonicated for crosslinking the two types of collagen. This collagen solution was further mixed with the diluted APTES solution in a magnetic stirrer for 2 hours in 1200 rpm to ensure proper mixing and enhancing the formation of the bond between the sols at a volume ratio of APTES to collagen 3:10. This mixing had been performed in an ice bath and temperature had been constantly monitored to prevent premature gelation which may occur in higher elevated temperature near room temperature. The solution so obtained is highly acidic. It had been neutralized by 1M NaOH stock solution at 7.43 pH.

The solution had been incubated for 48hours at room temperature for curing to form a gel which is hydrophilic and which can readily solubilize in any liquid medium. The gel so formed is further centrifuged in 15000rpm to extract the pure gel. The extracted gel was poured in petridishes and freezed to -20°C temperature and further lyophilized at -60°C for 48 hours to ensure complete extraction of moisture from the material. The composite so obtained was further washed with Phosphate Buffer Saline (PBS) and incubated for further 48 hours at room temperature of 37°C to ensure and mimic the environment around the composite similar to tissue fluids. The complete process has been schematized in Figure 6.3 a and b.

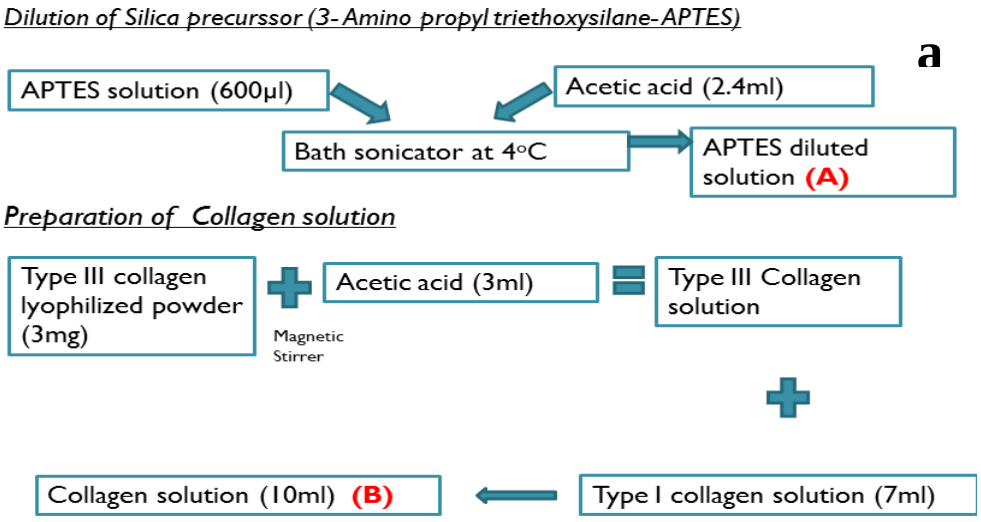

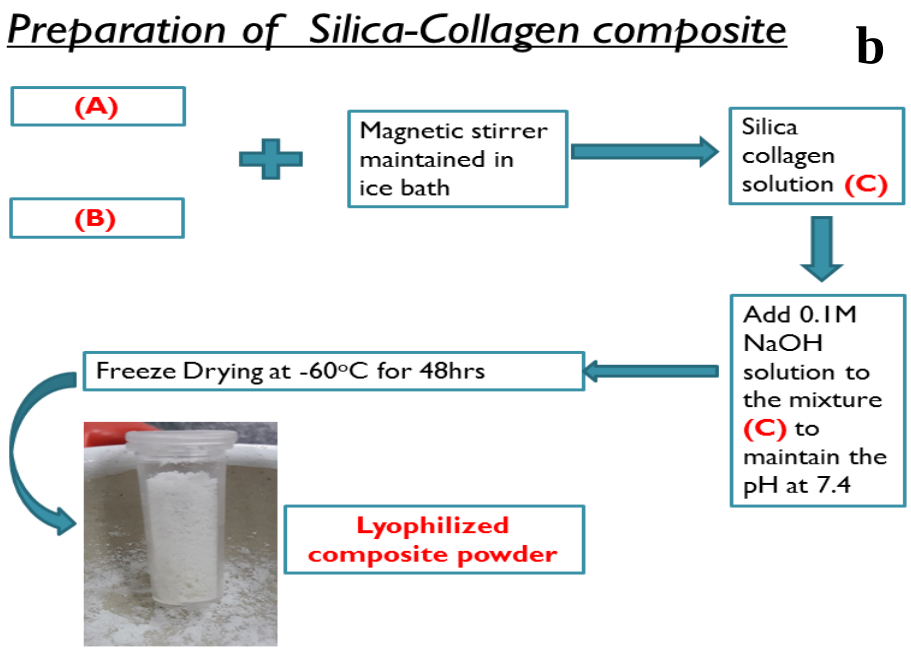

Fig 6.3 a & b: *Schematic diagram for the process of developing Silica Collagen Composite*

The composite now formed is a lyophilized xerogel which had been further characterized to study the microstructure with the help of Scanning Electron Microscopy. Optical properties had been studied in UV-Vis photometer. Further XRD and FTIR patterns had been studied.

6.2 EXTRACTION OF COLLAGEN FROM INDIAN CATFISH (*Sperata Aor*)

Beyond all this research there remains a constraint and that lies on the price of commercial collagen and extensive delay of delivery to Indian states from foreign companies. This is the reason which has given path to extraction of nascent collagen from fish skin in this research.

6.2.1 Collagen extraction process

Collagen can be fundamentally extracted by chemical hydrolysis and enzymatic hydrolysis (*Zavareze et al., 2009*). Chemical hydrolysis is all the more ordinarily utilized as a part of industry, however organic procedures that utilization the expansion of chemicals are additionally encouraging when items with high healthful esteem and enhanced usefulness are required (*Martins et al., 2009*). In addition, enzymatic procedures produce less waste and may diminish the preparing time, however they are more costly. To separate collagen it is important to expel various covalent intra-and

intermolecular cross-links, which fundamentally includes buildups of lysine and hydroxy-lysine, ester securities and different bonds with saccharides, all of which makes the procedure very complex (*Ran and Wang, 2014*).

Prior to the collagen extraction a pre-treatment is performed utilizing a acidic or alkaline process, which varies as per the inception of the crude material. The pre-treatment is utilized to expel non-collagenous substances and to acquire higher yields simultaneously. The most normally utilized extraction techniques depend on the dissolvability of collagen in unbiased saline arrangements, acidic arrangements, and acidic arrangements with included chemicals.

6.2.2 Pre-treatment

Due to the nature of the cross-linked collagen that is available in the connective tissue of creatures, it breaks up gradually, even in bubbling water. Subsequently, a partial chemical treatment is important to break these cross-interfaces previously extraction (*Schreiber and Gareis, 2007*). To this end, weakened acids and bases are utilized, and the collagen is subjected to partial hydrolysis, which keeps up the collagen chains in place however the cross-links are cleaved (*Prestes, 2013*).

In the acidic type of pre-treatment the crude material is drenched in acidic solution until the point when the solution enters all through the material. As the solution infiltrates the structure of the skin at a controlled temperature it swells to a few times its underlying volume and the cleavage of the non-covalent between and intra-molecular bonds occurs (*Ledward, 2000*). The acidic procedure is more appropriate for more delicate crude materials with less interlaced collagen strands, for example, porcine and fish skins (*Almeida, 2012b*).

The alkaline procedure comprises of treating the crude material with a basic solution, normally sodium hydroxide (NaOH), for a period that can take from a couple of days to half a month (*Prestes, 2013*). This procedure is utilized for thicker materials that require a more forceful entrance by the treatment specialists, for example, bovine ossein or shavings (*Ledward, 2000*). NaOH and $Ca(OH)_2$ are regularly utilized for pre-treatment, yet NaOH is better for pre-treating skins since it causes huge swelling, which encourages the extraction of collagen by expanding the exchange rate of the mass in the tissue network (*Liu et al., 2015*).

An examination by Liu et al. (2015) assessed the impact of antacid pre-treatment on the extraction of acid soluble collagen (ASC) from the skin of grass carp (Ctenopharyngodonidella). Concentrations of NaOH from 0.05 to 0.1 M were powerful in

expelling non-collagenous proteins without losing the ASC and basic changes at temperatures of 4, 10, 15 and 20°C. Be that as it may, 0.2M and 0.5M NaOH caused a critical loss of ASC, and 0.5M NaOH brought about auxiliary alteration in the collagen at 15 and 20°C. Notwithstanding the utilization of acids and bases, catalysts or chemicals may likewise be utilized to cut the cross-linked bonds to get products with various qualities (*Schrieber and Gareis, 2007*).

6.2.3 Chemicals, Instruments and Materials:

The list of chemicals required are listed below in Table 6.2

Table 6.2: *List of Chemicals for extraction of Collagen*

Sl. No.	Chemicals	Company
1.	Butyl Alcohol	Merck Germany
2.	NaOH Pellets	Merck Germany
3.	Acetic Acid 99.9%	Sigma Aldrich India
4.	NaCl powder	Merck Germany
5.	DeIonized water	Merck Germany

Fish Skin had been bought from local market. Alongwith these above mentioned chemicals various materials and instruments had been used, viz. 125mm Filter Paper, Electronic balance, Vacuum Filtration unit, Refrigerated Centrifuge machine (Remi C-24BL) and Freeze Dryer.

6.2.4: Methodology

The step has been summarized in figure 6.4. *Sperata Aor* or commonly known as Indian Catfish has a thick layer of epidermal tissue which is a reserve of basic protein, collagen and fats. The fish skin had been bought from local market and preserved in ice before further treatment. The skins were thawed and washed thoroughly first by running tap water and then by deionized water which was kept at ice cool temperature. Skins were further cleaned with 0.8 M NaCl (1:6 w/v), again in the Stephan homogenizer at 5° C for 10 min, and were rinsed with abundant running tap water. This process was repeated for atleast 2 to 3 times and excess water as removed by manual squeezing. The skin was further cut into small pieces and further treated to remove any non-collagenous parts.

For loosening the skin, i.e, for removing non collagenous parts the skin was treated with 0.1M NaOH and thoroughly mixed in a sonicator. After this vigorous mixing the mixture had been kept in normal freezer for 24 hours to enhance proper loosening of the thick fibres. After 24 hours the skin was filtered through double filtration paper and further cleaned with cold deionized water until the pH falls to 7. Following this process the skin was treated with 15% butyl alcohol to remove fats. To make 1 litre of 15% butyl alcohol, 150 ml of the alcohol was mixed in 850 ml of deionized water. The skin was treated in two consequent batches. First 500 ml of butyl alcohol was used to treat the skin mass for 24 hours, then another 500 ml was used for another 24 hours in a normal freezer.

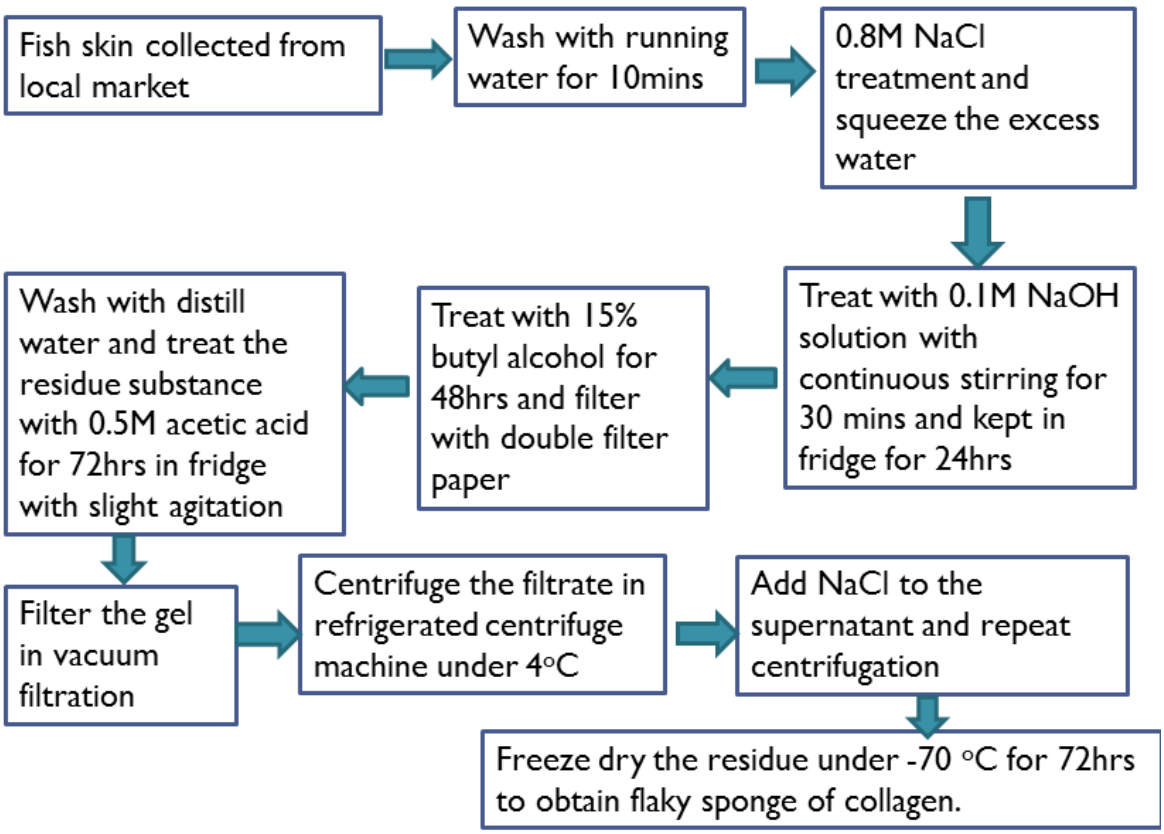

Fig 6.4: *Schematic of the process of Collagen Extraction*

After 48 hours of butyl alcohol suspension, the skin was filtered and washed thoroughly and 1 litre of 0.5M acetic acid had been added to the skin and stirred intermittently. This process is again repeated for another 24 hours. After 72 hours of acid treatment the quasi fluid mixture was filtered in a vacuum filtration unit to ensure that only soluble collagenous parts are filtered as shown in figure 6.5.

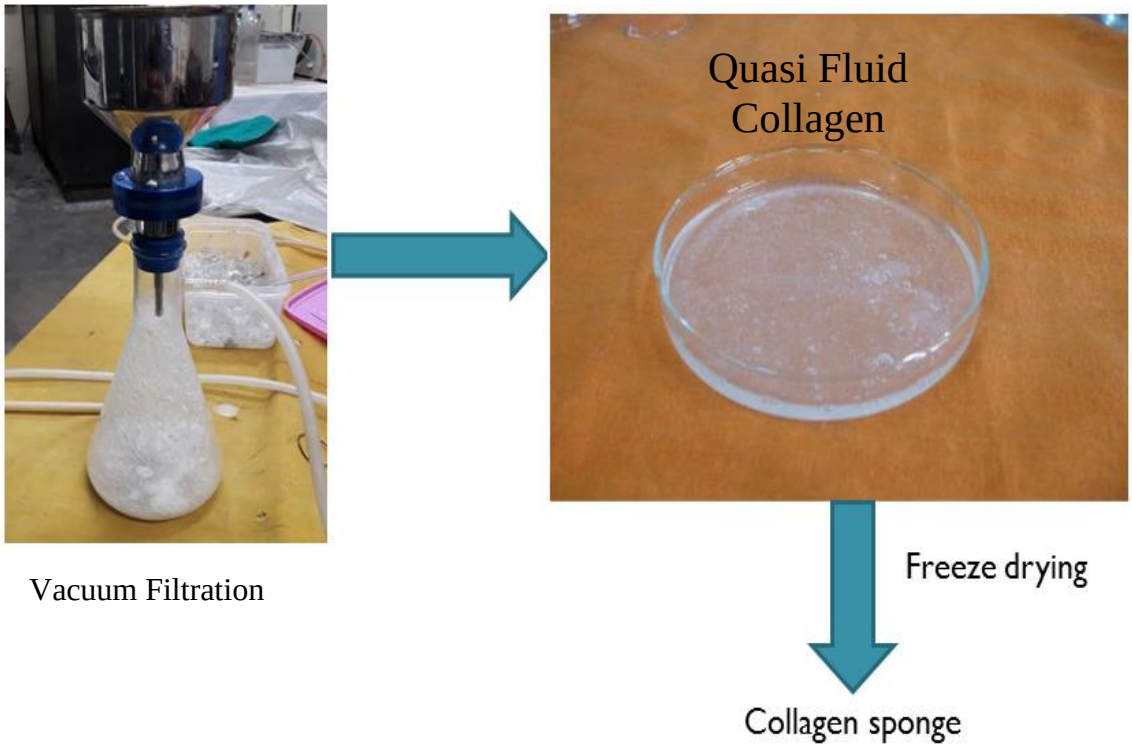

Fig 6.5: *The vacuum filtration unit*

6.3 RESULTS AND DISCUSSION

6.3.1 Fourier Transform Infrared Spectroscopy*:* The FTIR spectra of extracted collagen and silica-collagen composites are presented in Fig. 6.6 a and b. Amide A band corresponds to N-H stretching vibrations was found in the wave range 3419.79 cm^{-1}. Generally Amide A band is obtained in the range of 3400-3440 cm^{-1} *(Tylingo, 2016)* which is an indication that, hydrogen bond network has been constructed for this material. Amide I bond corresponds to carbonyl group stretching vibrations is generally found in the range of 1600-1700 cm^{-1}, here which is found at 1668.43 cm^{-1} *(Li et al.,2013).* Amide II bond corresponds to CN stretching vibrations is found at 1535.34cm^{-1} *(Wang et al. 2008).* The absorbance peak at 1238.30 cm^{-1} corresponds to the peak responsible for Amide III *(Sasmal and Begam, 2014).*

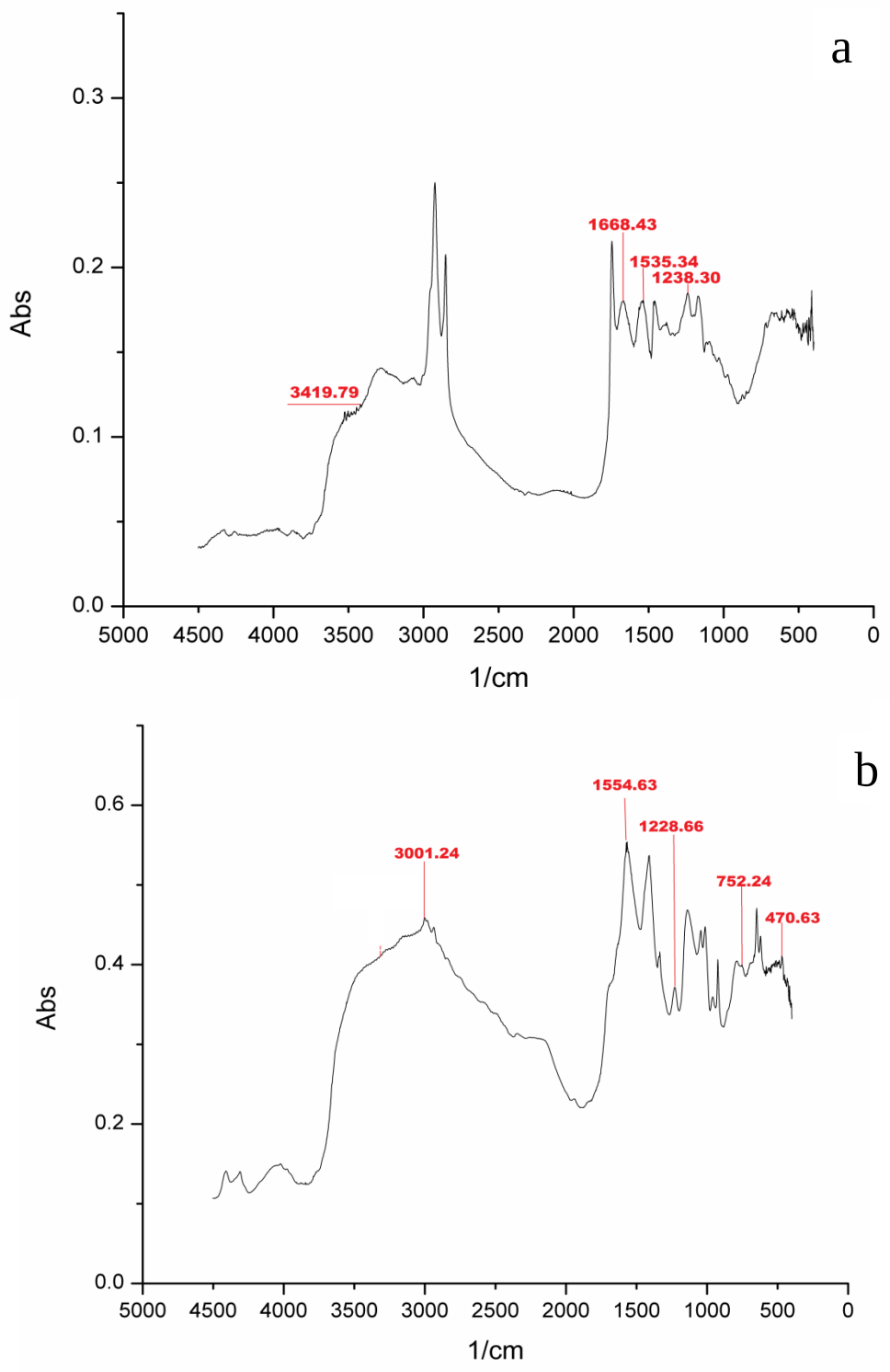

Fig 6.6: *FTIR analysis of* ***(a)****Extracted Collagen and* ***(b)****Silica-Collagen Composite respectively*

From the FTIR Spectra of Silica-collagen composite it was observed that the composite consist characteristic peaks of collagen and silica both. Amide A band was observed at

the wavelength 3001.24 cm^{-1}. Amide II and Amide III was found in the wave range 1554.63 cm^{-1} and 1228.66 cm^{-1} respectively. The stretching mode of Si-OH linkage is observed at 752.24 cm^{-1}. The band at 470.63cm^{-1} is assigned to stretching and bending mode of Si-O-Si of the gel network *(Padmaja, 2001).*

6.3.2 X-ray Diffraction Study: The XRD pattern of extracted collagen and Silica-collagen composite was shown in figure 6.7. It was observed from the diffraction pattern that the specimen consist of Silica phases and there were no other secondary phase. Major peaks were observed at 22, 28, 29, 36, 37, 38, 43 and 48 corresponding to peaks of silica, (002), (210), (211), (112), (130), (222) and (213) planes, respectively. The similar trend was observed by Najafizadeh in 2016 for the peak of Si.

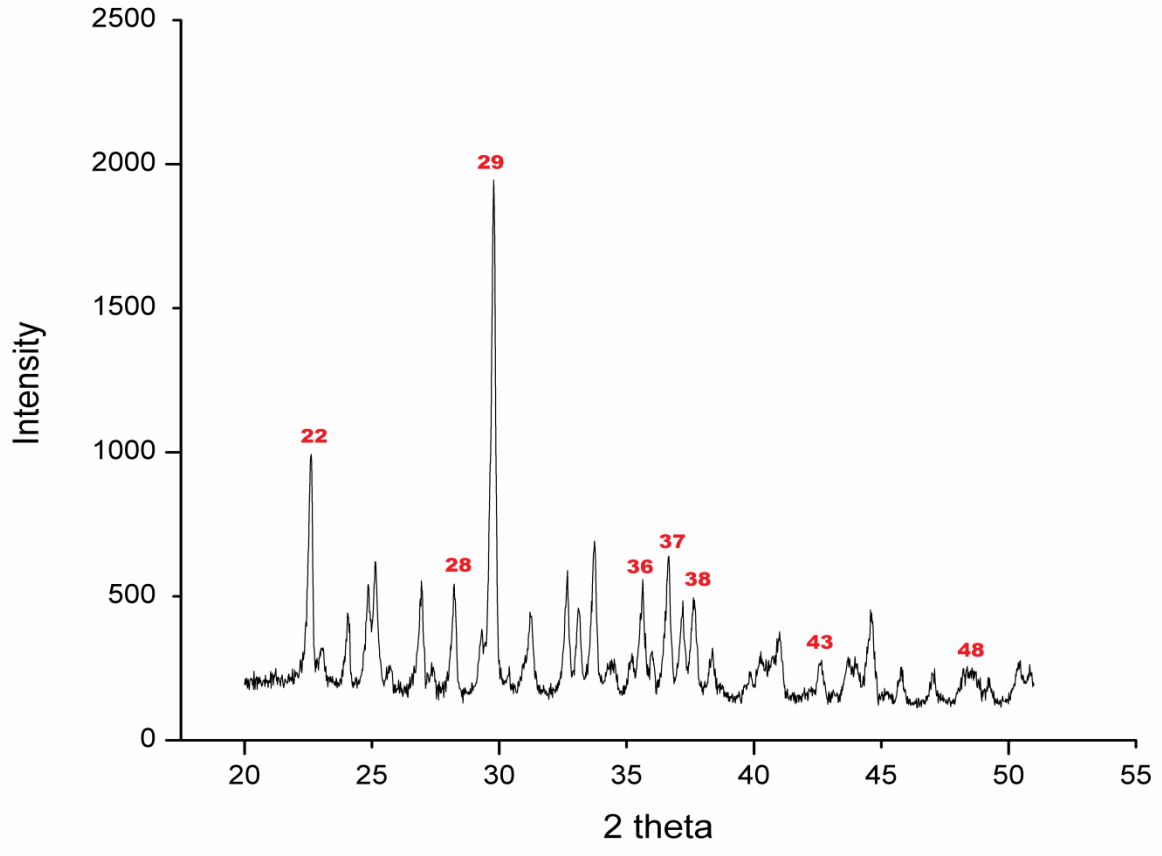

Fig. 6.7: *XRD analysis plot of Silica Collagen composite*

6.3.3 Scanning Electron Microscopy: The microstructure of extracted collagen and silica-collagen composite were investigated by FESEM. The micrograph of extracted collagen in figure 6.8 shows almost spiral structure with few open spaces. Where, in case of silica-collagen composite the particles obtained are spherical in nature with few amorphous aggregates which is porous in nature as shown in figure 6.9.

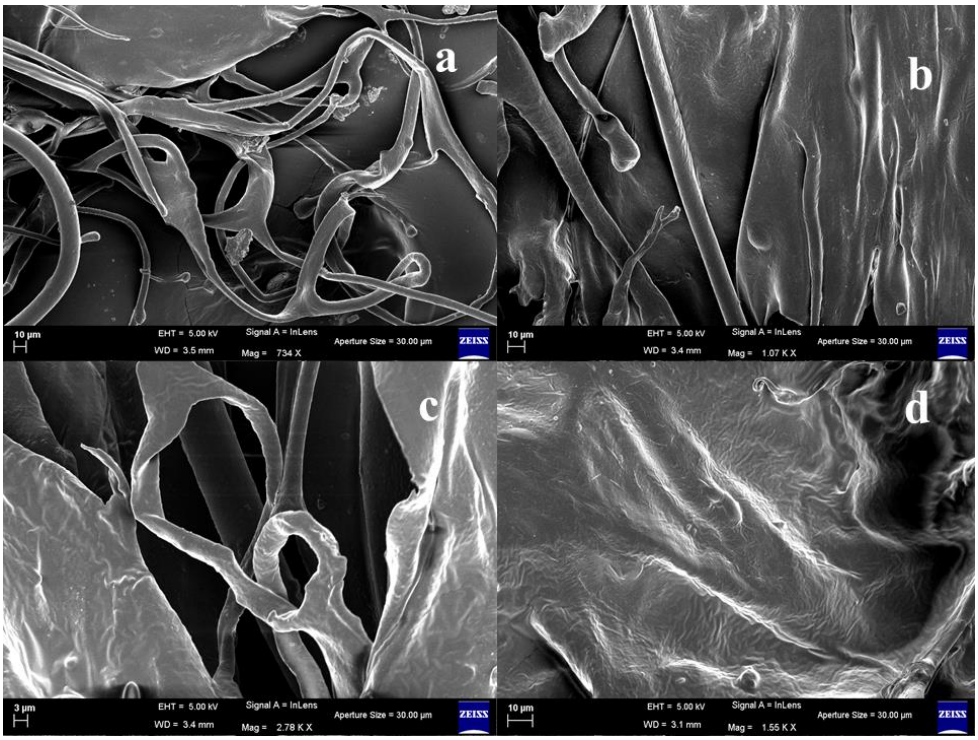

Fig. 6.8: *SEM of extracted collagen at different zooming magnitude showing knotted fibrillar structures*

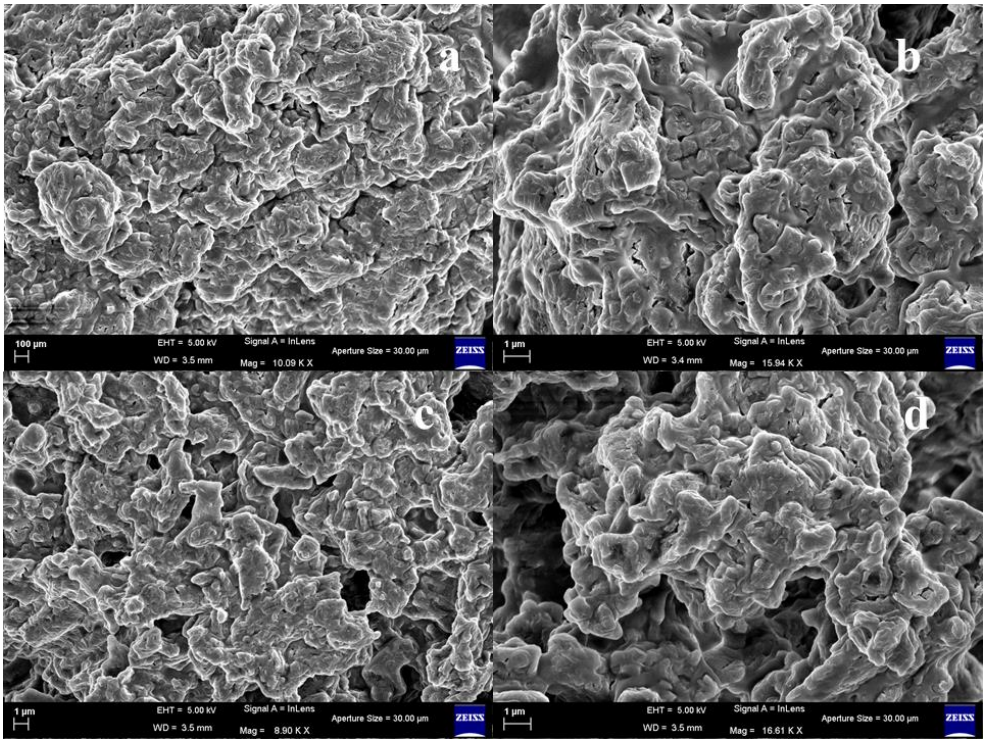

Fig. 6.9:*FESEM of Silica Collagen composite showing porous phases at different magnification levels*

6.3.4 Optical study: Transmittance is the ratio of transmitted light intensity to incident light intensity, which was measured in UV-Vis Meter. A 50 µL of the gel formed was pipetted into the cuvette and allowed to cure at ambient humidity. The transmittance was calculated between 300 to 800nm covering the visible light spectrum. Figure 6.10 shows the plot of transmittance, which shows that the transmittance increases as the wavelength shifts from ultraviolet to infrared regions. The value of transmittance is between 0.8 to 1.0 in the range of 600 to 800 nm and 0.6 to 0.6 for lower wavelength range between 300 to 600. Therefore there is need to work further on the model for improving its optical characteristics.

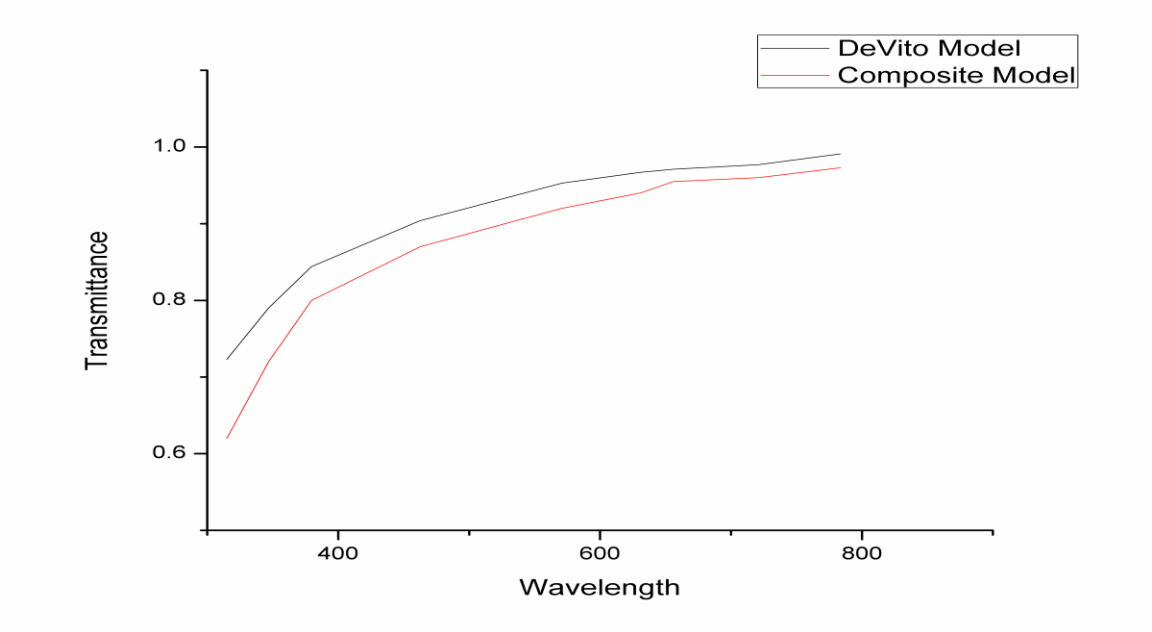

Fig. 6.10: *Transmittance curve for silica collagen composite compared with DeVito Model, 2012*

6.4 CONCLUSION

The extracted material from fish skin showed characteristics absorption peaks for Amide A and Amide I, II and III which is the identification characteristics of Collagen type I. The microstructure of the collagen is fibrillar with some knotted structure and few spaces which has determined its spongy nature. These characteristics confirm the material as predominantly collagen type I.

The FTIR curve of the Silica-Collagen composite showed the characteristic peaks for both collagen and silica phase. The stretching mode of Si-OH and stretching and bending of Si-O-Si can also be seen from the curve which determines proper linking of the two phase while gelation. As collagen is amorphous so the XRD plot shows intensity peaks Si phase at various degrees of rotation among those some are of very high intensity magnitude. The SEM micrograph has a porous phase which is very much likely for any scaffold for tissue growth, regeneration, cell proliferation and targeted drug delivery.

Furthermore there are lots of areas of improving the microstructure and characteristics of these biomaterials like the curing technique could be varied to examine the characteristics of the materials as curing is a very important step in forming the microstructure in nano-science. The swelling nature could be studied for any post-operative swelling of the implant and amount of water absorption. The bonding and linking could be made stronger with some additives like glutaraldehyde or poly vinyl alcohol or some commercial plasticizers. These are the future research interest in these fields to enhance the property and suitability of the collagen and composite to ensure them to be a part of the implant synthesis and the implant itself.

References:

Abahussin M., Hayes S., Knox Cartwright N., Kamma-Lorger C., Khan Y., Marshall J., et al. 2009. 3D collagen orientation study in human cornea using X-ray diffraction and femtosecond laser technology, Invest. Ophthalmol. Vis. Sci. 50, 5159–5164.

Almeida P.F., Vanalle R.M., Santana J.C.C. 2012b. Produção de Gelatina: Uma perspectivacompetitivapara a cadeiaprodutiva de frango de corte. Produto and Produção 13(2), 22-39.

Baldock C., Gilpin C.J., Koster A.J., Ziese U., Kadler K.E., Kielty C.M., Holmes D.F. 2002. Three-dimensional reconstructions of extracellular matrix polymers using automated electron tomography. J. Struct. Biol. 138, 130-136.

Beems E., Van Best J. 1990. Light transmission of the cornea in whole human eyes. Exp. Eye Res. 50, 393–395.

Boote C., Dennis S., Newton R.H., Puri H., Meek K.M. 2003. Collagen fibrils appear more closely packed in the prepupilliary cornea-optical and biomechanical implications. Invest. Ophthalmol. Vis. Sci. 44, 2941–2948.

Boote C., Hayes S., Abahussin M., Meek K. 2006. Mapping collagen organisation in the human cornea: left and right eyes are structurally distinct. Invest. Ophthalmol. Vis. Sci. 47, 901–908.

Carlsson D.J., Li F., Shimmura S., Griffith M. 2003. Bioengineered corneas: how close are we? Curr. Opin. Ophthalmol. 14, 192-197.

Daxer A., Misof K., Grabner B., Ettl A., Fratzl P. 1998. Collagen fibrils in the human Corneal stroma: structure and ageing. Invest. Ophthalmol. Vis. Sci. 39, 644–648.

Dohlman C.H. 1971. The function of the corneal epithelium in health and disease. Invest. Ophthalmol. 10, 383-407.

Goodfellow J.M., Elliot G.F., Woolgar A.E. 1978. X-ray diffraction studies of the Corneal stroma. J. Mol. Biol. 119, 237–252.

Hart R.W., Farrell R.A. 1969. Light scattering in the cornea. J. Opt. Soc. Am. 59, 766-774.

Hayes S., Boote C., Lewis J., Sheppard J., Abahussin M., Quantock A.J., et al. 2007. Comparative study of fibrillar collagen arrangement in the corneas of primates and other mammals. Anat. Rec. Adv. Integr. Anat. Evol. Biol. 290, 1542–1550.

Holmes D.F., Kadler K.E. 2005. The precision of lateral size control in the assembly of corneal collagen fibrils. J. Mol. Biol. 345, 773-784.

Ihanamaki T.T., Pelliniemi L.J., Vuorio E. 2004. Collagens and collagen-related matrix components in the human and mouse eye. Prog. Retinal Eye Res. 23, 403–404.

Ledward D.A. 2000. Gelatin. In Handbook of hydrocolloids, ed G. O. Philips, P.A. Williams. p. 67- 86.Woodhead Publishing Limited.

Li Z., Wang B., Zhang Q., Gong Y., Tang J., Luo H., Ding G. 2013. Isolation and characterization of acid soluble collagens from the skin and bone of Spanish Mackerel (Scomberomorousniphonius). Food Hydro Colloids 31, 103-113.

Liu D., Wei G., Li T., Hu J., Lu N., Regenstein J. M., Zhou, P. 2015. Effects of alkaline pretreatments and acid extraction conditions on the acid-soluble collagen from grass carp (Ctenopharyngodonidella) skin. Food Chemistry 172,836-843.

Maurice D.M. 1957. The structure and transparency of the cornea. J. Physiol. 136, 263–286.

Maurice D.M. 2016. The cornea and sclera, in: H. Davson (Ed.), The Eye, 3rd ed., Academic Press, New York, 1–158.

Meek K.M., Elliot G.F., Sayers Z., Whitburn S.B., Koch M.H.J. 1981.Interpretation of themeridional X-ray diffraction pattern from collagen fibrils in corneal stroma. J. Mol. Biol. 149, 477–488.

Meek K.M., Holmes D.F. 1983. Interpretation of the electron microscopical appearance of collagen fibrils in the corneal stroma. Int. J. Biol. Macromol. 5, 17-25.

Meek K.M., Elliott G.F., Nave C. 1986. A synchrotron X-Ray-diffraction study of bovine cornea stained with cupromeronic blue. Coll. Relat. Res. 6, 203–218.

Meek K., Blamires T., Elliot G., Gyi T.J., Nave C. 1987. The organisation of collagen fibrils in the human corneal stroma: a synchrotron X-ray diffraction study. Curr. Eye Res. 6, 841–846.

Meek K.M., Leonard, D.W. 1993. Ultrastructure of the corneal stroma: a comparative study. Biophys. J. 64, 273-280.

Najafizadeh F., Sadjadi M.B.S., Fateami S.J., Mobarakeh M.K., Afshar R.M. 2016. The Effects of Silica and a Nature Polymer on the Size and Properties of nano-Hydroxyapatite. Oriental Journal of Chemistry 32(3), 1639-1647.

Ottani V., Martini D., Franchi M., Ruggeri A., Raspanti M. 2002. Hierarchical structures in fibrillar collagens. Micron 33, 587-596.

Padmaja P., Anilkumar G.M., Mukundan P., Aruldhas G., Warrier K.G.K. 2001. Characterization of stoichiometric sol-gel mullite by fourier transform infrared spectroscopy. Int. J. Ing. Mat. 3, 693-698.

Peterson D.S. Sol-Gel Technique, Encyclopedia of Microfluidics and Nanofluidics, DOI: https://doi.org/10.1007/978-3-642-27758-0_1432-2

Prestes R.C. 2013. Colágeno e seusderivados: características e aplicaçõesemprodutoscárneos. Revista Unopar Científica Ciências Biológicas e da Saúde 15(1), 65-74.

Reinstein D.Z., Archer T.J., Gobbe M., Silverman R.H., Coleman J.D. 2008. Epithelial thickness in the normal cornea: three-dimensional display with very high frequency ultrasound. J. Refract. Surg. 24, 571-581.

Sakka S., 2013, Chapter 11.1.2-Sol-Gel Process and Applications, Handbook of Advanced Ceramics, 2nd Edition, 883-910.

Sasmal P., Begam H. 2014. Extraction of type –I collagen from sea fish and synthesis of Hap/collagen composite. Procedia Materials Science 5, 1136-1140.

Schrieber R., Gareis H. 2007.Gelatine handbook: theory and industry practice. Hardcover. 348p.
Scott J. 1988. Proteoglycan–fibrillar collagen interactions. Biochem. J. 252, 313–323.

Tylingo R., Mania S., Panek A., Piątek R., Pawłowicz R. 2016. Isolation and Characterization of Acid Soluble Collagen from the Skin of African Catfish (Clarias gariepinus), Salmon (Salmo salar) and Baltic Cod (Gadus morhua). Journal of Biotechnology & Biomaterials 6(2), 1-6

Wang L., An X., Yang F., Xin Z., Zhao L., Hu Q. 2008. Isolation and characterization of collagen from the skin, scale and bone of deep-sea redfish (Sebastesmentella), Food Chemistry 108, 616-623.

Whitcher J.P., Scrinivasan M., Upadhyay M.P. 2002. Prevention of corneal ulceration in the developing world. Int. Ophthalmol. Clin. 42, 71-77.

CHAPTER 7
CONCLUSIONS & FUTURE PROSPECTS

7.1 CONCLUSION

The complete research work has been summarized in this thesis which includes seven chapters including the present one.

Chapter 1 is comprised of the introductory stage about the physiology and anatomy of human eye and its various tissue layer and their nature. The chapter also reflects the biomechanical properties of biological tissues which are mostly viscoelastic in nature.

Followed by chapter 1 the thesis contains various Literature reviews that has been supported the research work with the techniques and knowledge. This Literatures supported the research like the skeleton of a vertebrate and has been summarized in *Chapter 2*.

Chapter 3 is Numerical Foundation. This chapter explains the mathematical equations and derivation which formulates various elastic and viscoelastic models for simulating and designing biological tissue mechanics.

Impact Analysis is the chapter that follows and elaborately described in *Chapter 4*. In this research, a 3D FE model has been constructed in CAD software and basic material properties has been assigned and an impactor is simulated to impact the surface at various velocities. The Stress and Strain has been measured on the surface of the tissue. The study showed that cornea Elastic Model deforms much more than the Viscoelastic model. This confirms that cornea should be simulated as Viscoelastic material for any Impact Test. The Generalized Kelvin-Voigt Model that has been used in this study could provide a better alternative for donor cadaver cornea as this model with conjunction to the silica composite synthetic cornea can provide a far better viscoelastic barrier similar to collagen tissues. This behavior of material properties could also be used in artificial soft contact lenses to resist any damage to the prosthesis from crash injuries or environmental hazards.

Chapter 5 describes Fractional Derivative approach for conventional viscoelastic models. As a conclusion it can be said that the human cornea exhibits viscoelastic tissue behavior with the fractional element lying between the values of perfectly elastic and viscous values with a cling towards elasticity, i.e., the elasticity retains its nature more with a tendency of being viscous. Thus a human cornea actually mimics a viscoelastic soft tissue and can be modeled with fractional parameters. It can also be concluded from this study that the human cornea does not actually behaves a Maxwell viscoelastic tissue and thus does not obey the parameters that to be maintained for a fractional model to be a Maxwell Model i.e., $\alpha = \beta = 1$. As mentioned this particular case shows a large demarcation with

the experimental data observed in literature works. Study from nature of deformation for both FMM and KVFD on the other hand gives clear views of the validation of the two models. As far as experimental works are considered, KVFD depicts a very small change in deformation for the same range of stress applied thus giving out very less energy losses. As a result KVFD can be preferred to Fractional order Maxwell Model in case of implant design or synthesis for drug delivery related purposes. FMM on the other hand shows more close approximation with experimentally obtained data from cadaver cells. The results are more realistic as for the similar range of force; deformation is high and attains rupture within a shorter range of stress.

Chapter 6 explains the experimental investigation towards development of Corneal hybrid composite and Isolation of native collagen from Fish skin. The extracted material from fish skin showed characteristics absorption peaks for Amide A and Amide I, II and III which is the identification characteristics of Collagen type I. The microstructure of the collagen is fibrillar with some knotted structure and few spaces which has determined its spongy nature. These characteristics confirm the material as predominantly collagen I. The FTIR curve of the Silica-Collagen composite showed the characteristic peaks for both collagen and silica phase. The stretching mode of Si-OH and stretching and bending of Si-O-Si can also be seen from the curve which determines proper linking of the two phase while gelation. As collagen is amorphous so the XRD plot shows intensity peaks Si phase at various degrees of rotation among those some are of very high intensity magnitude. The SEM micrograph has a porous phase which is very much likely for any scaffold for tissue growth, regeneration, cell proliferation and targeted drug delivery.

7.2 FUTURE PROPSECTS

Human cornea tissue showing its wide range of deformation has been an area of immense interest recently. Few experimental works have been computed and performed regarding this topic, but a wide range of mathematical modeling is yet to be done in this respect. Fractional Calculus has already been an area of easy and understandable scope of designing and modeling various mechanical models including aerospace engineering. Works on modeling human eye and its nature with this Fractional calculus is yet to come up and more study is needed in this respect including all sorts of complex boundary conditions and non-linearity. More Fractional calculus mathematical models are yet to be studied for human corneal Viscoelasticity. Fractional Kelvin-Voigt Model, Fractional Voigt Maxwell Series (FVMS), Fractional Voigt Maxwell Parallel (FVMP) are few of the Fractional Calculus models which needs to be studied and model human cornea tissue in them. A simultaneous work on both experiments and mathematical modeling with these fractional calculus models will provide a better clarity of viscoelastic nature of lens and also help modeling it to create artificial lenses and cure ophthalmologic issues.

In impact analysis this study of the mechanical behavior of corneal tissues is going to be of immense help as the actual response of the tissues due to a blunt body foreign body on human cornea will depend greatly on the amount of elasticity or viscosity of the same. Any kind of ophthalmologic abnormality in which elasticity as well as viscosity varies can be well defined specially in case of impact analysis now. Likewise the mathematical modeling will also be of help in this regard with the specific values of the fractional parameters to obtain the exact nature mathematically even without any wet laboratory experiments.

Furthermore, there are lots of areas of improving the microstructure and characteristics of these Silica Collagen composite like the curing technique could be varied to examine the characteristics of the materials as curing is a very important step in forming the microstructure in nano-science which in return affects the porosity and mechanical strength of the material. The swelling nature could be studied for any post-operative swelling of the implant and amount of water absorption. The bonding and linking could be made stronger with some additives like glutaraldehyde or poly vinyl alcohol or some commercial plasticizers. These are the future research interest in these fields to enhance the property and suitability of the collagen and composite to ensure them to be a part of the implant synthesis and the implant itself.

Biomedical Research 2018; 29 (12): 2465-2470 *ISSN 0970-938X*
www.biomedres.info

Finite element approach towards impact analysis on biomechanical nature of cornea.

Dibyendu Mandal*, Himadri Chattopadhyay, Amit Karmakar, Kumaresh Halder

Department of Mechanical Engineering, Heat and Power Laboratory, Jadavpur University, Kolkata, India

Abstract

The present work is a computational analysis of a blunt body impact on corneal viscoelastic behavior; simultaneously comparison is drawn between the tissue behaviors with corresponding cases considering the tissue to be elastic in other simulated model. Three dimensional models of corneal tissue were subjected to blunt body impact at different velocities in ALTAIR platform to study the nature of injury on the tissue material. The variation in the strain due to impact on the cornea for the material behaviors, range in the order $10^{-2} \pm 0.002$ and that for the stress, the magnitude gets almost double for elastic nature of cornea. Results shows that the viscoelastic fractional derivative biomechanics of the tissue predict higher resistance to any foreign body impacting on the surface of cornea preventing it from further indentation into the tissue. The viscoelastic model provided in this work can be incorporated for the synthesis of artificial corneas and soft contact lenses.

Keywords: Cornea, Fractional kelvin voigt model, Biomechanical properties, Viscoelasticity, Finite element simulation.

Accepted on May 11, 2017

Introduction

Ocular injury can lead to extensive tissue damage which results in ocular emergency situations and serious morbidity of the delicate tissues of the eye [1]. Injuries due to larger impacting bodies cause wear and tear of the eye lid tissues, retinal detachment from choroid or equatorial expansion of the eye ball. But injury due to small foreign body can also lead to the injuries direct on the surface of cornea, which may lead to complete or partial tissue rupture leading to complete loss of vision or impaired vision. Eye is one of the major sense organ of our body. It has three membrane layers, sclera, choroid and retina from outer layer to inner layer that surrounds the eye. The sclera continues in front of the eye ball as a transparent layer named cornea which helps in reflection of the light into the eye and also protect the inner parts and tissues of the eye. Thus cornea is a part of major clinical and medical concern. Recently researchers are focusing on the biomechanical characteristics of the morbid eye tissues where increase in intraocular pressure (IOP) results in increase of stress which is a characteristic of the deformation of cornea [2]. To properly understand the process of these ocular diseases a better visualization and understanding of the mechanical nature of the corneal tissue is of prior importance. The main objective of this work is to focus on the material characteristics behavior of synthetic cornea or contact lenses which is subjected to regular impact. A three dimensional Finite Element Analysis (FEA) is applied for understanding and analyzing the impact of foreign body causing Intra-Ocular Foreign Body (IOFB) injuries. Blunt eye trauma comprises injuries to the closed globe where tissue damage can results from mechanical deformation alone or combined effect of direct delivery of energy to the tissue due to impact [3]. A particular tissue's behavior and deformation under stress is determined by its biomechanical properties.

Finite Element Modeling (FEM) is a numerical analytical approach, extensively used for simulation of multiphysics problems that involves complex structures and loading conditions [4]. This method, since past few years, is applied to biological systems, specifically to the eye for simulation of the stress-strain nature of the lamina cribrosa layer, the corneal tissue and the whole eye [5-7]. A simulation model of eye is set up based on the information of cadaver eyes done in the earlier works in this domain. The scope of the present work is to investigate an FEM analysis of a standardized corneal trauma due to blunt body impact where the tissue is considered to be viscoelastic in nature, and to draw a comparison between the tissue behaviors with corresponding cases considering elastic behavior only.

Materials and Methods

Cornea exhibits unique properties of stiffness, mechanical strength and optical transparency which enable it to provide protective barrier to the inner components of the globe and also the primary refractive medium of the eye. The fibrous microstructure of the stromal layer of cornea, which in humans constitutes 90% of the corneal thickness, results in this unique nature of the tissue. The stromal thickness is composed of around 200 lamellar sheets of collagen myofibrils implanted in hydrated matrix of glycoproteins, keratocyte cells and proteoglycans [8]. Cornea exhibits complex microstructure

strongly regulated by the human body itself. After death, the cornea swells and its optical clarity and tear film is lost. Thus the biomechanical properties of the eye changes due to the combined effect of these biomechanical changes along with tissue degradation and alteration in temperatures [9]. In addition, Kobayashi et al. explained that the cornea is not purely elastic but rather is viscoelastic, which means the loading rate applied on the tissue alters the calculated value of the Young modulus [10]. Due to the combination of all these factors, previous literatures has reported large range of Young's Modulus ranging from 0.159 MPa to 57 MPa [11,12]. Under loading condition, cornea shows instantaneous deformation which demonstrates purely elastic response followed by gradual and progressive deformation which signifies its viscoelastic nature [10,13]. These behaviors could be modeled fairly with a Hookian spring system for pure elastic nature and with a spring-dashpot system for the viscoelastic nature, where the dashpot represents time-dependent viscous resistance to an applied force. Here one spring-mass system is in series with a spring-mass damping system where the damping is parallel to the spring system.

For viscoelastic model, generalized Fractional Kelvin-Voigt Deravativehas been selected as other model (e.g. Maxwell model) continually to creeps indefinitely under load. In the cornea, creep approaches asymptotically [14]. Another limitation of Maxwell model is that it does not regain its original form after the load cease to act. The pure Kelvin-Voigt model was not selected because it does not possess a purely elastic component and thus no instantaneous deformation occurs. A simple graphical model has been developed in MATLAB for a corneal model with Young's modulus in the above mentioned range and viscosity of 9.02 KPa-s, which shows time-dependency of the deformation for a particular load. Figure 1 shows that the steepness of the curve increases as the stress increases and after the elastic limit it experiences no further deformation.

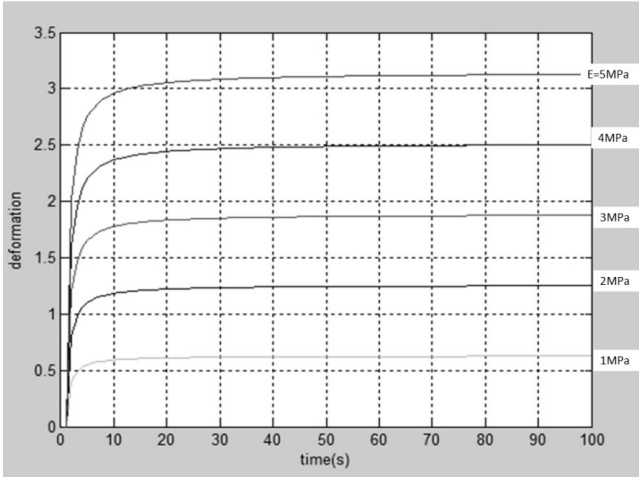

Figure 1. *Strain versus time for load varying from 110^5 to 5 10^5 Nm^{-2}.*

The elastic nature of the model is assumed to be an isotropic, linear elastic model obeying Hook's law and represents a linear relation between stress and strain. The stress-strain relationship could be presented as:

$$e_{ij} = \frac{1+\vartheta}{E}\sigma_{ij} - \frac{\vartheta}{E}\sigma_{kk}\delta_{ij} \rightarrow (1)$$

$$\sigma_{ij} = 2Ge_{ij} + \lambda e_{kk}\delta_{ij} \rightarrow (2)$$

Where, e_{ij} represents the Eulerian strain tensor and σ_{ij} represents Cauchy stress tensor's component [15].

KVFD governing equation 4 arises out of the conventional governing equation 3 of the K-V Model by replacing the ordinary integral derivatives with a fractional order. Order of the derivative of strain with respect to time is thus assumed to be a fraction and the corresponding stress-strain plot has been obtained. Stress has been varied between 1 MPa-9 MPa and the corneal tissue has a co-efficient of viscosity of 9.02 KPa and elastic limit of 11.05 MPa [16-18]. These data have been incorporated into the governing equation of KVFD to obtain the characteristic plots. The fractional order α takes up values such as 1/3, 2/3, 1/2, 1/4 and 3/4. When α=1, KVFD reduces to the conventional K-V Model.

$$\sigma(t) = E\varepsilon(t) + \eta\frac{d\varepsilon}{dt} \rightarrow (3)$$

$$\sigma(t) = E\varepsilon(t) + \eta\frac{d^{\alpha}\varepsilon}{dt^{\alpha}} \rightarrow (4)$$

Stress relaxation and Creep Compliance response for a KVFD model are obtained by taking a Heaviside function of the deformation and stress respectively. In the standard Kelvin-Voight model α=1, and the stress relaxation is equal to a delta function at time zero with a constant response after. No real material follows this function. In the KVFD model, where 0<α<1 the stress relaxation has the form $t^{-\alpha}$, where t is time. The creep compliance, J(t), and stress relaxation, G(t), functions, for the KVFD model are [19]:

$$J(t) = \frac{1}{E}\left[1 - E_{\alpha}\left\{-\left(\frac{Et}{\eta}\right)^{\alpha}\right\}\right] \rightarrow (5)$$

Where, E_{α} is the Mittag-Leffler function and is given by:

$$E_{\alpha}(x) = 1 + \sum_{n=0}^{\infty}\frac{x^n}{\Gamma(\alpha n + 1)}$$

And,

$$G(t) = E + \eta\frac{(1-\alpha)t^{-\alpha}}{\Gamma(2-\alpha)} \rightarrow (6)$$

Figure 2 shows that KVFD depicts predicted nature of plot for deformation against time, where the deformation is increasing exponentially in the beginning and then converges within a very short interval of time for various α values: 1/3, 2/3, ½ and 1.

Nguyen et al. suggested the development of a constitutive model based on the tissue microstructure for the nonlinear anisotropic viscoelastic tensile behavior of the stroma layer that comprise a explanation of fully nonlinear viscoelastic response of the lamellar level [20]. The model is based on a

newly developed general nonlinear constitutive framework for soft fiber-reinforced composites [21]. The model represents the stroma as a continuum mixture consisting of collagen fibrils structured into lamellae characterized by an in plane orientation angle and embedded in a soft isotropic matrix.

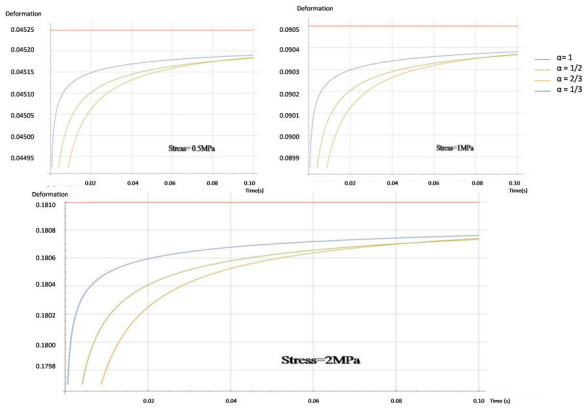

Figure 2. *KVFD Response for Deformation (mm/mm) vs. Time(s) for four different values of α for (1.1) Stress=0.5 MPa, (1.2) Stress=1 MPa, (1.3) Stress=2 MPa.*

The geometric model for the present work is based on the size, structure and dimensions of a generic human eye model. The model has been derived from our previous work which is a three-dimensional geometry of eye cornea that has been developed and imported in Altair Hyperworks 10.0 suite in Block 90 format and linear hexahedral volume mesh is generated throughout the thickness of the cornea and is constituted of eight nodes hexahedral element called hex8 element in Altair Hypermesh environment, containing total 3095 elements comprising off 3960 nodes shown in Figure 3a [22].

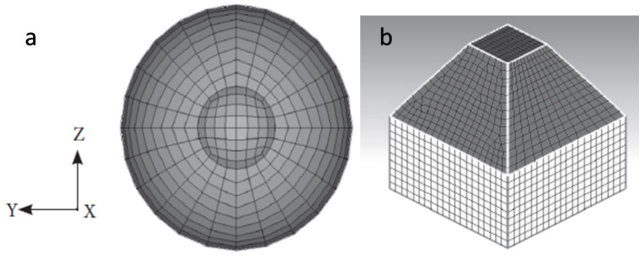

Figure 3. *A) Meshed eye model; B) The decahedron projectile.*

From the experiment report of Uchio et al. it was found that Poisson's ratio for cornea is 0.420 and it was assumed that rupture occurs at a strain of 18% in cornea, and at a stress of 9.4 MPa [23]. The blunt decahedron projectile, shown in Figure 3b, is generated based on previous work of Uchio et al. and Mousavi et al. [23,24]. Three different materials were considered for projectile i.e., aluminum, bone and stainless steel with corresponding material properties. The bullet projectile has been meshed with linear hexahedral brick element mesh comprising of total 980 elements with 1124 nodes.

The mechanical properties used for various materials are enumerated in Table 1 [25,26]. The base area of the projectile is 0.25 mm^2 whose mass varies depending on the material. The cornea geometry is constrained about all axes to prevent any linear or rotational movement in any directions and the projectile material is set to impact on the surface at variable speed of 25 ms^{-1}, 50 ms^{-1}, 75 ms^{-1} and 100 ms^{-1}. The computation has been performed in Z230 HP workstation.

Table 1. *Mechanical properties of various materials considered to be as the foreign body.*

Material	Density (gm/cm^3)	Young's Modulus (Mpa)	Poisson's Ratio
Bone	1.9	9000	0.30
Aluminium	2.7	69000	0.35
Steel	3.0	197000	0.29

Result and Discussions

It has been observed through the simulation result that when the corneal tissue is considered as viscoelastic in nature it offers better resistance to the impacting object. The magnitude of the von-Misses stress generated on the surface of the elastic nature cornea almost gets double compared to the viscoelastic nature of the tissue. In the case of strain rate it has been observed that the localized straining is more on the surface of the elastic tissue. The variation in the strain effect on the cornea surface for both the material behavior range in the order $10^{-2} \pm 0.002$. It is mainly observed how the strain behavior and von Misses stress behavior varies on the surface of the cornea when crashed with projectiles of such varied mechanical properties. Human cortical bone has the lowest range of Young's modulus and density among the three materials used, the other two being Aluminum and stainless steel of grade AISI 316. The results are plotted for both plastic strains and Von Misses stresses of the cornea for all the three impacting material and for both the mechanical nature of cornea. From the plots it could be easily said that the value of the result parameters increases with increase in velocities. The plots also depicts that the value of both the result parameters sharply varies with the mechanical properties of the impacting material used for given set of velocities as shown in Figures 4a and 4b.

The higher the Young's Modulus and density of the material higher is the value of plastic strain and von Misses stress at a particular velocity. Stress and strain are generated and transient behavior plot of the strain and stress on the tissue surface are developed which is shown in Figure 5 for the case of an aluminum projectile with a velocity of 50 ms^{-1}. From the transient response of the stress and strain, it is observed that the stress generated and strain effect on the tissue surface due to high velocity blunt body impact is comparably less for the viscoelastic nature of cornea than that of the elastic nature for similar test conditions. This leads to better energy absorption in

the model constituted with viscoelastic nature thus it could provide better and long term resistance to the impacting body before failure.

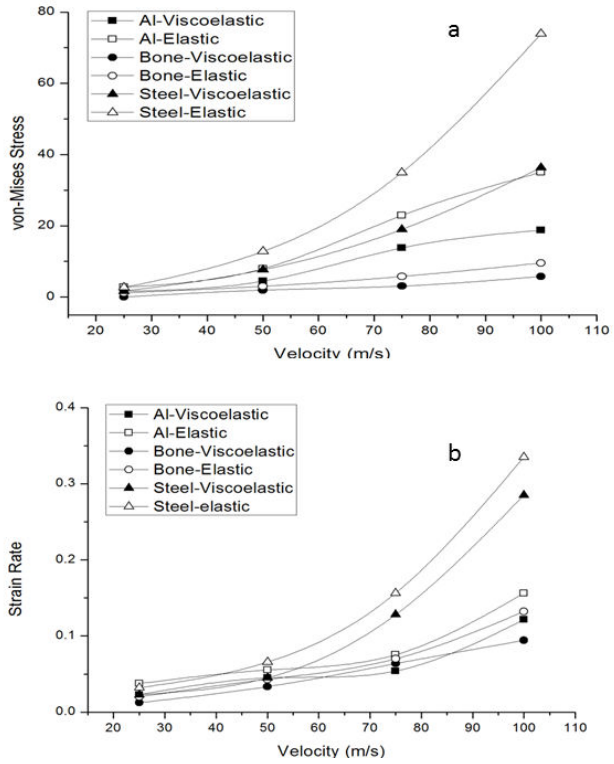

Figure 4. *A) Stress versus velocity curve; B) Strain rate versus velocity curve.*

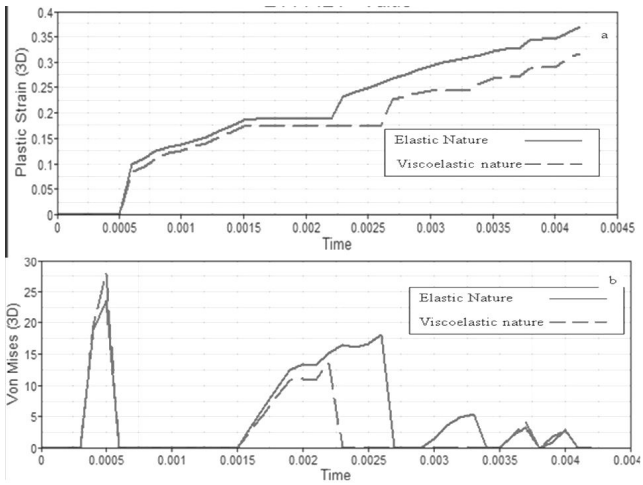

Figure 5. *Transient response of strain and stress with time (a) transient response of strain with time, (b) transient response of stress with time.*

In this study the displacement of the surface of the cornea is also studied. The transient response of the displacement is shown in Figure 6 where it is clearly explained that elastic nature shows instantaneous deformation and is short termed but viscoelastic nature shows prolonged and progressive deformation. Table 2 shows the duration of deformation for different material and projectile velocity combination. There in all the cases we can observe that for viscoelastic model the deformation is much gradual than the elastic model. In our range of maximum velocities, it has been observed that maximum duration for energy absorption is around 5.0, 5.5 and 6.5 milli-second respectively for each of the projectile material. However, the transient response time increases as the elastic moduli and density of the projectile increases. For example the duration of deformation for bone projectile impact is about 5.0 milli-seconds whereas for that of steel is around 6.5 milli-second.

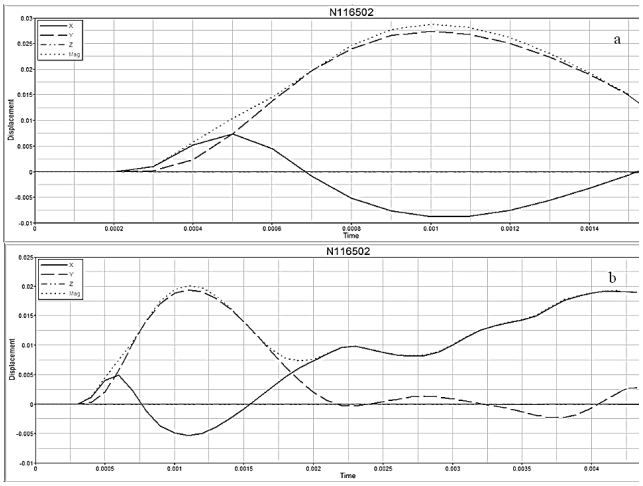

Figure 6. *Transient response of displacement of node N116502 (a) displacement for elastic cornea, (b) displacement for viscoelastic cornea, for aluminum projectile impacting at 50 ms^{-1}.*

Due to this prolonged deformation stage in viscoelastic model which is not an instantaneous shock to the material rather it follows a gradual deformation with respect to the force applied, this model could be used for further research in this area. Cadaver eye cornea transplant reported several issues of donor graft rejection, biocompatibility and such other issues and anti-rejection drugs are commonly administered which could lead to infections [27]. The Generalised Kelvin-Voigt Model that has been used in this study could provide a better alternative for donor cadaver cornea as this model with conjunction to the silica composite synthetic cornea can provide a far better viscoelastic barrier similar to collagen tissues. This behavior of material properties could also be used in artificial soft contact lenses to resist any damage to the prosthesis from crash injuries or environmental hazards.

Table 2. *Duration of deformation for different cornea material behavior and projectile velocity combination; E: Elastic model of cornea, VE: Viscoelastic model of cornea.*

Velocities (ms^{-1})	25		50		75		100		Projectile Material
	E	VE	E	VE	E	VE	E	VE	
Duration of Deformation (sec)	0.0007	0.0028	0.0010	0.0037	0.0016	0.0045	0.0021	0.0051	Bone
	0.0011	0.0035	0.0015	0.0043	0.0019	0.0051	0.0025	0.0056	Aluminum
	0.0016	0.0043	0.0022	0.0052	0.0026	0.0059	0.0031	0.0066	Steel

Acknowledgment

We would like to acknowledge the Altair India Support Team for their constant technical support during the research. I like to acknowledge JRF Fellowship of UGC, Government of India for financial support.

References

1. Vajpayee RB, Shekhar H, Sharma N, Jhanji V. Demographic and clinical profile of ocular chemical injuries in the pediatric age group. Ophthalmology 2014; 121: 377-380.
2. Glass DH, Roberts CJ, Litsky AS, Weber PA. A Viscoelastic Biomechanical Model of the Cornea Describing the Effect of Viscosity and Elasticity on Hysteresis. Invest Ophthalmol Vis Sci 2008; 49: 3919-3926.
3. Kuhn F, Morris R, Whiterspoon CD, Heimann K. A standardized classification of ocular trauma terminology. Ophthalmology 1996; 103: 240-243.
4. Rossi T, Boccassini B, Esposito L. The Pathogenesis of Retinal Damage in Blunt eye Trauma: Finite Element Modeling. Invest Ophthalmol Vis Sci 2011; 52: 3994-4002.
5. Roberts MD, Liang Y, Sigal IA. Correlation between local stress and strain and lamina cribrosa connective tissue volume fraction in normal monkey eyes. Invest Ophthalmol Vis Sci 2010; 51: 295-307.
6. Gefen A, Shalom R, Elad D, Mandel Y. Biomechanical analysis of the keratoconic cornea. J Mech Behav Biomed Mater 2009; 2: 224-236.
7. Amini R, Barocas VH. Anterior chamber angle opening during corneo-scleral indentation: the mechanism of whole eye globe deformation and the importance of the limbus. Invest Ophthalmol Vis Sci 2009; 50: 5288-5294.
8. Maurice DM. The structure and transparency of the cornea. J Physiol 1957; 136: 263-286.
9. Hjortdal JO. Extensibility of the normo-hydrated human cornea. Acta Ophthalmol Scand 1995; 73: 12-17.
10. Kobayashi AS, Staberg LG, Schelge WA. Viscoelastic properties of human cornea. Exp Mech 1973; 497-503.
11. Elsheikh A, Wang D, Brown M, Rama P, Campanelli M, Pye D. Assessment of corneal biomechanical properties and their variation with age. Curr Eye Res 2007; 32: 11-19.
12. Andreassen TT, Simonsen AH, Oxlund H. Biomechanical properties of keratoconus and normal corneas. Exp Eye Res 1980; 31: 435-441.
13. Edmund C. Corneal topography and elasticity in normal and keratoconic eyes. A methodological study concerning the pathogenesis of keratoconus. Acta Ophthalmol Suppl 1989; 193: 1-36.
14. Jue B, Maurice DM. The mechanical properties of the rabbit and human cornea. J Biomech 1986; 19: 847-853.
15. Material Laws. Large Displacement Finite element analysis-Part2. RADIOSS Theory Manual v10.0, 2009.
16. Uchio E, Watanabe Y, Kadonosono K, Matsuoka Y, Goto S. Simulation of airbag impact on eyes after photorefractive keratectomy by finite element analysis method. Graefe's Arch Clin Exp Ophthalmol 2003; 241: 497-504.
17. Glass DH, Roberts CJ, Litsky AS, Weber PA. A Viscoelastic Biomechanical Model of the Cornea Describing the Effect of Viscosity and Elasticity on Hysteresis. Invest Ophthalmol Vis Sci 2008; 49: 3919-3926.
18. Wua J, Nasseri MA, Eder M, Gavaldon MA, Lohmann CP, Knoll A. The 3D Eyeball FEA Model with Needle Rotation. APCBEE Procedia 2013; 7: 4-10.
19. Lawrence ST, Amy LL, Deborah JR, Kevin JP. A Kelvin-Voigt Fractional Derivative Model for Viscoelastic Characterization of Liver Tissue. ASME Int Mech Engg Congress and Exposition 2002.
20. Nguyen TD, Jones RE, Boyce BL. A Nonlinear Anisotropic Viscoelastic Model for the Tensile Behavior of Corneal Stroma. J Biomech Eng 2008; 130: 1-10.
21. Nguyen TD, Jones RE, Boyce BL. Modelling the Anisotropic Finite-Deformation Viscoelastic Behavior of Soft Fiber-Reinforced Composites. Int J Solids Struct 2007; 44: 8366-8389.
22. Mandal D. Simulation of eye Injury due to blunt body impact. DSpace of Jadavpur University 2013; Kolkata, India.
23. Uchio E1 Ohno S, Kudoh J, Aoki K, Kisielewicz LT. Simulation model of an eyeball based on finite element analysis on a supercomputer. Br J Ophthalmol 1999; 83: 1106-1111.
24. Mousavi SJ, Nassiri N, Masoumi N, Nassiri N, Majdi-N M, Farzaneh S, Djalilian AR, Peyman GA. Finite element analysis of blunt foreign body impact on the cornea after PRK and LASIK. J Refract Surg 2012; 28: 59-64.
25. Rupin F, Amena S, Dolmas D. Experimental determination of Young's Modulus and Poisson ratio in cortical bone tissue using high resolution Scanning Acoustic Microscopy

and Nanoindentation. J Acoustic Soc Am 2008; 123: 3785-3795.

26. Geringer J, Atmani F, Forest B. Friction Corrosion of AISI 316L/Bone Cement and AISI 316L/PMMA contacts: ionic strength on tribological behavior. Wear 2008; 267: 763-769.
27. http://webeye.ophth.uiowa.edu/eyeforum/tutorials/Cornea-Transplant-Intro/index.htm

***Correspondence to**

Dibyendu Mandal

Department of Mechanical Engineering

Heat and Power Laboratory

Jadavpur University

India